Mari Solheim
Ådne Magnus Viga Skretting

Fatigue assessment of a generic steel bridge

A comparison of NS-EN 1993-1-9 and DNVGL-RP-C203

Master's thesis

NTNU
Norwegian University of Science and Technology
Faculty of Engineering
Department of Structural Engineering

NTNU
Norwegian University of
Science and Technology

Mari Solheim
Ådne Magnus Viga Skretting

Fatigue assessment of a generic steel bridge

A comparison of NS-EN 1993-1-9 and DNVGL-RP-C203

NTNU
Norwegian University of
Science and Technology

Department of Structural Engineering
Faculty of Engineering
NTNU − Norwegian University of Science and Technology

MASTER THESIS 2021

SUBJECT AREA: Applied mechanics	DATE: 08.06.2021	NO. OF PAGES: 128

TITLE:

Fatigue assessment of a generic steel bridge

Utmattingsberegning på en generisk stålbro

BY:

Mari Solheim

Ådne Magnus Viga Skretting

SUMMARY:

Fatigue is the growth of defects into cracks due to repeated loads over time, which eventually cause failure of details in structures. Design against fatigue is governed by standards limited to specific environments or dimensions. This thesis investigates the relationship between NS-EN 1993-1-9 and DNVGL-RP-C203 fatigue calculation for welded details in a generic steel bridge. The bridge has a lifespan of 100 years, and is exposed to truck loads. DNVGL-RP-C203 is more detailed and an important question is how this standard holds up against NS-EN 1993-1-9 in areas where the latter is limited. Python scripting has been used to automate finite element analysis and damage calculation in the bridge. By considering every possible location for fatigue prone details, over 7000 data points have been generated. For the details in the orthotropic deck, DNVGL-RP-C203 gives comparable results to NS-EN 1993-1-9. By choosing an appropriate safety implementation for damage calculation with DNVGL-RP-C203, slightly conservative results relative to NS-EN 1993-1-9 are obtained. NS-EN 1993-1-9 is especially limited when applied to details in trusses, which is reflected in the results in this thesis. For fatigue in the trusses, DNVGL-RP-C203 turned out non-conservative relative to NS-EN 1993-1-9, regardless of safety implementation. Due to the limitations of NS-EN 1993-1-9, it is hard to create reasonable loads in the trusses. The report therefore concludes with suggestions for further work in this area.

RESPONSIBLE TEACHER: Professor Arild Holm Clausen

SUPERVISOR(S): Senior advisor Nils Arne Rakstad (Dr.techn. Olav Olsen AS)

CARRIED OUT AT: Norwegian University of Science and Technology

Abstract

In this thesis, the relationship between fatigue damage calculation in welded details in a generic bridge for NS-EN 1993-1-9 and DNVGL-RP-C203 have been investigated. The bridge consists of an orthotropic deck with trusses at each side. The orthotropic deck has trapezoidal longitudinal stringers, T-profile transverse beams and a steel cover plate, and the trusses have tubular braces and chords defined by right isosceles triangles.

NS-EN 1993-1-9 is the Norwegian approved version of the standard for fatigue design of steel structures, authored by the European Committee for Standardization (CEN). DNVGL-RP-C203 is a so called Recommended Practice (RP) issued by the Norwegian company DNV, and is a standard for fatigue design of offshore steel structures[1]. The two standards cover the same topic in a similar way, but are intended for use in different areas, as indicated by their names. NS-EN 1993-1-9 is however not very detailed in designating procedures and is, on multiple areas, vague and limited. This is especially true for trusses and fatigue analysis based on detailed Finite Element Analysis (hotspot analysis). DNVGL-RP-C203 provides detailed procedures in these areas, and a comparison between the two are thus of interest to see how DNVGL-RP-C203 holds up against NS-EN 1993-1-9.

With the standards diverging on multiple points, a qualitative approach was deemed to be necessary. The generic bridge has been loaded with lorries as defined in Fatigue Load Model 4 (FLM4) of NS-EN 1991-2, resulting in a large number of fatigue damage data points for comparison between the two standards. To be able to calculate fatigue damage for the large number of locations in the bridge, Python scripting was used in conjunction with the Finite Element Analysis (FEA) software Abaqus FEA to automate the process. This resulted in over 7000 data points to assess the two standards. A simpler nominal stress approach was used to calculate fatigue damages for the entire bridge, and detailed FEM analyses has been performed to assess the validity of the nominal analyses.

The use of a generic bridge was found to be a convenient tool for comparing NS-EN 1993-1-9 and DNVGL-RP-C203. By plotting damages calculated by the two standards against each other, clustering of damages reveals that one can risk unfortunate sampling by not calculating damages for the entire bridge. In the orthotropic deck, DNVGL-RP-C203 has been found to be consistently more conservative than NS-EN 1993-1-9, while the opposite is true in the trusses. This is in both cases mainly due to the difference in S-N curves in the standards, but thickness factors included in DNVGL-RP-C203 also contributes. For the orthotropic deck, DNVGL-RP-C203 is found to give similar results as NS-EN 1993-1-9 for fatigue damage analysis when applying the correct safety implementations given in DNVGL-RP-C203. In the trusses, DNVGL-RP-C203 gave a more reasonable result than NS-EN 1993-1-9, where NS-EN 1993-1-9 damage was found to be very sensitive to the magnitude of stress ranges due to how the standard defines S-N curves for joints.

---

[1]The company name was changed from DNV GL to DNV in March 2021. Standards issued by the company are by the time of writing still denoted with DNVGL (Lovegrove, 2021).

Sammendrag

Denne masteroppgaven har sammenlignet utmattingsberegning i sveiste detaljer i en generisk bro ved bruk av standardene NS-EN 1993-1-9 og DNVGL-RP-C203. Broen består av et ortotropisk dekke og fagverk på begge sidene. Det ortotropiske dekket har trapesformede langsgående stivere, tverrbjelker med T-profil og en stålplate øverst. Fagverket består av rørformede gurter og diagonaler, definert av rettvinklete likebente trekanter.

NS-EN 1993-1-9 er den norske fastsatte versjonen av den Europeiske Komitéen for Standardisering sin standard for utmattingspåkjente stålkonstruksjoner. DNVGL-RP-C203 er en anbefalt praksis utgitt av det norske selskapet DNV, som omhandler utmattingsdesign av offshore stålkonstruksjoner[2]. Begge standardene dekker det samme temaet på en lik måte, men er tiltenkt ulike bruksområder som indikert av navnene deres. NS-EN 1993-1-9 er ikke veldig detaljert når det kommer til utføring av beregninger, og er på flere områder vag og begrenset i omfang. Dette gjelder spesielt for fagverk og for utmattingsanalyse ved detaljerte elementanalyser (geometriske utmattingsanalyser). DNVGL-RP-C203 har på sin side detaljerte, fastsatte fremgangsmetoder på disse områdene, og dermed er det av interesse å utforske hvordan DNVGL-RP-C203 opptrer i domenet til NS-EN 1993-1-9.

Ettersom standardene avviker på flere punkter er en kvalitativ undersøkelse blitt gjennomført. Den generiske broen har blitt påført lastebillaster som definert i Fatigue Load Model 4 (FLM4) i NS-EN 1991-2. Bruk av Pythonscripting til å hente ut spenninger fra elementanalyser gjennomført i programmet Abaqus FEA har muliggjort utmattingsberegninger for detaljene for alle posisjoner i broen. Dette ga over 7000 datapunkter som grunnlag til å vurdere de to standardene opp mot hverandre. En enkel nominell spenningsmetode har blitt brukt til å generere utmattingsskadene for hele broa, mens detaljerte elementanalyser har blitt brukt til å vurdere rimeligheten av de nominelle analysene.

Den generiske broen var et nyttig verktøy til å sammenligne NS-EN 1993-1-9 og DNVGL-RP-C203. Ved å lage figurer som viser utmatting fra de to standardene på hver sin akse, observerte man klynging av datapunkter, noe som kunne gitt uheldige utvalg om man ikke sjekket utmatting for hele broen. I det ortotropiske dekket var DNVGL-RP-C203 konsistent mer konservativ enn NS-EN 1993-1-9, og det motsatte var tilfelle i fagverkene. Dette er i begge tilfellene hovedsakelig på grunn av S-N-kurvene i standardene, men også på grunn av tykkelsesbidraget som er tatt hensyn til i DNVGL-RP-C203. Ved å bruke riktig sikkerhetsimplementering i DNVGL-RP-C203 får man i det ortotropiske dekket samsvarende resultater som ved bruk av NS-EN 1993-1-9. I fagverket ga DNVGL-RP-C203 rimeligere resultater enn NS-EN 1993-1-9, hvor utmattingsberegning ved NS-EN 1993-1-9 viste seg å være veldig sensitiv for størrelsesordenen på spennviddene som følge av hvordan standarden definerer S-N-kurver for knutepunkt.

---

[2]DNV GL byttet navn til DNV i mars 2021. Standardene utgitt av selskapet er i skrivende stund fremdeles navngitt DNVGL (Lovegrove, 2021).

x

Preface

The authors would like to thank Dr.techn. Olav Olsen AS for suggesting and providing support with this thesis. We are particularly grateful for the time and advice given by Senior Advisor Nils Arne Rakstad at Dr.techn. Olav Olsen AS, who has provided technical guidance and advice on short notice on many occasions.

We would also like to thank Professor Arild Holm Clausen from the Department of Structural Engineering at the Norwegian University of Science and Technology, for his support with the thesis and guidance with this report.

Finally, we would like to thank Specialist Engineer and Senior Vice President Inge Lotsberg at DNV for taking the time to provide insight into the relationship between safety implementation in NS-EN 1993-1-9 and DNVGL-RP-C203.

Table of Contents

Nomenclature

The following lists contains the symbols and abbreviations used in this master thesis, as well as a short description of them.

Abbreviations

CAE   Complete Abaqus Environment

CAFL Constant Amplitude Fatigue Limit

CEN   Comité Européen de Normalisation - European Committee for Standardization

CSV   Comma Separated Variable

DFF   Design Fatigue Factor

EN   Europäische Norm - European Standard

FEA   Finite Element Analysis

FEM   Finite Element Method

FLM   Fatigue Load Model

HCF   High Cycle Fatigue

LCF   Low Cycle Fatigue

NA   National Annex

NS   Norsk Standard - Norwegian Standard

ODB   Output DataBase

RP   Recommended Practice

SCF   Stress Concentration Factor

SCF_{AC} Stress Concentration Factor for axial stress in K-joint crown

SCF_{AS} Stress Concentration Factor for axial stress in K-joint saddle

SCF_{MIP} Stress Concentration Factor for in-plane bending stress in K-joint

SCF_{MOP} Stress Concentration Factor for out-of-plane bending stress in K-joint

Symbols

$\Delta\sigma$ Stress range

ΔK Stress intensity range

ΔK_{th} Crack growth threshold

$\Delta\sigma_C$ Detail category stress range

$\Delta\sigma_D$ Constant Amplitude Fatigue Limit stress range

$\Delta\sigma_L$ Cut-off Limit stress range

η Usage factor

$\frac{da}{dN}$ Crack growth rate

γ_{Mf} Partial factor for fatigue strength

λ_e Material-dependent adjustment factor

$\log a$ Intercept with log N-axis in S-N diagram. Denoted $\log\bar{a}$ in DNVGL-RP-C203

σ Stress

σ_i Stress in K-joint brace-chord intersection, where i = 1, 2, ..., 8

σ_x Axial stress

σ_{my} In-plane bending stress

σ_{mz} Out-of-plane bending stress

σ_m Mean stress

a Crack length

a_{cr} Critical crack length

H Height

K Stress intensity factor

k Thickness exponent

K_{IC} Fracture toughness

m Negative slope of S-N curve

M_{IP} In-plane bending moment

M_{OP} Out-of-plane bending moment

N Load cycles

N_C Detail category load cycles

r Radius

t Thickness

t_0 Chord thickness

t_i Brace thickness

t_p Plate thickness

t_r Tubular insert thickness

t_{ref} Reference thickness for welded connections

W Width

1 Introduction

Fatigue analysis is a comprehensive field, and failures due to this phenomenon is still a major concern in engineering design. The knowledge about fatigue as a limit state is relatively novel and there is continuous research within the field. Mechanical failures caused by fatigue has been one of many subjects of engineering work for more than 150 years, with the work done by August Wöhler in the 1850s being especially noteworthy. Through his extensive testing of many metals under bending, torsion and axial loads, the development of design strategies for avoiding fatigue failure was begun (Dowling, 2013, p. 417).

As of today, fatigue failure remains a problem. It has been estimated that about 90 % of all mechanical service failures are caused by fatigue, and both prevention and failures can be costly (Campbell, 2008, p. 243). The consequences of improper fatigue design is exemplified by the disastrous failure of the Alexander Kielland platform in 1980. It was concluded that a fatigue crack had initiated and propagated from the fillet weld near a tubular brace supporting one of the vertical columns. The brace broke off as a consequence of said crack propagation, and the other five braces had to support the column alone. The remaining braces eventually failed due to overload, causing the column to separate from the platform. With the column separated, the platform became unstable and subsequently collapsed. There were 123 fatalities out of the 212 persons present (Dahle and Smith-Solbakken, 2020), underlining the importance of sound design against fatigue damage.

As such, there is a need for design codes that provide sufficient recommendation on how to design against fatigue. There are many design codes that cover this topic. In Europe, the Eurocodes replace the national design codes published in each country (European Committee for Standardization, 2021). Each country provides their own National Annex as a supplement to them.

Standard Norge is the organisation representing Norway in the European Committee of Standardisation (CEN), and has adopted CEN's standard for fatigue loaded steel structures NS-EN-1993-1-9, where NS denotes the Norwegian approved version (Standard Norge, 2021). This standard governs fatigue loaded structures in Norway, and is adequate for many applications. It is however not very extensive in some crucial areas such as fatigue in trusses and fatigue analysis using detailed finite element modelling. DNVGL-RP-C203 is a so-called recommended practice issued by the Norwegian company DNV. Though not a standard in name, it is structured as a standard, giving guidelines for fatigue design of offshore steel structures. Importantly, DNVGL-RP-C203 gives detailed instructions in the areas which NS-EN 1993-1-9 is lacking.

Dr.techn. Olav Olsen AS is a consultancy within structural engineering, and have suggested this thesis. As of today, they are involved in the design process of a steel bridge consisting of two longitudinal trusses and one orthotropic deck. Some of the details in this bridge have dimensions outside the scope of NS-EN 1993-1-9, and this thesis will employ a generic, simplified bridge to gain insight into the relationship between NS-EN 1993-1-9

and DNVGL-RP-C203.

This report will limit the presentation of theory by mostly presenting what is used to calculate fatigue damage in the generic bridge. These analyses are based on Stress range-Life cycle curves (S-N curves), which are defined in NS-EN 1993-1-9 and DNVGL-RP-C203. The relevant standards are then presented in Section 3, with emphasis on what is considered relevant for the thesis. Here, NS-EN 1993-1-9 and DNVGL-RP-C203 are presented separately, along with other standards and design codes needed to implement the theory into practical design. A comparison of NS-EN 1993-1-9 and DNVGL-RP-C203 is found at the end of this section to highlight the most prominent similarities and differences between the two design codes.

The implementation of the theory and rules for fatigue calculation in the generic bridge is then described in Section 4. This section discusses the geometries of the bridge, classification of details and how the bridge is modeled for finite element analysis. The latter focuses on finite element modeling choices of importance for fatigue calculation. The results from the fatigue assessment of the generic bridge using the finite element models are given in a Section 5. Here, the orthotropic deck, the trusses and a comparison study on safety implementation in NS-EN 1993-1-9 and DNVGL-RP-C203 are all presented, and later discussed in Section 6. Finally, the report concludes with some closing thoughts in Section 7 on the usefulness of the generic bridge as a tool for generating realistic data points, as well as limitations and suggestions for further work.

2 Theory

In this section, the theory governing fatigue calculation as implemented in this thesis is discussed. This elaboration of the subject is not extensive, and other aspects of fatigue analysis are only briefly mentioned. Information in this section is primarily based on the following works: Dowling, 2013, Lotsberg, 2016 and Nussbaumer et al., 2011.

2.1 Fatigue - a short introduction

When metal components are subjected to cyclic loading, the resulting stresses can lead to microscopic damage in the material - even when the stresses are well below the yield limit. Over time, the damage might accumulate and form a crack if continued cyclic loading is applied. Eventually, the component will fail. Damage accumulation and eventual failure is what is known as fatigue.

According to ASM International, there are three main factors that cause fatigue (Campbell, 2008, p. 243). They are listed as follows:

- A maximum (and sufficiently high) tensile stress

- A fluctuation in applied stress of a sufficient magnitude

- A high enough number of cycles accompanying the applied stress

Cyclic stress can be both a variation between maximum and minimum stress levels of constant value (called constant amplitude stressing (Dowling, 2013, p. 418)), or it could vary between different maximum and minimum stress levels. The main point is to be able to define the stress ranges, as they are the ones that are used in most fatigue life calculations. The stress range is always positive, because $\sigma_{max} \geq \sigma_{min}$, and is defined in Equation (1) below:

$$\Delta\sigma = \sigma_{max} - \sigma_{min} \tag{1}$$

The mean stress (denoted σ_m) is defined as:

$$\sigma_m = \frac{\sigma_{max} - \sigma_{min}}{2} \tag{2}$$

The mean stress may have an effect on a component's fatigue life, in cases where σ_m has a value other than zero. This effect is called the mean stress effect. In general, tensile mean stresses tend to have a bad influence on fatigue life. According to Dowling, "[...]

tensile mean stresses give shorter fatigue lives than for zero mean stress, and compressive mean stresses give longer lives" (Dowling, 2013, p. 443). The mean stress effect is not relevant for the case studied here, therefore it will not be discussed further.

A certain number of cycles associated with the applied stresses, is the third and final factor affecting fatigue life, according to ASM. This has to do with what is called High Cycle Fatigue (HCF) and Low Cycle Fatigue (LCF). The latter is characterized by strain levels well above yield, and therefore large stress ranges and repeated plastic deformations in each cycle. Large deformations which occur in the plastic domain are not preferable for in-service structures like bridges. The high stresses associated with LCF also give a relatively short lifespan, which makes LCF of little relevance when designing a bridge. An exception is for analyses regarding accidental limit states. HCF on the other hand, involves a higher number of cycles. The line between LCF and HCF is often drawn at $N = 10^4$ cycles (Nussbaumer et al., 2011, p. 9). It is normal to plot data from HCF-testing in a so-called Stress-Life curve (S-N curve from now on).

2.2 Crack formation and propagation

It is unusual that cracks of a critical size already exist in a component. A more common situation is a small defect initially present growing into a crack over time, where the application of cyclic stress can cause the growth from defect to crack. This crack will eventually reach a critical size and cause failure of the component. Welding of components is an example of such a situation, as welds are rarely flawless. There can be numerous defects on a microscopic level that may act as stress raisers, which again can lead to stress localization. A lot of the reason behind this lies in the process of welding itself, as such a process can cause tensile mean stresses to arise. As previously mentioned, such mean stresses tend to shorten the total fatigue life. Consequently, the fatigue strength of a welded joint will *not* correlate to the fatigue strength of the base material.

The crack growth process can be described as shown in Figure 1. Here, the relationship between cyclic crack growth rate (denoted da/dN, where this fraction describes the crack growth rate pr. cycle) and the stress intensity range (denoted ΔK) describes the crack propagation process along with test data for one material and a fitted curve. From this figure, three stages of crack growth behavior can be deduced:

1. Micro-crack initiation

2. Stable crack propagation

3. Final rupture

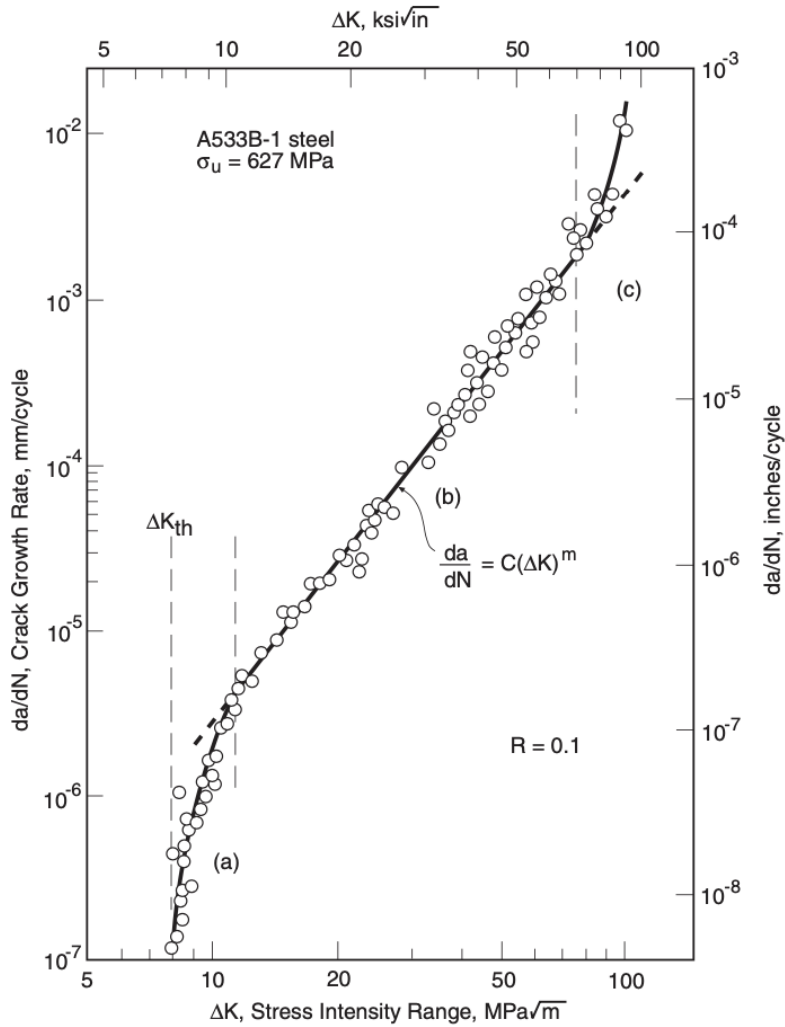The three stages are marked with (a), (b), and (c) in the figure below.

Figure 1: Fatigue crack growth rates over a range of stress intensities for a given material (Dowling, 2013, Figure 11.3, p. 565).

The figure is based on material testing where the thick, black line is curve fitted to the test data represented by dots. At the intermediate values of ΔK, this fitted line is as good as straight. Equation (3) below is known as the Paris law, and is used in application of fracture mechanics to calculate fatigue. It has the following equation:

$$\frac{da}{dN} = C(\Delta K)^m \tag{3}$$

Region (a), also known as the short crack growth propagation stage in Figure 1, is the stage where the crack initiates. The growth rate is low, but the curve is steep and it approaches what looks like a vertical asymptote denoted the fatigue crack growth threshold (denoted ΔK_{th}). This threshold value is, according to Dowling, "[...] interpreted as a lower limiting value of ΔK below which crack growth does not ordinarily occur"(Dowling, 2013, p. 565).

For small ΔK, crack propagation is hard to predict, because it depends on the micro structure and flow properties in the material (e.g particle size distribution). The crack will propagate until it reaches a microstructural barrier (a grain boundary for example), causing it to decelerate. The growth *may* even come to an arrest in this region. To guarantee that the crack will no longer propagate, grain refinement of some sort is a good remedy to increase fatigue strength of the component. This can be obtained by shot peening or surface rolling, resulting in flattening of the grains and more grain boundaries for the crack to overcome (Total Materia, 2010). Shot peening and other surface treatments are also great for inducing compressive surface residual stresses (or relieving tensile residual stresses) (Vinogradov, 2019b, slide 25).

As a consequence of either an increased applied load or continued crack growth, the stress intensity factor K will increase. Parts of the crystal lattice will glide along each other, changing the geometry of the material. In other words, dislocations will start moving within the material along so-called slip planes. This is what initiates stage 2 (or region (b) in Figure 1). The crack propagates in a stable manner here, and is represented by the linear relationship presented in Equation (3). This is also where the crack will spend a large part of its fatigue life (Total Materia, 2010).

In some materials, fatigue cracks will propagate more quickly along the grain boundaries than through the grains. In this case, using materials with elongated grains transverse to the direction of the crack growth direction might slow things down. Also, any treatment that will increase the yield strength of the material will be beneficial. This is because the stress level needed to produce slip will increase, and as a consequence, the resistance against fatigue will also increase (Vinogradov, 2019b, slide 25).

The last region in Figure 1 is region (c). As ΔK_{th} is the threshold value in region (a), K now approaches the other extremal value - namely the fracture toughness K_{IC}. At this point rapid and unstable crack growth occurs, and the crack size will eventually cause the component to fail (Total Materia, 2010). This happens when the critical crack length a_{cr} is exceeded, which is a parameter dependent upon the material's fracture toughness. The critical crack length may thus be increased by choosing a material with a high fracture toughness. Such materials are generally better suited for fatigue applications, as final rupture occurs by exceeding the magnitude of the fracture toughness (Vinogradov, 2019b, slide 25).

The region of a fracture surface formed during the crack propagation stage (region (b) in Figure 1) is characterized by the shape of the markings. Examples of such markings are beach marks and striations. Both markings indicate the position of the crack tip at some point in time. An example of what beach marks look like are shown in the area marked as *Fatigue* in Figure 2. The area denoted *Overload* in this figure is linked to the rapid and unstable crack growth in region (c) of Figure 1 and is usually rough in texture. The roughness of this area depends on the magnitude of the cyclic loading. For lower cyclic loads, the crack propagation phase lasts longer, and the area of the fracture corresponding to the fast rupture would be a lot smoother because the failure would be of a more ductile manner.
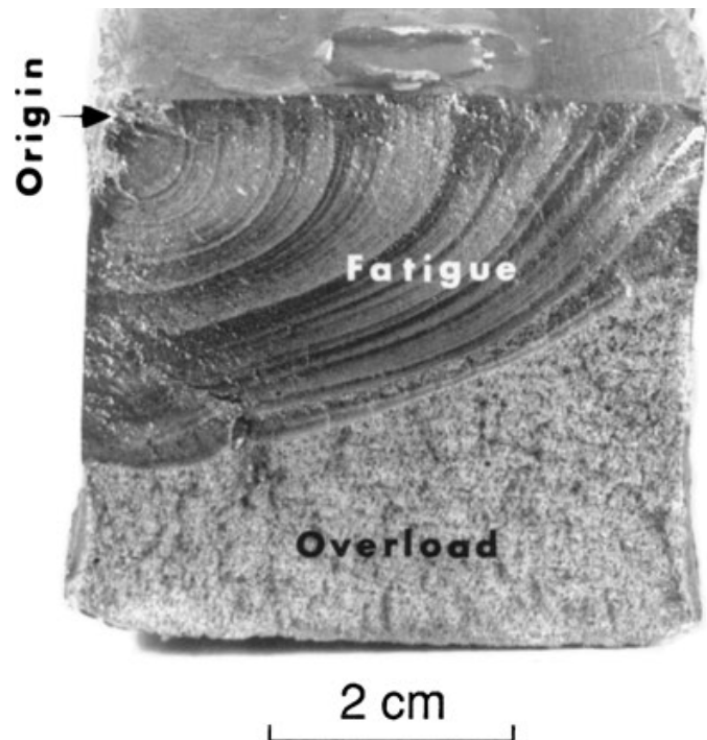
Figure 2: Fracture surface for fatigue and final fracture of a 18 Mn steel member (Dowling, 2013, Figure 9.21 (Photo courtesy of A. Madeyski, Westinghouse Science and Technology Ctr., Pittsburgh, PA.), p. 440).

The beach marks are of macroscopic dimension and may be observed with the unaided eye. They appear as concentric ridges that expand away from the crack initiation site, frequently in a circular or semicircular pattern (Callister, 2015, p. 311). The crack initiation site is shown as *Origin* in Figure 2 and it corresponds to region (a) in Figure 1. The beach marks indicate changes in the fracture surface as a consequence of the crack being delayed or accelerated. This may happen due to alternating stress levels or temperature, to name a few examples (Dowling, 2013, p. 441). Each beach mark band represents a period of time over which crack growth occurred.

Striations, on the other hand, are marks produced on the fracture surface that show the incremental growth of a crack. They are microscopic in size, and they are not guaranteed to be present. Striations mark the position of the crack tip at the time it was made, and each striation is the result of a single loading cycle. The striation width, being controlled by the dislocation activity at the crack tip, depends on, and increases with, the increasing stress range (Callister, 2015, p. 311).

The presence of beach marks and/or striations are used as an indication that a fatigue crack has been growing. Although both beach marks and striations are fatigue fracture surface features having similar appearances, they are nevertheless different, both in origin

7

and size. There may be literally thousands of striations within a single beach mark (Callister, 2015, p. 311).

2.3 S-N Curves

The basis for fatigue design in this thesis is S-N curves derived from component testing. The parameters of a function are curve fitted to test data for N number of cycles until failure for a stress range $\Delta\sigma$ in the S-N diagrams, commonly presented on a logarithmic scale. As there are significant scatter in test data used to create S-N curves, two standard-deviations are subtracted from the mean of the experimental data, which gives a 97.7% chance of survival (Lotsberg, 2016). This is illustrated in Figure 3 below.
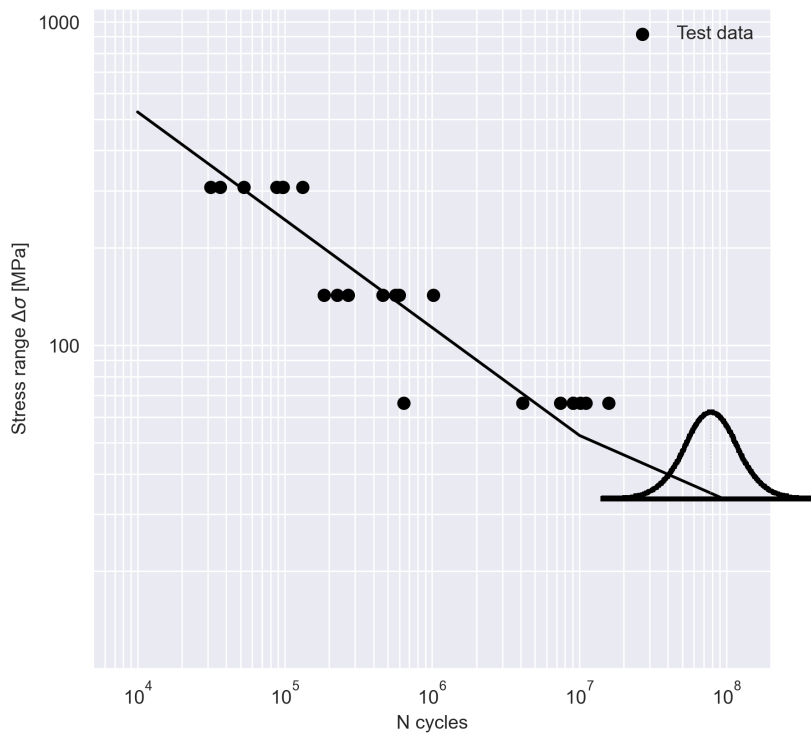
Figure 3: S-N curve generated from test data. Inspired by Figure 4.16 in Lotsberg, 2016, p. 159.

As fatigue properties are mainly a result from laboratory tests, it is useful to know about various factors that might cause scatter in the fatigue data. Some factors are controllable, while others are not - the statistical nature of damage itself being one of them. Such factors are called systematic factors, and will help the designer gain better understanding about the phenomenon. Variations in the sample-materials, internal defect sizes and imperfect control of test variables (such as specimen alignment and humidity) are some examples factors affecting fatigue life (Vinogradov, 2019c, slide 20-23).

Observe from Figure 3 that there is more scatter for high stress levels than there is for lower stress levels. This is because there is almost always microcracks present in a component at the beginning stages of a crack nucleation. If a higher stress level is applied in this initiation stage, stresses localize in these microcracks anyway and cause a rapid growth of the microcracks. As a result, the scatter tend to be low in these beginning stages.

If a low stress level was applied, factors such as the surface condition has to be included as a factor influencing the extent of scatter in fatigue data. Crack initiation is dependent on the condition of the surface - if it is rough, there might be some weak spots or other surface damage where the stresses can localize and eventually turn into a crack. The surface condition varies from specimen to specimen, and since it varies so much, it tends to create more scatter for lower stress levels (Schijve, 2004, p. 312).

2.4   Stress calculation for fatigue design

For fatigue design with the use of S-N curves, three approaches can be considered: the nominal stress approach, the hotspot stress approach and the notch stress approach. These three approaches are differentiated by how one calculates the stress ranges used to determine the number of cycles to failure. This is visualized in Figure 4, where the stress field in the detail is decomposed according to which part of the detail causes it.
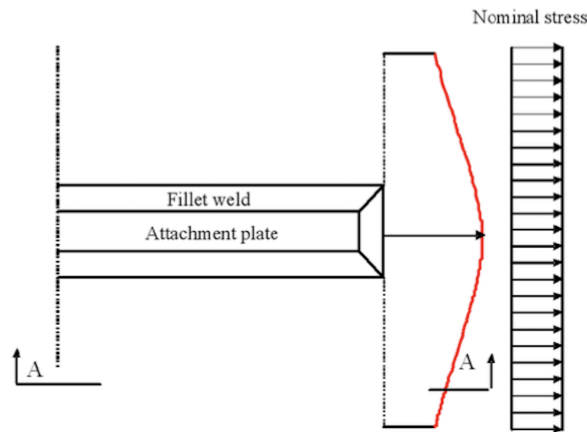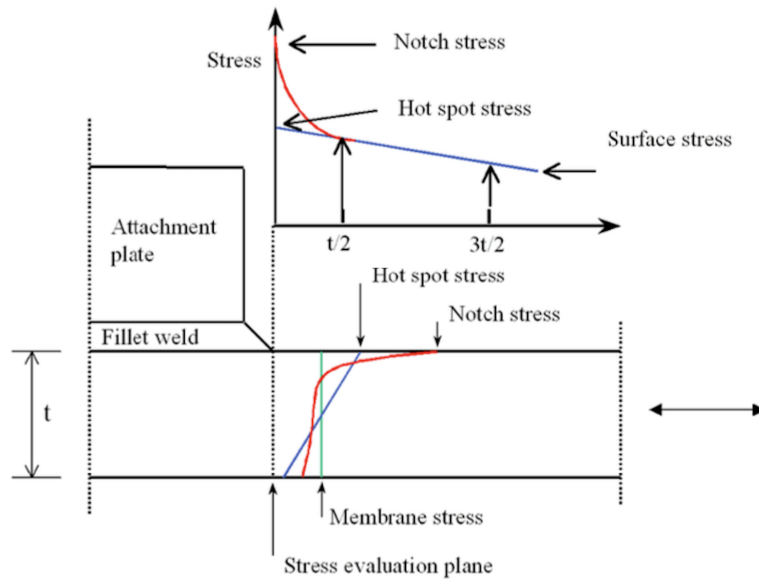
Figure 4: Nominal, hotspot and notch stress distribution in detail (DNV AS, 2019b, Figure 4-2, p. 84).

2.4.1 Nominal stress calculation

Excluding the attachment plate and the weld of the detail in Figure 4 results in a uniform stress field. This uniform stress field is denoted membrane stress in the Figure. This is the basis for the nominal stress approach, which considers stresses that can be determined by classical beam and plate theory (Nussbaumer et al., 2011, p. 96-97). Stress concentrations due to component geometry or the weld notch are not accounted for explicitly, but are instead included in the choice of S-N curves. As such, there is a wide range of S-N curves corresponding to the details considered for fatigue analysis with the nominal stress approach. Some stress raising effects are not included in the nominal S-N curves, and require the use of modified nominal stresses. Such stresses can be obtained by multiplying

nominal stresses with so-called Stress Concentration Factors (SCFs) from the literature (Nussbaumer et al., 2011, p. 106-107).

2.4.2 Hotspot stress calculation

The attachment plate in Figure 4 causes a linear stress distribution, denoted as hotspot stress. The hotspot method includes this linear stress distribution, but the non-linear effects of the weld notch is accounted for by the S-N curve in the same manner as for the nominal stress approach. Stresses at hotspots are determined by finite element analysis using shell or thin plate elements and the method requires extrapolation of stresses from integration points of the finite elements to the hotspot. This extrapolation is shown in Figure 5, where the intersection line is the intersection of two shell plates. Element size for the mesh at the detail is recommended for shell or thin plate elements to be between $t \cdot t$ and $2t \cdot 2t$ for a conservative result, where t is the element thickness (DNV AS, 2019b, p. 78). For a mesh with element size of $t \cdot t$, linear extrapolation of the hotspot stress can be used as in Figure 5. For other mesh sizes, a second order polynomial is recommended.
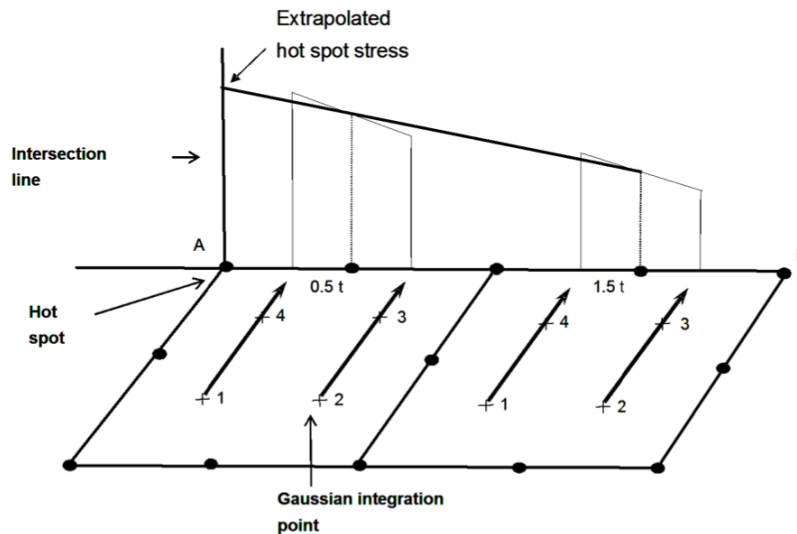
Figure 5: Stress extrapolation of hot spot stress (DNV AS, 2019b, Figure 4-3, p. 85).

2.4.3 Notch stress calculation

Including the effects of the weld notch in Figure 4 results in a non-linear stress distribution denoted as notch stress. The notch stress method requires more complex modelling of a detail, e.g. with solid elements and including the weld itself. This approach is not applied in this report, and will not be further elaborated.

11

2.4.4 Mesh calibration

It is recommended to calibrate element size and type against a known case when finite element analysis is used to calculate hotspot- and notch stresses for fatigue life calculations (Standard Norge, 2010b, NA.6.1). Lotsberg suggests calibration against the documented cases presented in Appendix D in DNVGL-RP-C203, where SCFs in plates are plotted for construction details, such as in Figure 6 (Lotsberg, 2016, p. 284). The SCF plot takes in dimensions of the detail, and returns a SCF. The calibration of the element is then verified by comparing the SCF from the element analysis with the SCF from the plot in the DNVGL-RP-C203 appendix.
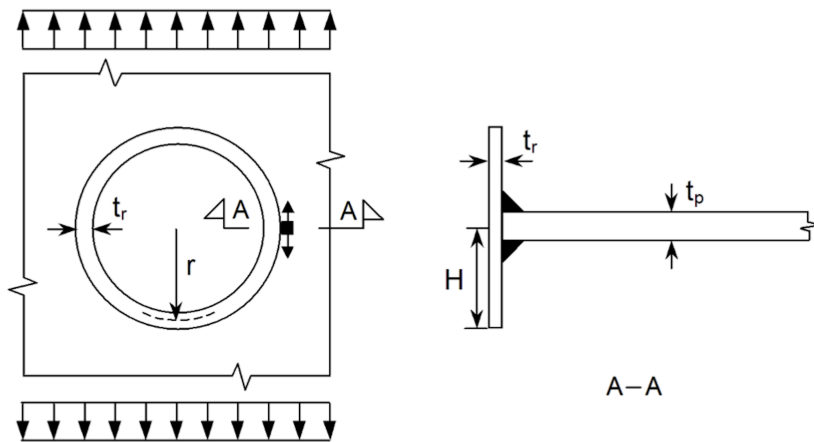

Figure 6: Plate with tubular insert (DNV AS, 2019b, Figure C-4, p. 178).

2.5 Damage calculation

Damage of a component can be calculated by what is known as the Palmgren-Miner rule for damage accumulation, with the assumption of linear cumulative damage (Lotsberg, 2016, p. 114). The rule is presented in Equation (4) below, and states that fatigue failure is to be expected as soon as the sum of the life fractions is greater than or equal to unity (Dowling, 2013, p. 468).

The rule considers that over the life of a component each stress range $\Delta\sigma_i$ occurs n_i times. A stress range is associated with N_i cycles until failure for the range. Thus, a partial damage for each stress range $\Delta\sigma_i$ can be calculated as n_i/N_i. The partial damage is also known as a life fraction, as it represents the percentage used of the total life.

For a continuous stress range distribution, the summation is replaced by an integral, as seen in the last part of Equation (4). The arguments of the Palmgren-Miner rule and the difference between a discrete and continuous stress range distribution is illustrated in Figure 7.

$$D = \frac{n_1}{N_1} + \frac{n_2}{N_2} + \frac{n_3}{N_3} + ... = \sum_{i=1}^{n_{tot}} \frac{n_i}{N_i} \approx \int \frac{dn}{N} \leq 1 \qquad (4)$$
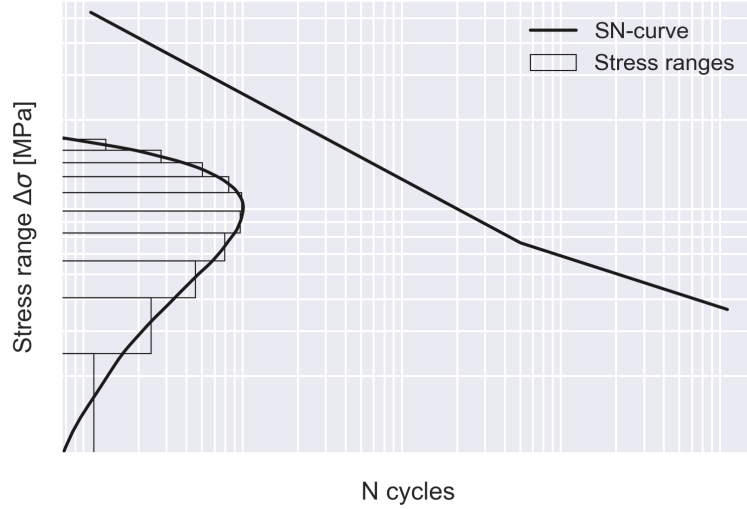

Figure 7: Damage calculation for discrete and continuous stress range distribution.

2.5.1 Limitations of the Palmgren-Miner rule

The Palmgren-Miner rule is not a flawless rule, however, it is still the main fatigue damage accumulation rule in the field. There are some important limitations that needs to be addressed, where the main flaw is the core assumption of it: the linearity of damage accumulation, which is related to when the different cycles are applied. Linear damage simply means that damage calculated from one life fraction is added on top of another life fraction and so on, as opposed to an exponential model, where more damage added to a already weakened part means that it becomes significantly more weak. As damage is not a linear phenomenon, the consequences of this is accounted for in practical design by the use of safety factors (Nussbaumer et al., 2011, p. 14).

The second limitation worth mentioning is that the rule does not consider sequence effects. Such effects might have a say on the fatigue life, depending on whether low or high stress amplitudes occur first in the loading history. Sometimes, cycles with low stress levels followed by an abrupt change to high load levels can cause more damage before failure than the Palmgren-Miner rule can predict. If a high stress level is followed by a low stress level, the damage may be less. This is because the abrupt change from high loading to low loading may cause compressive residual stresses (Dewesoft, 2021, slide 8). Already mentioned in Section 2.1, compressive stresses are considered more favorable than tensile stresses when it comes to fatigue, as they can slow down the crack growth. Sequence

effects are definitely observed in many cases in real life, which is why not including them in the Palmgren-Miner is a huge problem.

The third important limitation is that the Palmgren-Miner rule states that the damage accumulation is independent of stress level. According to Lotsberg, Miner himself did not include stress ranges below the fatigue limit, because he believed that these cycles did not contribute to damage. But for some structures, e.g. marine structures, there are a significant number of cycles below the fatigue limit that occur. As previously discussed and shown in Figure (1), cycles do not contribute to crack growth *if* the cracks are small enough (meaning that the stress intensity factor is below the threshold value K_{th}). However, if the crack is large enough, more stress cycles will contribute to crack growth (Lotsberg, 2016, p. 114-115).

The use of the Palmgren-Miner rule is also restricted to damage calculation resulting from one loading process. Adding together the damage from for example traffic and environmental loading is non-conservative (DNV AS, 2019b, appendix F.3)

2.5.2 Cycle counting

Structures are realistically exposed to varying loads, resulting in highly irregular stress-time histories. As a consequence of this, it might be challenging to define and isolate even one cycle for later use in the Palmgren-Miner summation rule. For practical design purposes, the stress-time history is simplified to a manageable format where the characteristics of the loading is retained.

There are a number of different ways to handle such irregular stress histories. Two of these methods are presented in NS-EN 1993-1-9 - namely the reservoir cycle counting method and the rainflow cycle counting method. According to Dowling, there is an consensus that the latter method is the better of the two (Dowling, 2013, p. 471). The rainflow cycle counting method has been applied in this thesis, and other counting methods will not be discussed further.

Early cycle counting methods were based on peaks, level crossings or simple ranges. In 1968, Matsuishi and Endo proposed the rainflow cycle counting method. Today, this method is standardized as one of many cycle counting methods in ASTM E1049:85(2017): Standard Practices for Cycle Counting in Fatigue Analysis. The reader is referred to this document for detailed instructions on how to use the rainflow cycle counting method.

In short, the rainflow cycle counting method works as follows: In an irregular stress-time history, there are numerous peaks and valleys. These are points where the loading changes direction. The stress ranges are measured between these points. What the rainflow cycle counting method does, is to identify the peaks and valleys. This is because only the maximum and the minimum values within a cycle matter when calculating damage. The cycle with the largest stress range value will therefore be found between the highest peak and the lowest valley. The rest of the cycles will be so-called half-cycles of different stress-

range magnitudes. Some of the ranges can be of such a small magnitude that they can be neglected. Filtering out the cycles with small stress-range such that only the cycles contributing the most to damage accumulation are included is beneficial with respect to calculation time (Hiatt, 2019). In the end, half-cycles with the same stress-range magnitude (but of *opposite* signs) are paired together to count the number of complete cycles. Typically, there will be some half-cycles left that cannot be paired up (Vinogradov, 2019a).

In this thesis, cycle counting is performed in Python, for which the rainflow cycle counting algorithm described in ASTM E1049:85(2017) is available as its own module online (Janiszewski, 2020).

2.6 Finite Element Method

In order to solve complex physical problems, a numerical method is applied. One such method is the Finite Element Method (FEM). It consists of mathematical modeling of the physical problem, discretization of the mathematical model and numerical solving of the discretized problem. In this report the software Abaqus FEA is used, which performs all these tasks.

2.6.1 Modeling

For a structural problem, an idealized and simplified version of reality is needed when it comes to geometry, material properties, loads and boundary conditions. These simplifications introduce a discrepancy between simulation and reality, and must be chosen to minimize what is called the modeling error.

2.6.2 Discretization

The finite element method discretizes the problem by subdividing the mathematical model into a number of finite elements constituting the mesh. This takes a continuous field problem to a piecewise continuous problem. How the finite elements approximate the field and the resolution of the mesh determines how closely the discretized model represents the mathematical model. The error introduced by discretization is called the discretization error (Cook et al., 2002, p. 4).

Factors on how the finite elements approximate the mathematical model includes the shape, nodes, degrees of freedom and integration points. Shape, nodes and degrees of freedom relates to which shapes can be represented geometrically, and the deformations which can be recreated. Integration points determine where the numerical integration of the field problem is sampled. They can be positioned in order to save computational effort, or to avoid numerical issues (Bell, 2014, p. 150).

2.6.3   Numerical Solving

The discretized problem can be solved numerically, either explicitly or implicitly. Where explicit methods find the displacement values based on equilibrium conditions at the previous time step, implicit methods find the displacement values based on equilibrium conditions at the current time step. This necessitates equation solving for implicit methods, which is computationally costly. Implicit methods are generally more stable, and some schemes are stable for any step size. This allows for fewer and larger steps in total, compensating for the cost per step calculated. Explicit methods are cheaply computed with no equation solving, but are bounded in their step size as the solving schemes are only conditionally stable. Explicit solving therefore requires many but cheap steps ((Cook et al., 2002, p. 150-155); (Hellevik, 2020)). Both methods are available in Abaqus, with implicit methods called Abaqus/Standard, and explicit methods called Abaqus Explicit (Simulia, 2020).

3 Standards and other regulations

There are many standards related to the topic of fatigue design, giving recommendations and guidelines for fatigue design in structures. In this thesis, a combination of three Eurocodes and one handbook from the Norwegian Public Roads Administration have been compared to the procedures and rules for fatigue design given in DNVGL-RP-C203. The standards studied are presented in Table 1 below.

Table 1: Relevant standards for this thesis.

Standard	Name
Håndbok N400	Bruprosjektering*
NS-EN 1993-2	Eurocode 3: Design of steel structures - Part 2: Steel bridges
NS-EN 1991-2	Eurocode 1: Actions on structures - Part 2: Traffic loads on bridges
NS-EN 1993-1-9	Eurocode 3: Design of steel structures - Part 1-9: Fatigue
DNVGL-RP-C203	Fatigue design of offshore steel structures (Recommended Practice)

* Norwegian Public Roads Administration handbook for design of bridges. Only available in Norwegian.

N400 describes in general how to design bridges and other large structures, as well as stating how long the design life of the structure should be (Statens Vegvesen, 2015). It also explains which Eurocodes to turn to when designing for different limit states, and when they come into play. The handbook is not to be considered a standard - but it can be used as a National Annex (NA), like those in the Eurocodes.

Most of what is described in N400 is recited in NS-EN 1993-2. Appendix C of the latter has been important for this thesis, as it provides a thorough description of orthotropic decks and its components, how to design the components of the orthotropic deck as well as which factors may cause fatigue in them (Standard Norge, 2009, p. 68-77).

Together, N400 and NS-EN 1993-2 form a foundation for bridge design, as they describe what to take into account for the different limit states. For the fatigue limit state, they both refer to NS-EN 1991-2, which is the Eurocode that covers traffic loads on bridges. Such loads are variable loads that produce stress spectra in details which may cause fatigue cracks to initiate in specific locations in the components of the orthotropic deck. These stress spectra depend on factors such as the geometry of the vehicle, axle loads, the composition of traffic and the dynamic effects of it (Standard Norge, 2010a, 4.6.1(1)). Information from this Eurocode is then linked to NS-EN 1993-1-9 for guidance on performing the fatigue assessment.

NS-EN 1993-1-9 gives the overall guidelines on how to perform the fatigue analysis for load-bearing steel structures. It is also valid for all types of steel subject to HCF. The standards in the Eurocode-series are intended to complete each other, and they should

not be used in combination with other standards outside the series. But - NS-EN 1993-1-9 is not valid for all dimensions and is sometimes unclear on how to proceed further. This is where DNVGL-RP-C203 comes in, which is a Recommended Practice valid for steel components in offshore steel structures subject to fatigue. It is based on data from fatigue tests as well as fracture mechanics, and is valid for steel components in the HCF-region. There are many documents referring to this standard when there is lack of available information, NORSOK N-004 being one of them (Aardal, 2012, p. 6).

3.1   NS-EN 1991-2

To perform a fatigue assessment of a road bridge, realistic loads are required. NS-EN 1991-2 supplies five different Fatigue Load Models (FLM), with differing complexity and areas of application. They all specify the loads as trucks traversing the bridge. Which one to choose depends on many factors, summarized in the following bullet point list below:

- If the goal is to determine the maximum and minimum stresses resulting from the loads on the bridge, FLM1, 2 or 3 may be an appropriate choice. For determination of the stress range spectra, FLM4 or 5 may be considered

- FLM1 and 2 are to be used when there is a need to check whether the fatigue life is unlimited for a load history with a constant stress amplitude. FLM3, 4, and 5 should not be used to check for infinite life.

- FLM3, 4 and 5 are intended to be used in combination with the fatigue strength curves given in Eurocodes NS-EN 1992 through NS-EN 1999, depending on the material in question

- FLM3 is a simplified method that can be used for direct verification of a designed structure. This load model makes use of a material-dependent adjustment factor, defined by λ_e, that takes the influence from the traffic volume and some dimensions of the structure into account

- FLM4 gives more accurate results than FLM3, and for that reason, it requires a more elaborate analysis

- The most general load model is FLM5, and is based on already recorded traffic data

The Norwegian National Annex in NS-EN 1991-2 gives some more notes on how to decide which FLM to choose. It clearly states that FLM2 is not to be used in Norway, and that FLM1 is used as a check to decide whether there is a need for a more accurate fatigue assessment. The Norwegian National Annex specifies that unless a thorough fatigue analysis is designated for the project, a modified version of FLM3 is to be used (Standard Norge, 2010a, NA.4.6.1). As comparison of NS-EN 1993-1-9 and DNVGL-RP-C203 is the goal of this thesis, the detailed FLM4 was suggested by supervisor Nils Arne Rakstad.

FLM4 consists of a set of five standard lorries where each of them cross the bridge individually. The number of lorries crossing the bridge during the entire design life is chosen based on a traffic category and a traffic type, which are selected from two separate tables - namely Table 4.5(n) and Table 4.7 in NS-EN 1991-2. Table 4.5(n) indicates the number of heavy vehicles pr. slow lane (a lane used mostly by lorries (Standard Norge, 2010a, 4.6.1(3))), based on a yearly estimation. This estimated number of lorries is denoted N_{obs}. In this thesis, traffic category 4 and $N_{obs} = 50000$ were chosen.

Table 4.5(n) alone does not provide enough information to perform the fatigue assessment. A further characterization of the traffic is therefore needed. Table 4.7 gives this information in the form of percentages of lorries present on the bridge for a given traffic type. These percentages multiplied with N_{obs} and the design life in years provides the estimated number of each standard lorry present on the bridge. The traffic type was chosen as *local*.

The percentages of each lorry defined in table 4.7 in NS-EN 1991-2 are linked to $N_{obs} = 50000$. From this, the number of cycles caused by each individual lorry during the design life of the bridge can be calculated. In this thesis, this will be represented by n_i, and their values are presented in Table 2 below.

Table 2: Information gathered from Table 4.5(n) and Table 4.7 in NS-EN 1991-2.

Vehicle	Percentage	n_i during one year	n_i in 100 years
1	80 %	40 000	4×10^6
2	5 %	2 500	0.25×10^6
3	5 %	2 500	0.25×10^6
4	5 %	2 500	0.25×10^6
5	5 %	2 500	0.25×10^6
Sum	100 %	50 000	5×10^6

Applying FLM4 on a bridge gives realistic loads in a structure assessed for fatigue. A stress spectrum can be extracted such that a Palmgren-Miner summation can be performed in the details where a fatigue crack *could* initiate. Such details are to be classified according to NS-EN 1993-1-9 (and in this case, DNVGL-RP-C203 as well).

3.2   NS-EN 1993-1-9

NS-EN 1993-1-9 gives detailed guidance on how to perform a fatigue assessment of different types of steel components. The methods are based on data from elaborate fatigue testing, with both geometrical and structural imperfections of the specimen included. The test data form a basis for the detail categories and their associated S-N curves. NS-EN 1993-1-9 presents ten of these detail categories, numbered between 36 and 160. The category number indicates the constant amplitude stress range at 2 million cycles, given in MPa. The corresponding S-N curve is then constructed based on test data for specimens

of standard geometry tested at different stress levels, as discussed in Section 2.3. Each category number corresponds to their own S-N curve.

Some detail categories also have an asterisk, meaning that these details are "classified one detail category lower than their fatigue strength at 2 million cycles would require from them" (Standard Norge, 2010b, 7.1(3) NOTE 3). What this means is that they would provide non-conservative results if they were classified as if the asterisk was neglected. This applies to detail categories 36^*, 45^* and 56^*.

The S-N curves presented in this Eurocode are all offset from each other, and they follow Equation (5) given below:

$$\log N = \log a - m \log \Delta \sigma \tag{5}$$

where

- N: (Assumed) Cycles to failure for the given stress range

- $\log a$: Intercept with $\log N$-axis

- m: Negative slope of S-N curve, works as a relation between stress range and fatigue life

- $\Delta \sigma$: Stress range

To choose an appropriate curve, the Eurocode refers to table 8.1 through table 8.10 for categorization of the details. From these tables, the designer must choose the correct detail for the situation, and then choose the corresponding S-N curve. The curves are presented in Figure 8 below.
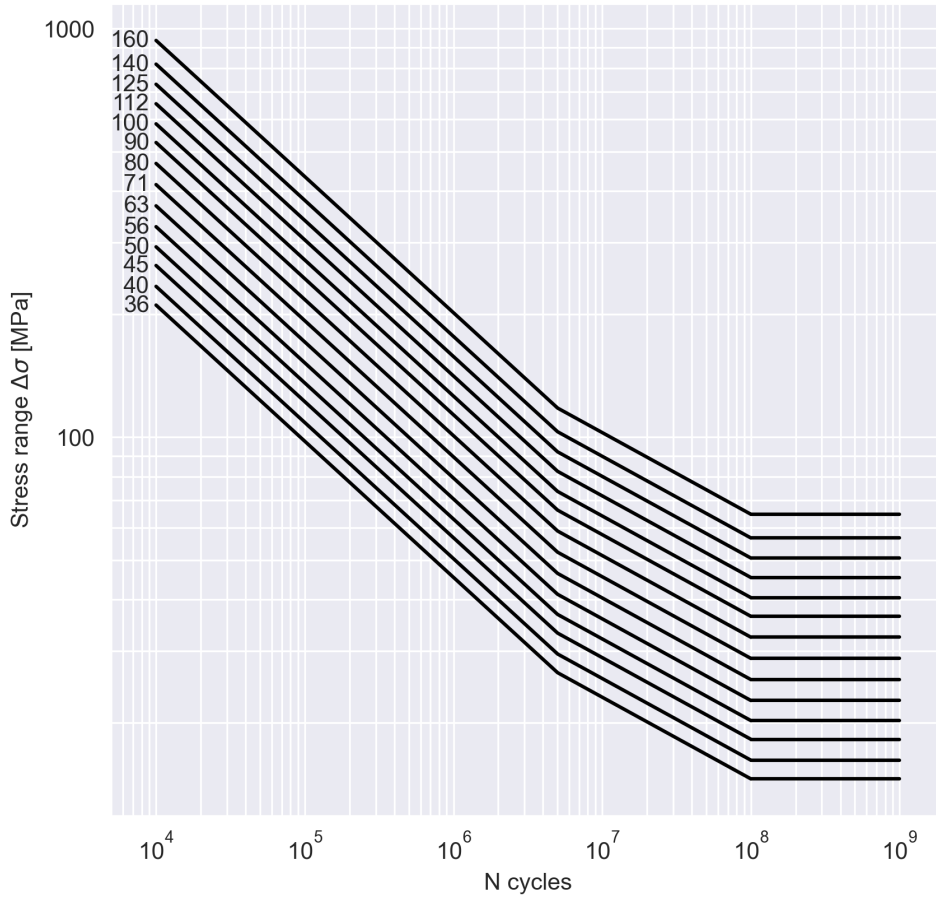
Figure 8: S-N curves as presented in Figure 7.3 in NS-EN 1993-1-9.

All S-N curves have a negative slope $m = 3$ up to $N = 5 \times 10^6$, which is where the constant amplitude fatigue limit $\Delta\sigma_D$ (CAFL) is. Constant amplitude loading is a cyclic loading of both constant amplitude and mean load. Following this, the CAFL is then a stress level marking that fatigue failure will not happen below this limit *for constant amplitude loading*. If the stress range amplitude varies, they will contribute to the total damage, even if they are below the CAFL (Larsen, 2010, p. 492). Note that not every detail category follows this form of the S-N curves. Details in table 8.7 (which covers lattice girder node joints) has one constant slope of $m = 5$.

From $N = 5 \times 10^6$ to $N = 10^8$ in Figure 8, the slope changes from $m = 3$ to $m = 5$. From $N = 10^8$ cycles, the curve is a horizontal line. This point is known as the cut-off limit, denoted by $\Delta\sigma_L$. The same principle for the CAFL ($\Delta\sigma_D$) applies to the cut-off limit at $N \geq 10^8$ cycles as well. Stress ranges below this stress limit can be repeated an infinite number of times, and they do not contribute to the fatigue damage in total.

At which stress range the CAFL and the cut-off limit are defined, depends on the choice of S-N curve. Both of them have to be calculated, and are found as follows:

CAFL:

$$\Delta\sigma_D = \left(\frac{2}{5}\right)^{1/3} \approx 0.737\Delta\sigma_C \tag{6}$$

Cut-off limit:

$$\Delta\sigma_L = \left(\frac{5}{100}\right)^{1/5} \approx 0.549\Delta\sigma_D \tag{7}$$

where $\Delta\sigma_C$ is the same as the detail category number. It is named after the stress range value of the S-N curve at $N_C = 2 \times 10^6$ load cycles.

NS-EN 1993-1-9 gives two methods to implement safety in fatigue life calculation. These are the damage tolerant method and the safe life method. The damage tolerant method should provide an acceptable level of reliability ensuring that the structure performs satisfactorily for its entire design life (Standard Norge, 2010b, p. 10). The reliability of the structure is taken care of by choosing details, materials and an adequate stress level that can ensure that the cracks will grow slowly, such that the critical crack length (denoted a_{cr}) at which point failure occurs, is of a large size. To be able to ensure this however, there must be an inspection and maintenance regime provided, such that cracks can be detected before the critical crack length is reached. For the safe life method, there should not be a need for regular inspection of the structure. According to Larsen, this method should be used in cases where the formation of local cracks in a component can lead to a sudden collapse of the structure. Which method to use for different purposes can be specified by the standard. It is recommended that the safe life method is utilized when designing bridges (Larsen, 2010, p. 489-490).

An acceptable reliability level corresponding to the chosen method is achieved by adjusting the so-called partial factor for fatigue strength γ_{Mf} (Standard Norge, 2010b, 3(3)). The value of this partial factor depends on the safety method, but also the consequence of an eventual failure of the structure. The values of γ_{Mf} in table 3 presented below are as given in the Norwegian National Annex NA.3.1 in NS-EN 1993-1-9.

Table 3: Partial factors for fatigue design according to NS-EN 1993-1-9, Norwegian National Annex (Standard Norge, 2010b, tab. NA.3.1).

Assessment method	Consequence of failure	
	Low consequence	High consequence
Damage tolerant	1.0	1.15
Safe life	1.35	2.0

When using damage accumulation, NS-EN 1993-1-9 demands that the total damage is less than unity, and that the total number of cycles N_i for a stress range $\Delta\sigma_i$ is adjusted

for the partial factor γ_{Mf} (Standard Norge, 2010b, App. A.5). Visually, this can be seen as lowering the S-N curve by a factor of γ_{Mf}, illustrated for NS-EN 1993-1-9 S-N curve 90 in Figure 9.
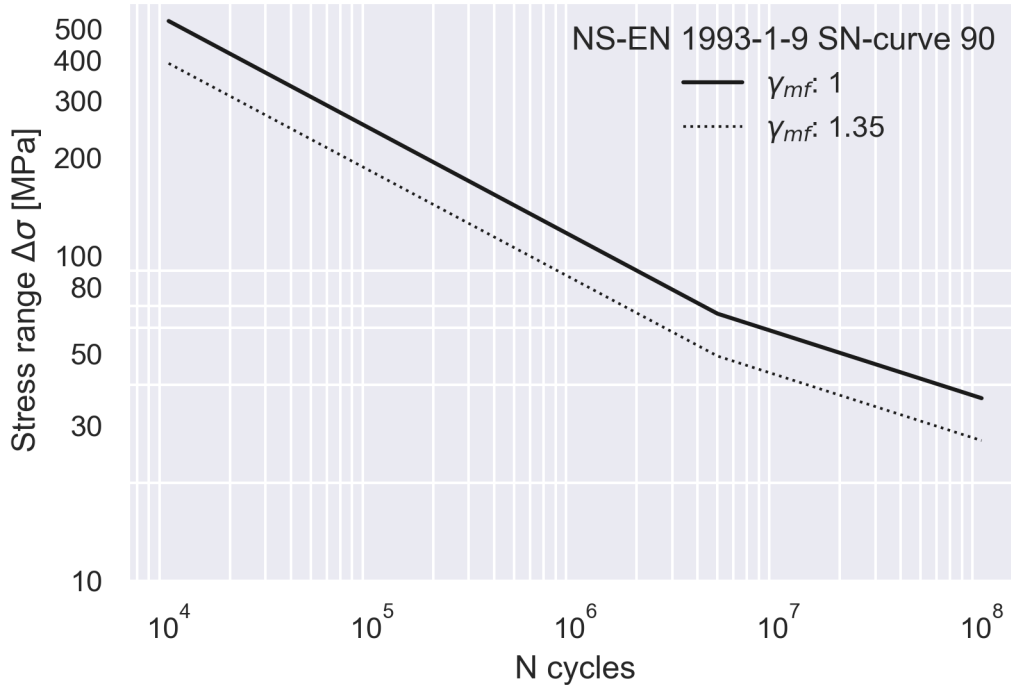

Figure 9: Adjustment of S-N curve by partial factor in damage calculation.

For the safe life method, the value of the partial factor γ_{Mf} can be either 1.35 or 2.0, as presented in Table 3. It is important to choose the correct value, as it will affect the life calculations drastically if chosen wrong. In this thesis, $\gamma_{Mf} = 1.35$, following the table notes from table NA.3.1 in the National Annex of NS-EN 1993-1-9.

3.3 DNVGL-RP-C203

DNVGL-RP-C203 is a recommended practice covering fatigue design of offshore steel structures. The standard is based on S-N data, depending on the environment the detail is in in. Furthermore, detailed procedures for performing fatigue assessment by finite element modelling is given. The standard also includes in its appendices a rich collection of stress concentration factors (SCFs), which are especially relevant for the trusses in the generic bridge in this thesis.

DNVGL-RP-C203 sorts the details into ten detail categories, denoted by a combination of letters and numbers, e.g. B1, C, and D, which are shown in Figure 10. Similar to the NS-EN 1993-1-9, the detail category corresponds to a given S-N curve, where the B1-curve is the least strict curve, and the W3-curve is the most strict curve in terms of

fatigue resistance. The D-curve is found in the middle and acts a hotspot S-N curve. This curve takes weld notch effects into account, but has no inherent stress concentrations due to the geometry of the detail considered. Because of these properties, it also used as a reference curve (Lotsberg, 2016, p. 125).

As mentioned, DNVGL-RP-C203 presents different S-N curve values for the detail categories based on the environment they are in. Reflecting the nature of a standard intended for offshore structures, the different environment classes are based on corrosiveness related to exposure to seawater. In this thesis, the air environment detail classes have been chosen, as this was deemed to best represent the environment NS-EN 1993-1-9 classes are intended for. DNVGL-RP-C203 has its own detail category for tubular joints, namely the T-category, which is also differentiated by environments.
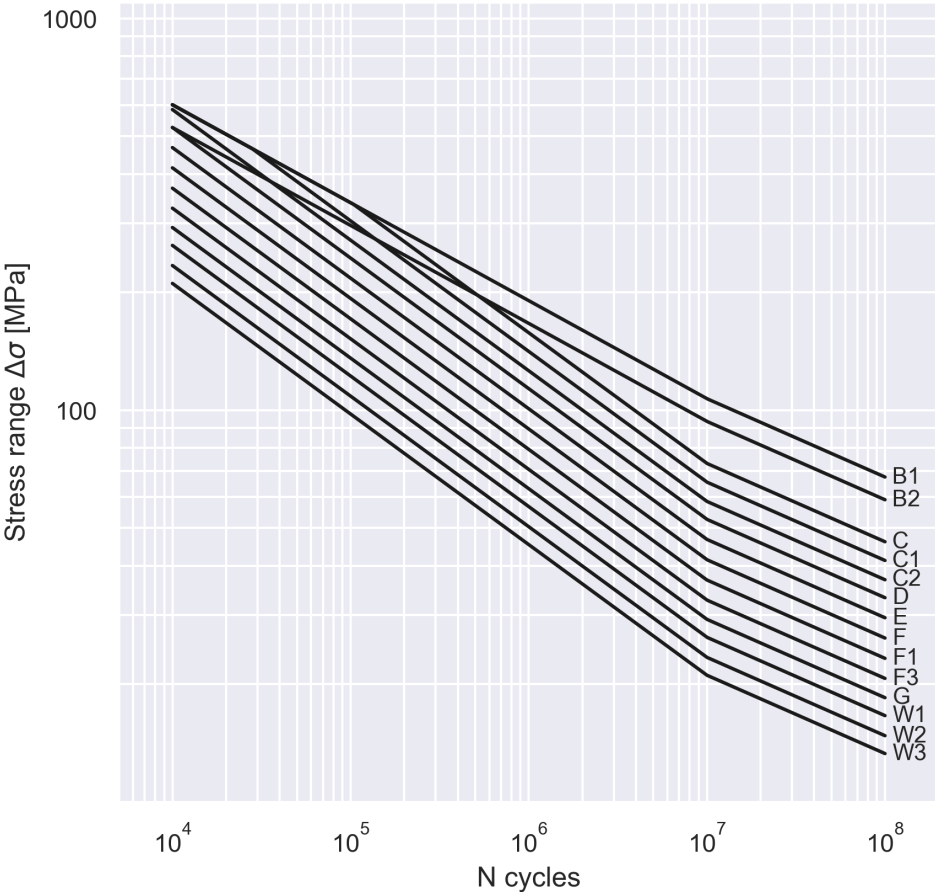

Figure 10: S-N curves in air as presented in Figure 2-8 in DNVGL-RP-C203.

Cut-off limits are not shown specifically in the S-N curves in DNVGL-RP-C203. This means that the curves are only presented as two-sloped. Change of slope occurs at $N = 10^7$ cycles. What would have been the cut-off limit in DNVGL-RP-C203 is shown at $N = 10^8$ cycles, if it is assumed to cut-off at the end of the N-axis. Based on these guidelines, the basic design S-N curve is given as follows:

$$\log N = \log \bar{a} - m \log \left(\Delta\sigma \left(\frac{t}{t_{ref}} \right)^k \right) \tag{8}$$

where

- N: (Assumed) Cycles to failure for the given stress range

- $\log \bar{a}$: Intercept with $\log N$-axis

- $m = $ Negative slope of curve

- $\Delta\sigma$: Stress range

- t: The thickness through which a crack will probably grow

- t_{ref}: Reference thickness for welded connections

- k: Thickness exponent

For some geometries, the details deviate from the assigned S-N curves. The reference thickness is such a geometry-dependent variable, which DNVGL-RP-C203 sets at 25 mm for welded connections in plated structures, and 16 mm for tubular joints. DNVGL-RP-C203 corrects for this by lowering the curves with the term $(t/t_{ref})^k$ in Equation 8. For thickness values t below t_{ref}, this term is ignored.

Safety in fatigue calculations in DNVGL-RP-C203 is introduced with Design Fatigue Factors (DFFs). This safety is introduced after Palmgren-Miner damage calculation by requiring that the accumulated damage over the service life is not less than unity, but less than a usage factor $\eta = 1/DFF$ (DNV AS, 2019b, p. 20). DNVGL-RP-C203 refers to DNVGL-OS-C101 for the choice of DFFs. Shown in Table 4, which DFF to apply is determined based the ease and interval of inspections. A DFF of 3 somewhat resembles the safe life method in NS-EN 1993-1-9, as a DFF of 3 is applied to details which are not planned to be inspected. Though DFFs are specified for DNVGL-RP-C203, Specialist Engineer and Senior Vice President at DNV Inge Lotsberg has confirmed by e-mail that one can apply the partial factors from NS-EN 1993-1-9 for fatigue calculation with DNVGL-RP-C203. The reason is that the definition of safety is similar for the S-N curves in both standards (personal communication, 8 March 2021). This is the default for analyses in the report, with a separate study investigating the relationship between partial factors and DFFs.

Table 4: Design fatigue factors for fatigue design according to DNVGL-RP-C203 (DNV AS, 2019a, Table 1, p. 58).

Structural element	DFF related to survey cycle	
	5-year inspection interval, carried out in dry dock	5-year inspection interval, carried out afloat
External structure, accessible for regular inspection and repair in dry and clean conditions	1	1
External structure, accessible for inspection but not accessible for repair in dry and clean conditions	1	$2^{1)2)}$
Internal structure, accessible and not welded directly to the submerged shell plate	1	1
Internal structure, accessible and welded directly to the submerged shell plate	1	2
Non-accessible areas, not planned to be accessible for inspection and repairs during operation	3	3

[1] For units that are planned to be inspected afloat at a sheltered location:
- DFF of 1 from 1 m above lowest inspection waterline and upwards.
- DFF of 2 from 1 m above the lowest inspection waterline and downwards.

[2] For units intended for prolonged stay at location:
- DFF of 1 above the splash zone.
- DFF of 2 below the splash zone.
- DFF of 3 in the splash zone.

Splash zone is the area that not is accessible, due to typically waves and current. The splash zone shall be defined for the unit, as relevant.

3.4 Comparison of NS-EN 1993-1-9 and DNVGL-RP-C203

As NS-EN 1993-1-9 and DNVGL-RP-C203 are two different standards covering fatigue for onshore and offshore structures, there are bound to be some differences between the two of them. But - there are also some similarities. A general comparison of the two documents will be presented in the following subsections.

3.4.1 Detail categories

The detail categories assigning S-N curves for fatigue calculations in NS-EN 1993-1-9 have counterparts in DNVGL-RP-C203, as presented in Table 5 below (DNV AS, 2019b, p. 237). The relationship for DNVGL-RP-C203 curves B1, B2, C1 and C2 is only approximate with their NS-EN 1993-1-9 counterpart. The reason is that these DNVGL-RP-C203 curves have a slope of $m = 4$ and not $m = 3$ as most other curves for lower load cycle ranges. Corresponding NS-EN 1993-1-9 and DNVGL-RP-C203 S-N curves are similar for less than 5×10^6 load cycles, as the standards changes the slope m of the curves at different numbers of load cycles N. This is visualized in Figure 11 for curve pairs D/90 and F/71, which are the curves most relevant for this report. Although the stress ratio at any number of load cycles N is less than 1.1, this is significant. E.g. for curves F and 71, the difference for a stress range of 30 MPa is 30 000 000 cycles. Remaining pairs of S-N curves are plotted in the Appendix A.1.

Table 5: Comparison between detail categories in DNVGL-RP-C203 and NS-EN 1993-1-9 3.

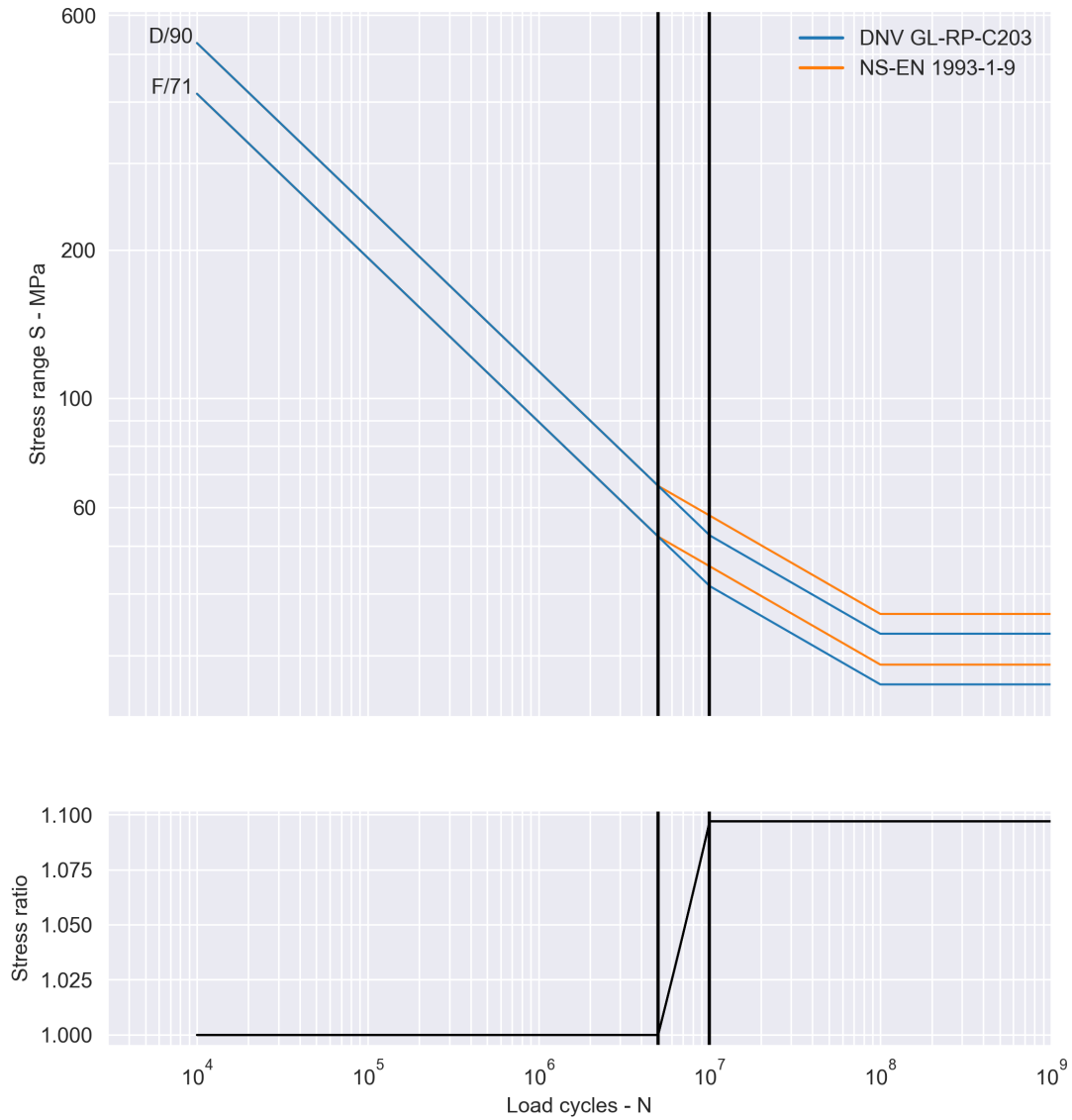| NS-EN 1993-1-9	DNVGL-RP-C203
160	B1
140	B2
125	C
112	C1
100	C2
90	D
80	E
71	F
63	F1
56	F3
50	G
45	W1
40	W2
36	W3
-	T

Figure 11: S-N curve pairs D/90 and F/71 for DNVGL-RP-C203 and NS-EN 1993-1-9.

For hotspot analysis, NS-EN 1993-1-9 and DNVGL-RP-C203 differ, with DNVGL-RP-C203 being more detailed. DNVGL-RP-C203 designates its S-N curve D for hotspot fatigue analysis, with exceptions for some joints. NS-EN 1993-1-9 Annex B prescribes hotspot analysis S-N curves based on weld type. The welds covered in this annex are however not extensive, and all details listed are given S-N curves either equal to S-N curve D from DNVGL-RP-C203, or less conservative. Since the details mentioned for

hotspot analysis with NS-EN 1993-1-9 are assigned S-N curves equal or less conservative than DNVGL-RP-C203, the authors have decided to use the S-N curve pair D/90 for all hotspot analyses.

3.4.2   Tubular joints

Fatigue calculation of tubular joints for NS-EN 1993-1-9 and DNVGL-RP-C203 is based on their own S-N curves, as already discussed in Sections 3.2 and 3.3. NS-EN 1993-1-9 does not have its own S-N curve for tubular joints, but the same categorization system is used as for the details in the deck, with one important exception - that the curves are to be implemented with a *constant* slope $m = 5$. For tubular joints found in the generic bridge, curves 45 and 90 are used. The choice of tubular joint S-N curve for NS-EN 1993-1-9 is based on the thickness ratio of chords and braces, denoted t_0/t_i. For a thickness ratio equal to 1 curve 45 is used, and for a ratio equal to 2 or more, curve 90 is used. For intermediate values a linearly interpolated curve between 45 and 90 is applied (Standard Norge, 2010b, p. 27). In DNVGL-RP-C203, the curve used is the T-curve. The curves mentioned are shown in Figure 12.
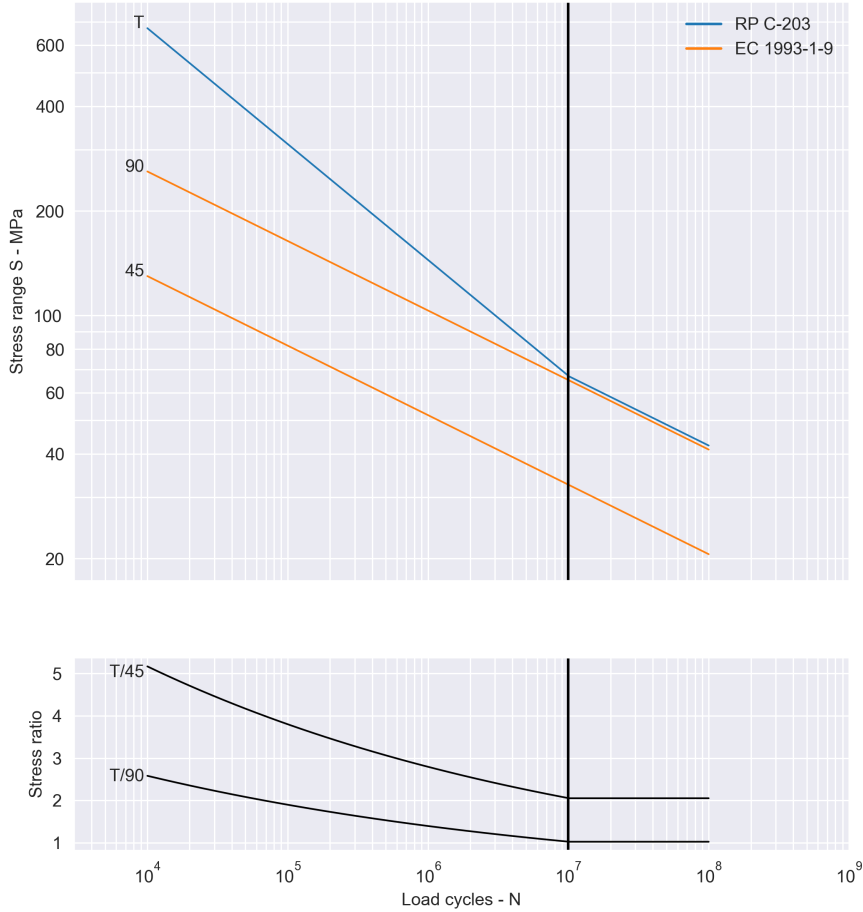
Figure 12: S-N curves for tubular joints.

Due to the single slope of NS-EN 1993-1-9 tubular joint S-N curves, the difference of S-N curves for NS-EN 1993-1-9 and DNVGL-RP-C203 is greatest for large stress ranges. The stress ratio plot of Figure 12 reveals how drastic this difference is. At $N = 10^4$ load cycles between 2.5 to over 5 times the stress magnitude can be applied before failure occurs for the DNVGL-RP-C203 T curve, compared to the NS-EN 1993-1-9 45 and 90 curves. For thickness ratios of 2 and more, the S-N curves of the two standards can however be close to similar, at least for smaller stress ranges.

For DNVGL-RP-C203, the stresses in tubular joints are calculated at the crown and saddle points, shown in Figure 13 below. These are the sites where stress concentration is most likely to occur.
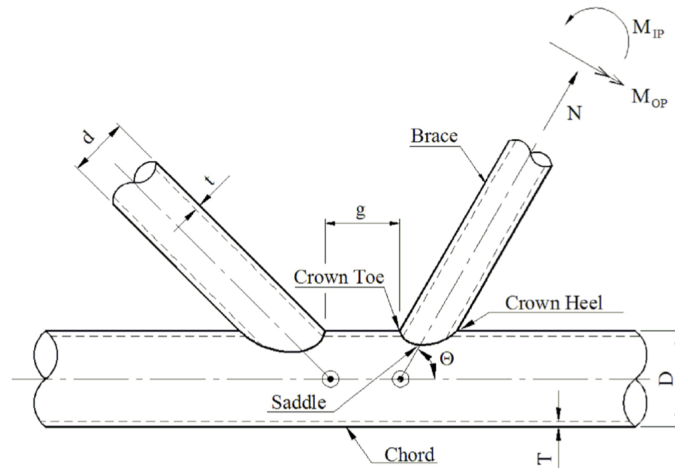
Figure 13: Geometrical definitions of a typical K-joint (DNV AS, 2019b, Figure 3-7, p. 55).

DNVGL-RP-C203 uses SCFs in conjunction with the T-curve. A SCF is defined as the ratio of the hotspot stress to the nominal stress (DNV AS, 2019b, p. 47). They are used to determine the hotspot stress at a given location. This is what is happening for point 1, 3, 5 and 7 in Figure 14 below. For the other four points between the saddle and the crown, a linear interpolation is performed to derive the last four hot spot stresses. The linear interpolation is needed "[...] due to the axial action at the crown and saddle and a sinusoidal variation of the bending stress resulting from in-plane and out of plane bending" (DNV AS, 2019b, p. 54).
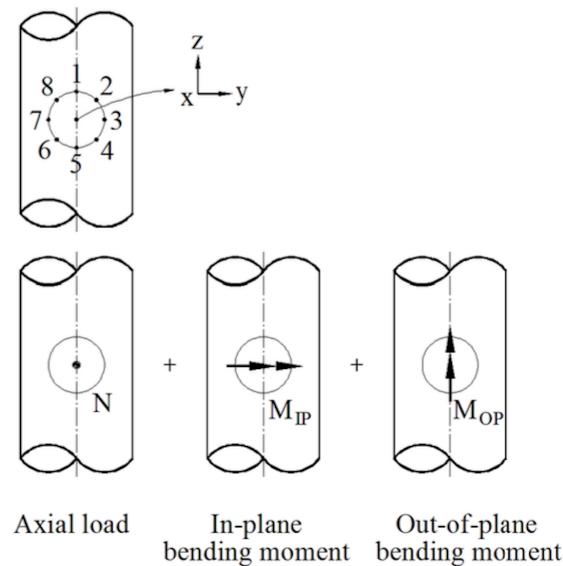

Figure 14: The eight spots around the circumference of the intersection where the hotspot stresses are evaluated (DNV AS, 2019b, Figure 3-7, p. 54).

In each of the intersection points, a summation of the axial stresses and bending stresses is performed. The stress terms are associated with SCF and linear interpolation terms as presented in the following eight equations:

$$\sigma_1 = SCF_{AC}\sigma_x + SCF_{MIP}\sigma_{my} \tag{9}$$

$$\sigma_2 = \frac{1}{2}(SCF_{AC} + SCF_{AS})\sigma_x + \frac{1}{2}\sqrt{2}SCF_{MIP}\sigma_{my} - \frac{1}{2}\sqrt{2}SCF_{MOP}\sigma_{mz} \tag{10}$$

$$\sigma_3 = SCF_{AS}\sigma_x - SCF_{MOP}\sigma_{mz} \tag{11}$$

$$\sigma_4 = \frac{1}{2}(SCF_{AC} + SCF_{AS})\sigma_x - \frac{1}{2}\sqrt{2}SCF_{MIP}\sigma_{my} - \frac{1}{2}\sqrt{2}SCF_{MOP}\sigma_{mz} \tag{12}$$

$$\sigma_5 = SCF_{AC}\sigma_x - SCF_{MIP}\sigma_{my} \tag{13}$$

$$\sigma_6 = \frac{1}{2}(SCF_{AC} + SCF_{AS})\sigma_x - \frac{1}{2}\sqrt{2}SCF_{MIP}\sigma_{my} + \frac{1}{2}\sqrt{2}SCF_{MOP}\sigma_{mz} \tag{14}$$

$$\sigma_7 = SCF_{AS}\sigma_x + SCF_{MOP}\sigma_{mz} \tag{15}$$

$$\sigma_8 = \frac{1}{2}(SCF_{AC} + SCF_{AS})\sigma_x + \frac{1}{2}\sqrt{2}SCF_{MIP}\sigma_{my} + \frac{1}{2}\sqrt{2}SCF_{MOP}\sigma_{mz} \tag{16}$$

σ_x, σ_{my} and σ_{mz} are the axial stress, in-plane bending stress and out-of-plane bending stress, respectively. Furthermore, SCF_{AC} is the SCF for axial loading in the crowns, and SCF_{AS} is the SCF for axial loading in the saddles, which are shown in Figure 13. The subscripts MIP and MOP stands for Moment In Plane and Moment Out of Plane, respectively.

The SCFs are found in the appendix of DNVGL-RP-C203 and they are calculated based on multiple factors such as the thickness of braces and chords, the diameters of braces and chords, angles between braces and chords, and the length of the joint. Calculation of SCFs have in this thesis been implemented in a Python script, which can be found in Appendix A.9.3. The Python script has been verified against an online calculator (CRM Engineering Services, 2021).

Use of SCFs is not stated explicitly in NS-EN 1993-1-9, but the standard demands that for nominal stresses, one shall take stress concentrations not included in the detail category

into account (Nussbaumer et al., 2011, p. 105). For the sake of comparison for analyses on tubular joints, the SCFs from DNVGL-RP-C203 are also used for NS-EN 1993-1-9 in this thesis. A visual representation of the implementation of SCFs is shown in Figures 15 and 16. On the depth axis of Figure 15, the thickness ratio is plotted, showing the invariance of the T-curve for this parameter, whereas the NS-EN 1993-1-9 curve is interpolated for thickness ratios between 1 and 2. Figure 16 intends to illustrate the effect of SCFs by lowering the S-N curves. It should be noted that this is purely a visualization approach, as the SCFs are applied to the stresses in the detail, and not the S-N curves. The same approach can be used for other parameters when calculating SCFs, but as long as the same SCFs are used for both standards, DNVGL-RP-C203 will be less conservative than NS-EN-1993-1-9.
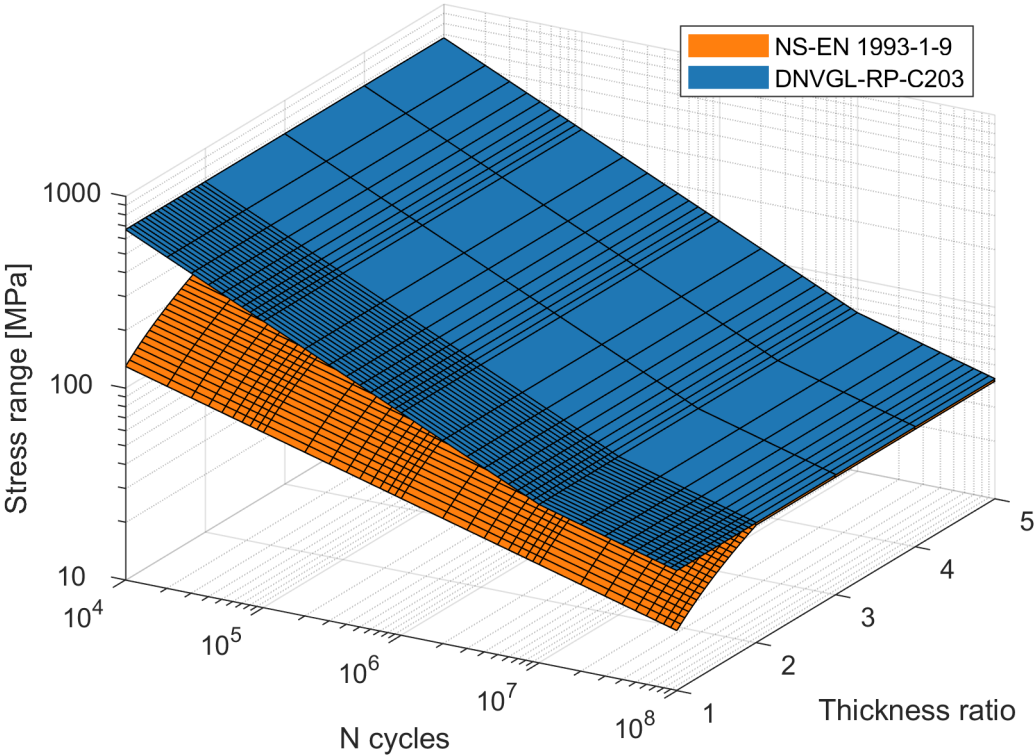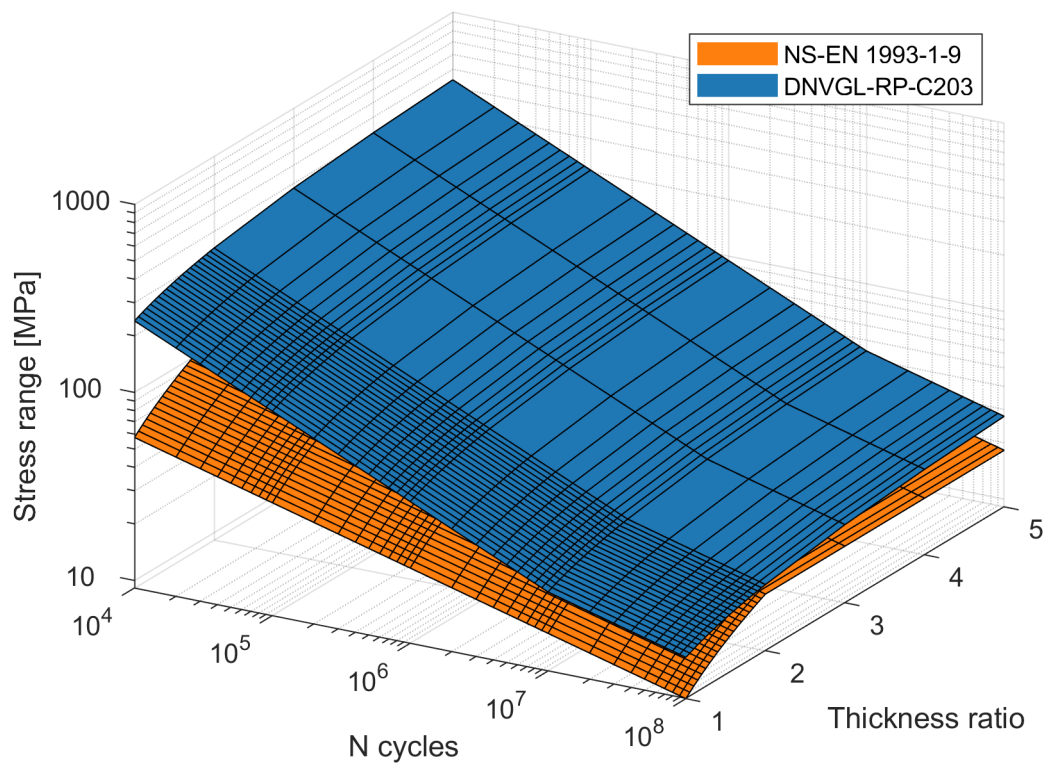

Figure 15: S-N surface without SCFs.

Figure 16: S-N surface with SCFs.

4 Generic bridge

The generic bridge shown in Figure 17 was suggested by Senior Advisor Nils Arne Rakstad at Dr.techn. Olav Olsen AS and is described in this section. Emphasis is given to the geometries of the bridge, classifications of details assessed for fatigue, and the finite element modelling of the bridge.
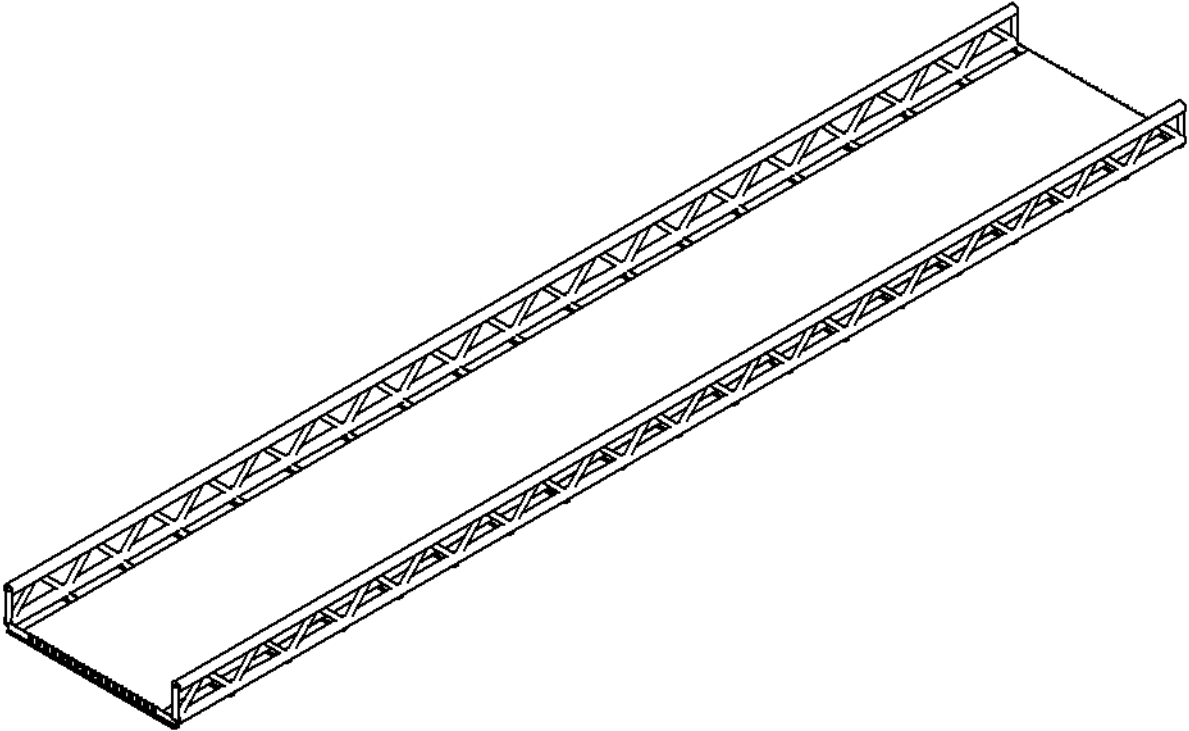

Figure 17: Generic bridge.

4.1 Description of the bridge

Complete construction drawings of the bridge can be found in the Appendix, Section A.2. As illustrated in Figure 18, the bridge is simply supported with three spans over 72 meters. The intermediate supports are columns supporting the ends of the transverse beams.
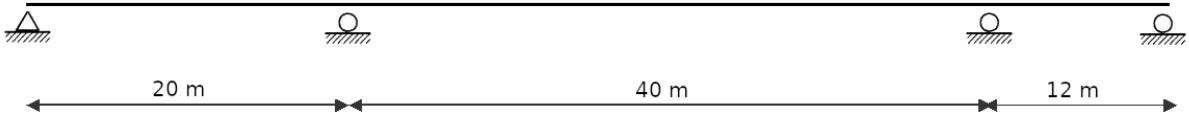

Figure 18: Layout of bridge supports.

The orthotropic deck has a width of 10 meters, consisting of a 14 mm thick steel cover, 17 trapezoidal, longitudinal stringers and 19 T-profile transverse beams. Transverse T-profile beams are spaced 4 meters apart, with cutouts for longitudinal stringers in accordance with NS-EN 1993-2 Section C.1.3.5.2. Trapezoidal stringers are spaced 0.55 meters apart, splice welded to form continuous members. Profile geometries are as specified in Figure 19.

(a) Trapezoidal stringer.
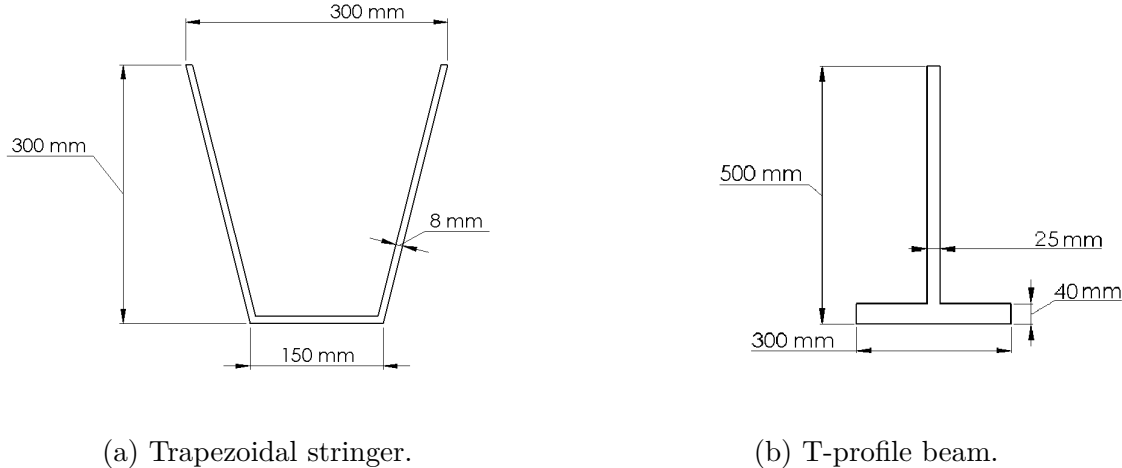(b) T-profile beam.

Figure 19: Orthotropic deck profile geometries.

The trusses, illustrated in Figure 20, support the bridge at each side and consist of K-joints with braces angled 45° relative to the chords. Brace thicknesses and diameters are 12.5 mm and 323.9 mm respectively. Chord thicknesses and diameters are 20 mm and 610 mm respectively.
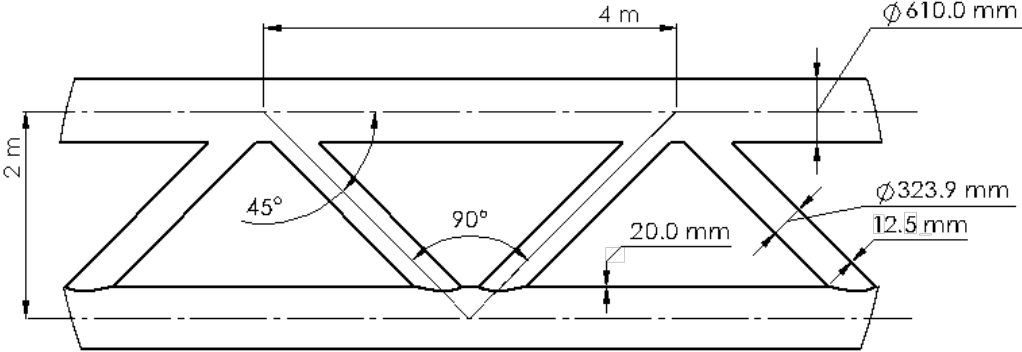

Figure 20: Layout of bridge truss.

4.2 Details considered for fatigue analysis

NS-EN 1993-1-9 specifies several details in an orthotropic deck to be assessed for fatigue. In order to narrow the scope, a selection of details suggested by Nils Arne Rakstad as representative has been analysed. These details are shown in Figure 21 below.
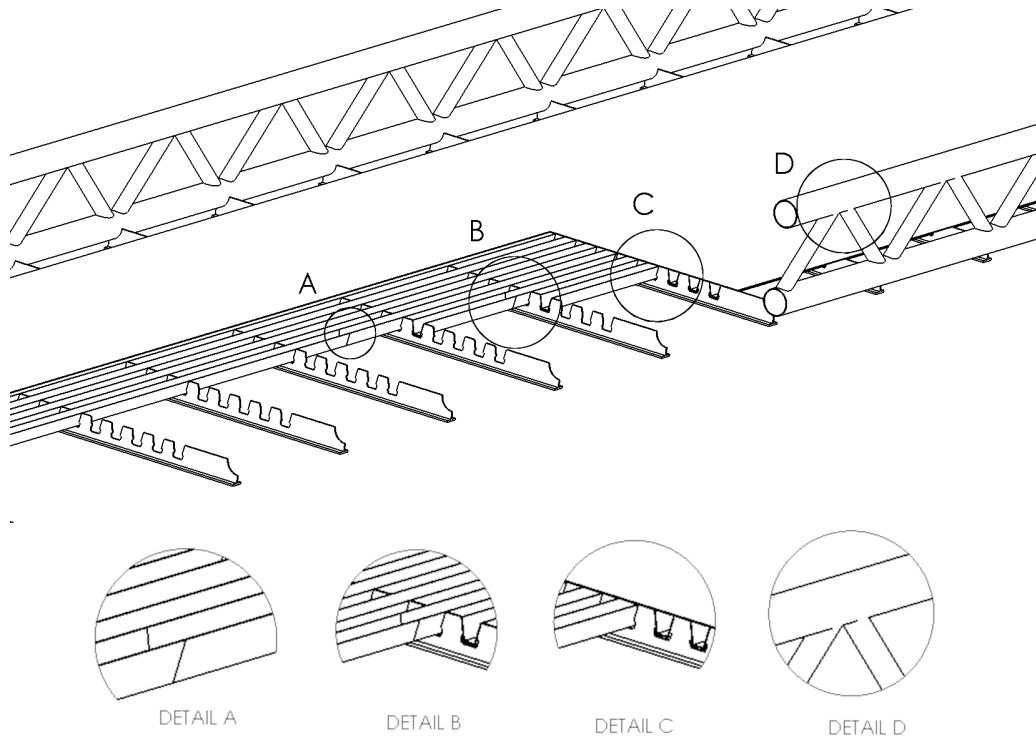

Figure 21: Details considered for fatigue analysis.

4.2.1 Detail A: Weld between the orthotropic deck cover and stringer

Stringers are welded to the cover of the orthotropic deck, where it has been assumed full penetration welds, or partial penetration welds with thickness greater than the stringer web thickness. Note that the vertical lines of detail A in Figure 21 does not indicate a weld, but are included to help identify the position of the stress sampling for the detail, which is in the mid-span between the transverse beams.

With these weld type assumptions, detail A is classified as detail 7 from Table 8.8 in NS-EN 1993-1-9, (Figure 22). The standard specifies that stresses for fatigue calculation is to be determined based on bending in the plate. This detail is found in DNVGL-RP-C203 as detail 9 from Table A.8, giving the detail category as F, with the same specifications for stress sampling.
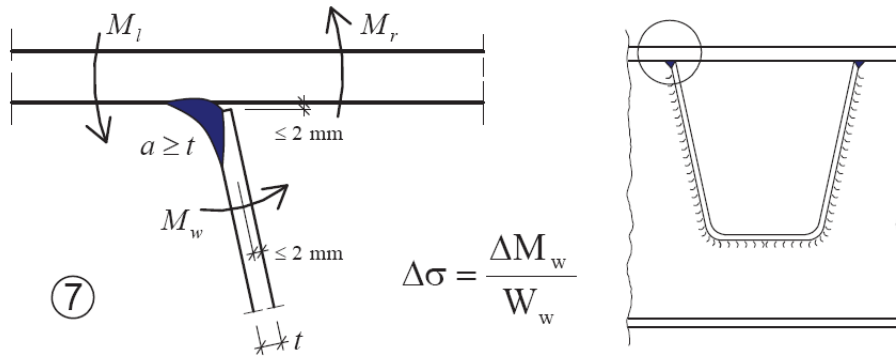
Figure 22: Detail 7 Table 8.8 NS-EN 1993-1-9.

4.2.2 Detail B: Trapezoidal stringer splice weld

Joints connecting stringers are assumed to be full penetration butt welds with backing plates as specified in NS-EN-1993-2 Table C.4, detail 6. They are located 550 mm away from the transverse beams and longitudinal stringer intersections, in accordance with NS-EN 1993-2 Section C.1.3.4.

Based on these assumptions, NS-EN 1993-1-9 classifies detail B of Figure 21 as detail 4 from Table 8.8 (Figure 23), with detail category 71. The standard specifies the stress to be sampled for fatigue calculation as the stress in the stringer.

DNVGL-RP-C203 does not specify detail B explicitly, but detail 2 from Table A.6 fits, which is a butt weld transverse to the load direction with a temporary or permanent backing plate. The detail category for this butt weld is specified as F, with no specifications on stress sampling.
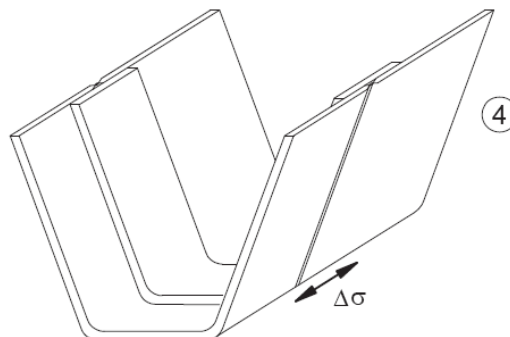

Figure 23: Detail 4 Table 8.8 NS-EN 1993-1-9.

38

4.2.3 Detail C: Weld between T-beam and trapezoidal stringer

At intersections between stringers and T-profile beams, cutouts are made in the beams to accommodate continuous stringers, as described in Section 4.1. With cutouts included in the transverse beams, this detail is classified as detail 1 from Table 8.8 in NS-EN 1993-1-9 (Figure 24). Category assignment is dependent on the web thickness of the T-profile, which is 25 mm. This gives a detail category equal to 71, with the stress range to be sampled in the longitudinal stringer.

This detail is not listed explicitly in DNVGL-RP-C203, but resembles detail 8 from Table A.7, which is a plate with transverse attachment. Its detail category is assigned based on the thickness of this attachment, which corresponds to the web thickness of the transverse T-profile beam. For thicknesses less than or equal to 25, detail category E is assigned and F else. For the sake of comparison in this thesis, detail category F has been chosen regardless. This is in conflict with the rules stipulated, but the T-profile beam web thickness of 25 mm are on the limits of category classification. The choice of category F is based on the fact that curve F is similar to curve 71, which makes the DNVGL-RP-C203 classification similar to the NS-EN-1993-1-9 classification.
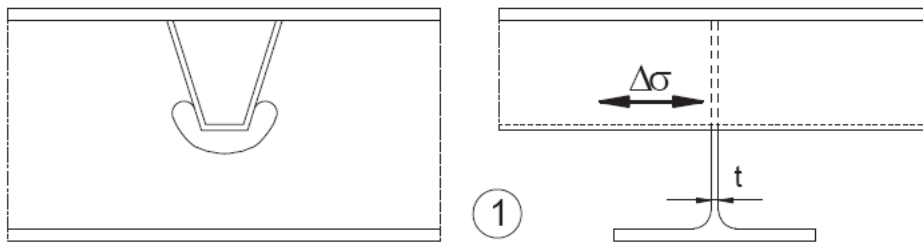

Figure 24: Detail 2 Table 8.8 NS-EN 1993-1-9.

4.2.4 Detail D: K-joint

End joints with 90° members are not considered, as they are few and thus gives a small data set to assess the difference in outcome for fatigue damage using NS-EN 1993-1-9 and DNVGL-RP-C203. The tubular members have thicknesses larger than the maximum of 8 mm wall-thickness set by NS-EN 1993-1-9. There is no such limitation in DNVGL-RP-C203.

The K-joint in detail D in Figure 21 can be classified as detail 1 from Table 8.7 in NS-EN 1993-1-9 (Figure 25). The detail category is dependent on the thickness ratio between chord and braces. In the generic bridge, this ratio is found as $t_0/t_i = 20/12.5 = 1.6$. In ranges between 1 and 2, this entails a S-N curve linearly interpolated between category 45 and 90.

DNVGL-RP-C203 classifies all tubular joints as detail category T. The standard has a detailed list of stress concentration factors to be applied in conjunction with stresses sampled for fatigue analysis. These SCFs are also applied in damage calculations for K-joints when using NS EN-1993-1-9. As Eurocodes supplies no SCFs of their own, it is suggested to obtain modified nominal stresses in accordance with stress concentrations not included in the detail category (Nussbaumer et al., 2011, p. 105).
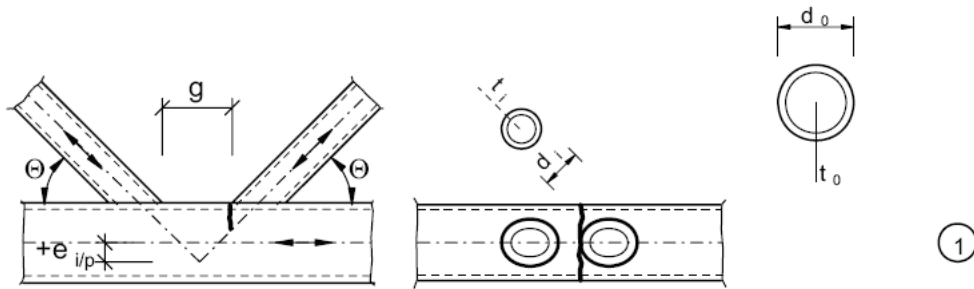

Figure 25: Detail 1 Table 8.7 NS-EN 1993-1-9.

4.3 Finite element analysis of bridge

Finite element analysis modeling choices to determine stresses for fatigue calculation are strongly connected to the detail in question, and therefore multiple models are required. All the details presented in Section 4.2 are assessed for fatigue damage with the nominal stress approach discussed in Section 2.4.1. This approach requires less modeling effort at the detail location and allows for efficient fatigue analysis on all details in the bridge. As mentioned in Section 2.4.1, the nominal stress approach requires that stresses used for fatigue calculation are in accordance with what can be determined by classical beam and plate theory. To comply with this demand, it is suggested to use a simplified model for the T-profile cutout welds and stringer-cover welds (Nussbaumer et al., 2011, p. 304). The hotspot approach discussed in Section 2.4.2 requires considerable more effort and is used less extensively. In the most damaged locations for the details according to the nominal analyses, hotspot analyses has been performed to assess the validity of the nominal stress approach damage calculation.

Five models in total have been created, summarized in Table (6). Two nominal stress approach models have been created, one full and one simplified. For hotspot stress analysis, three models have been created, one for each orthotropic deck detail.

Table 6: Finite element models.

Model	Stress approach	Element types	# elements	Global element size - mm	Local element size - mm
Full	Nominal	S4R, B31	82573	20	-
Simplified	Nominal	S4R, B31	70454	20	-
Stringer-cover weld	Hotspot	S8R, B31	33696	50	8
Stringer splice weld	Hotspot	S8R, B31	33723	50	8
T-profile cutout weld	Hotspot	S8R, B31	34421	50	8

4.3.1 Nominal stress approach models

Full model

The deck, including longitudinal stringers and transverse beams, are modelled with shell elements. As every possible location for the details is considered, a rather fine mesh with global size of 20 mm is needed, thus four-noded reduced integration shell elements (S4R) with five-point Simpson thickness integration are used to to save computational expense, which is important as there are approximately twice as many elements in the nominal models as there are in the hotspot models. The S4R elements also simplifies the stress sampling as the element has only one integration point. Trusses are included in this model as specified in Section 4.3.3.

Simplified model

As mentioned in Section 2.4.1, the nominal stress approach requires that stresses used for fatigue calculation are in accordance with what can be determined by classical beam and plate theory. To comply with this demand, it is suggested to use a simplified model for the T-profile cutout welds and stringer-cover welds (Nussbaumer et al., 2011, p. 304). In this simplified model, the transverse beams are not included, as the cutouts in these cause stress localization, which is in violation with the nominal stress method. Instead, the stringers will rest on elastic supports, with stiffness determined by sampling deflection stiffness of a clamped T-profile beam. This is associated with both conservativity and non-conservativity, as the transverse beams are not fully clamped in reality. However, some torsional stiffness is lost when introducing the beams as elastic supports. With transverse beams removed, trusses are not included.

4.3.2 Hotspot approach models

For hotspot stress analyses the orthotropic deck is modeled with shell elements, and eight-node reduced integration shell elements (S8R) are used in accordance with the recommendations in DNVGL-RP-C203 (DNV AS, 2019b, p. 78). Higher order elements are necessary for the hotspot method due to extrapolation of stresses. Similar to the S4R elements in the nominal models, a five-point Simpson rule is used for thickness integration. The three hotspot models also include trusses as specified in Section 4.3.3.

To obtain a regular mesh with element size $8mm \cdot 8mm$ in the vicinity of the weld detail considered, partitions were used. 200 mm to each side of the detail has been used for the regular mesh area, with further 100 mm to act as a transition zone for the regular fine mesh and the coarse mesh. This has been done to ensure a regular mesh at the hotspot, and avoid numerical issues due to too abrupt changes in element size (Cook et al., 2002, p. 340-342). Figure 26 illustrates the process of partitioning and meshing for the stringer-cover weld detail. Note that the view of the figure is from beneath the bridge and up.
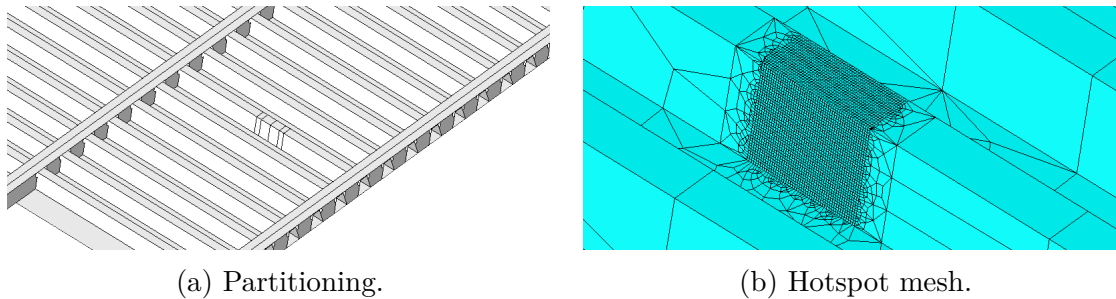

| (a) Partitioning. | (b) Hotspot mesh. |

Figure 26: Abaqus FEA model partitioning and local mesh for hotspot analysis of stringer-cover weld.

4.3.3 Trusses

The truss in Figure 20 is modelled with three-dimensional linear two-node beam elements (B31), which are constrained to the transverse T-profile beam end points using a tie constraint with tolerance 0.05 meters. For the K-joints in the truss, the full nominal model has been used to calculate fatigue damage.

4.3.4 Boundary conditions

Boundary conditions in Figure 18 are introduced by constraining translations in all directions along the leftmost edge of the deck. At the rightmost edge, all translations, except in the bridge's longitudinal direction, are constrained. At intermediate supports, a modeling

choice was made to only constrain translation in the vertical direction, reflecting columns supporting the truss structure. Boundary conditions at intermediate supports are point boundary conditions, as opposed to the ones at the leftmost and rightmost edge of the bridge, which are line boundary conditions.

4.3.5 Loads

NS-EN 1991-2 truck loads, as presented in Section 3.1, are introduced by modelling tyre contact surfaces as rectangular planar shells. The axle loads are placed on these and interaction with the bridge is achieved with a tie constraint to the steel cover. The stiffness of the asphalt cover is neglected, but the effect the asphalt has on load distribution is included. As specified in NS-EN 1991-2, the contact area of the tyres is extended by a 1:1 ratio for the depth of the asphalt to the mid surface of the steel plate. An asphalt depth of 80 mm has been assumed, extending the tyre contact surfaces (as defined in FLM4) 80 mm outwards. The loads introduced by the trucks defined in FLM4 are applied onto the bridge as static loads. Lorries are placed in the center of the bridge, with the sides considered pedestrian lanes.

4.3.6 Input file and output generation with Python scripting

A Python script supplied by thesis supervisor Nils Arne Rakstad generates multiple Abaqus input files, where the position of the lorry is stepped across the bridge. For the nominal model, a step size of 0.5 meters has been used, whereas the hotspot models use 0.3 in the vicinity of the detail, and up to 1.5 meter else.

Relevant element sets for the detail considered is defined, and output from Abaqus CAE Output DataBase files (ODB) is stored in a Comma Separated Variable file (CSV) by another Python script. Generalized input and output scripts are given in the Appendix, Section A.9.

4.3.7 Mesh calibration

Element size of $t \cdot t$ and element type for hotspot analysis were validated for use for hotspot analysis by calibration, as described in Section 2.4.4. The results of this calibration are presented in the Appendix, Section A.3.

5 Results

The results of the analyses as described in Section 4 are presented here. Results for details in the orthotropic deck are presented in Section 5.1, and results for the K-joints in the truss are given in Section 5.2. Section 5.3 presents results for the use of DFFs for DNVGL-RP-C203 damage calculation in the orthotropic deck. An overview of the scope of the analyses is given in Table 7.

Table 7: Damage calculations on generic bridge.

Detail	Location	Analysis	Positions considered *
Stringer-cover weld	Orthotropic deck	Nominal stress method	612
		Hotspot method	2
Stringer splice weld	Orthotropic deck	Nominal stress method	612
		Hotspot method	1
T-beam cutout weld	Orthotropic deck	Nominal stress method	1224
		Hotspot method	2
K-joint brace	Truss	Nominal stress method	152
K-joint chord	Truss	Nominal stress method	148

* Includes all possible locations of the detail in the analysed bridge, not necessarily ones relevant in a built structure.

5.1 Orthotropic deck

Fatigue analysis in the orthotropic deck performed with FLM4 from NS-EN 1991-2, resulted in 6743 data points distributed among the details as specified in Table 8, allowing for a quantitative investigation of the difference in outcome when applying NS-EN 1993-1-9 and DNVGL-RP-C203. Results in this section are presented using the partial factor γ_{Mf} from NS-EN 1993-1-9 on the S-N curves from both standards. Results for the details using DFFs from DNVGL-OS-C101 are found in the Appendix, Section A.5.

The most damaged welds according to the nominal analyses on the full and simplified model has been investigated further by performing a hotspot analysis on these welds. Load spectra and damage calculation plots at these locations were made to assess the validity of the nominal models by comparing with the hotspot models. In this section, the load spectra plots for Lorry 3 of FLM4 are presented. Complete load spectra plots are found in the Appendix, Section A.4.

Table 8: Data points generated for details in orthotropic deck.

Detail	Data points		
	Full model	Simplified model	Total
T-beam cutout weld	1224	1851	3075
Stringer splice weld	1224	-	1224
Stringer-cover weld	1224	1220	2444

5.1.1 Stringer-cover weld

Damage calculated in the stringer-cover welds differ significantly between the two nominal models, which can be seen in Figure 27. For the simplified model, there is little difference between damage calculated with NS-EN 1993-1-9 and DNVGL-RP-C203. For the damages of magnitude 1.5 and above, the standards give equal results. The damage calculated from the simplified model is clustered around two points, one below 0.5 and one above 1.5. Resulting damages from the full nominal analysis are of less magnitude.

Figure 28 shows how the simplified nominal model calculated the most damaged weld at the mid span of the bridge, while the full nominal model calculated it at the rightmost edge. The black lines in Figure 28 represent the stringers and the transverse beams of the deck.
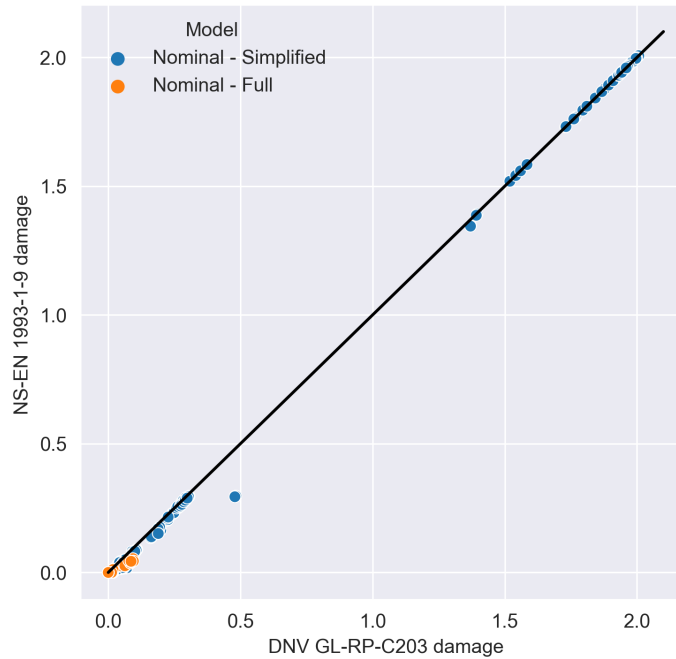

Figure 27: Nominal stress method damage for string-cover welds in orthotropic deck.
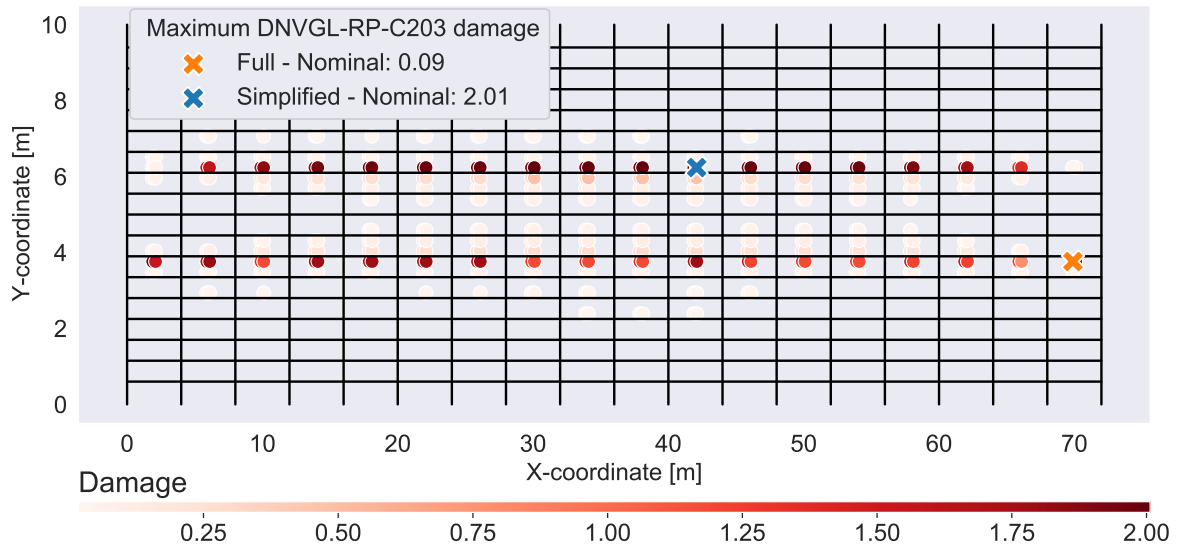
Figure 28: Stringer-cover weld damage distribution in orthotropic deck.

Figures 29 and 30 show load spectra and damage calculated at the most damaged weld according to the full nominal analysis. The load spectra shows a close resemblance of loading for the finite element models. Lower damage for the hotspot model compared to the full nominal model is therefore as expected given the less strict S-N curve for hotspot analysis. The difference in damage calculation for NS-EN 1993-1-9 and DNVGL-RP-C203 for the full nominal model is reasonable, given Figure 30a. It shows that most stress ranges are below the range where the two standards' S-N curves are not equal.
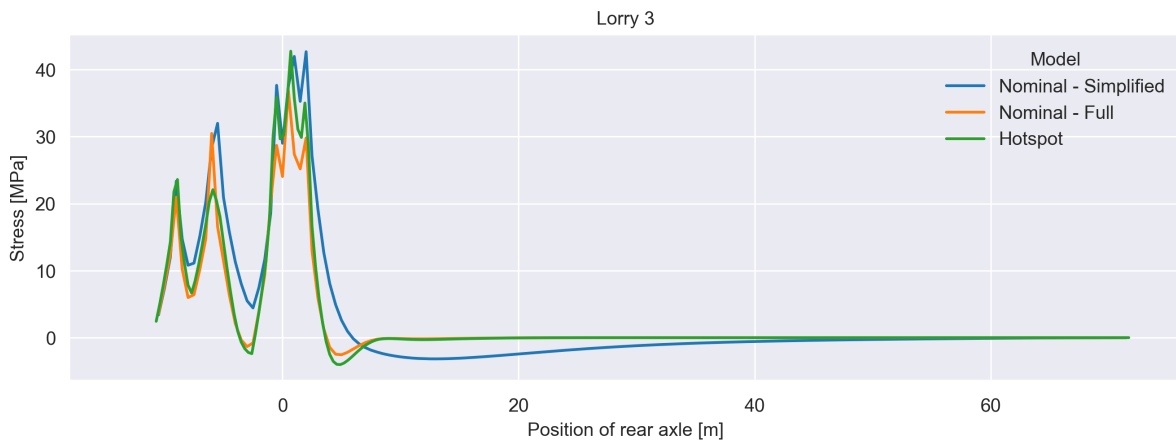

Figure 29: Stringer-cover weld load spectra at most damaged location according to full nominal analysis.
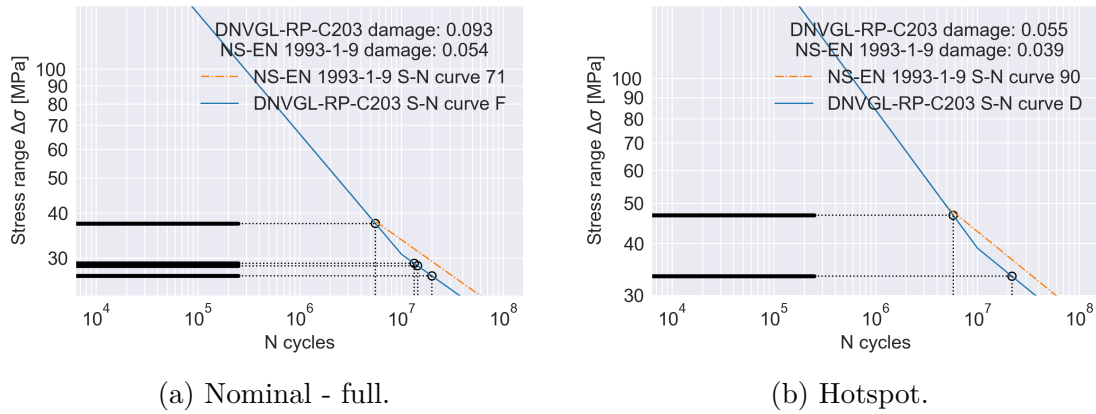
(a) Nominal - full.

(b) Hotspot.

Figure 30: Stinger cover weld damage calculation at most damaged location according to full nominal analysis.

At the most damaged location according to the simplified nominal analysis, the loading for the simplified model exceeds the hotspot and full nominal model loading, shown in Figure 31. This is *not* as expected, as stress concentrations from hotspot analyses are accounted for by the finite element model and not by the choice of S-N curve. The result of this large loading is that stress ranges used in damage calculation are above the stress range at which NS-EN 1993-1-9 and DNVGL-RP-C203 S-N curves are equal. This gives a rather large maximum calculated damage, as visualized in Figure 32a. The figure shows that stress ranges are located solely in the range where S-N curves for both standards overlaps - which explains why the large damages calculated for the simplified nominal model are equal.
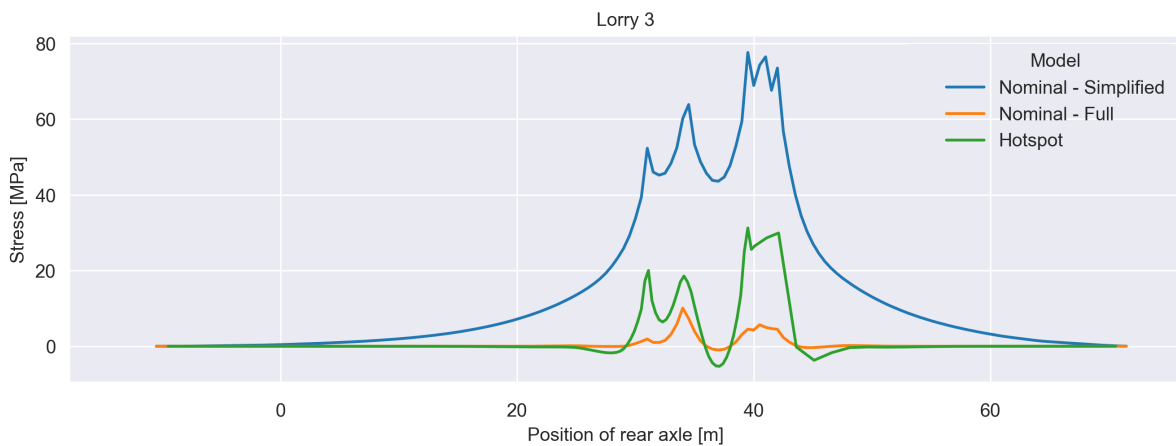

Figure 31: Stringer-cover weld load spectra at most damaged location according to simplified nominal analysis.

47

(a) Nominal - simplified.

(b) Hotspot.
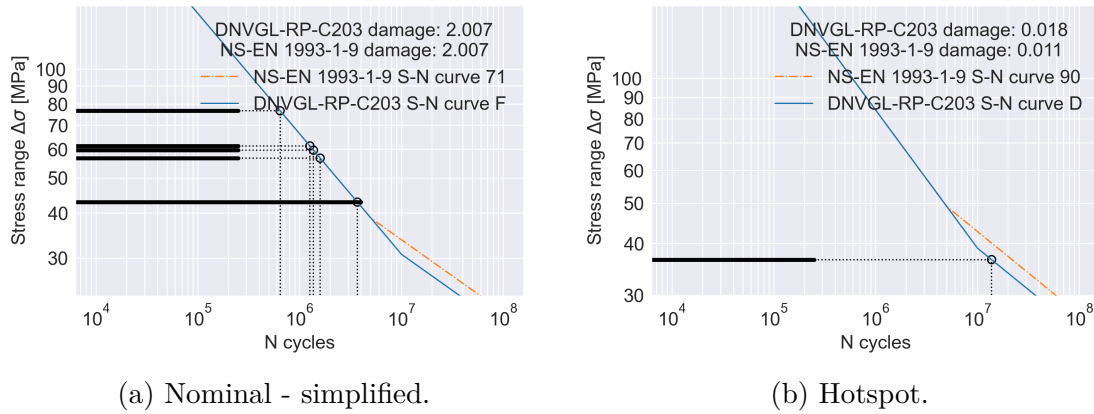
Figure 32: Stinger cover weld damage calculation at most damaged location according to simplified nominal analysis.

5.1.2 Stringer splice welds

As the stringer splice welds are not located in the vicinity of any stress concentrating geometries, no special modelling consideration are required. Consequently, damages are only calculated based on the full nominal model. All larger damages are more conservative for DNVGL-RP-C203 than NS-EN 1993-1-9, as seen in Figure 33. The most damaged weld is located at the first transverse T-profile beam, shown in Figure 34.
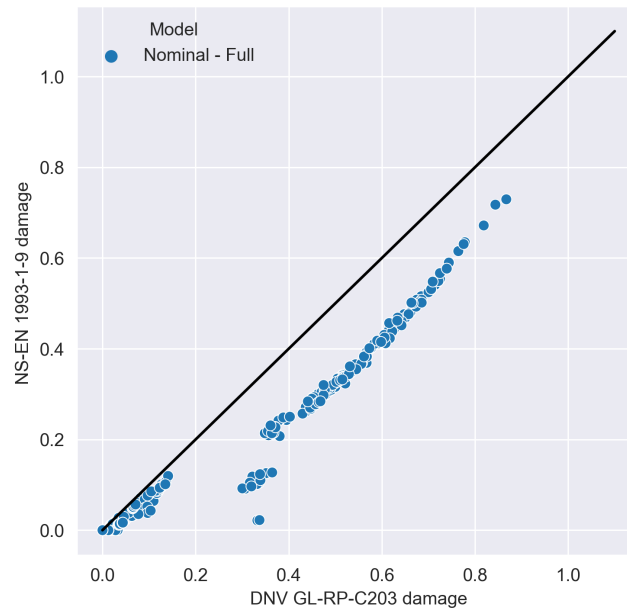
Figure 33: Nominal stress method damage for stringer splices in orthotropic deck.
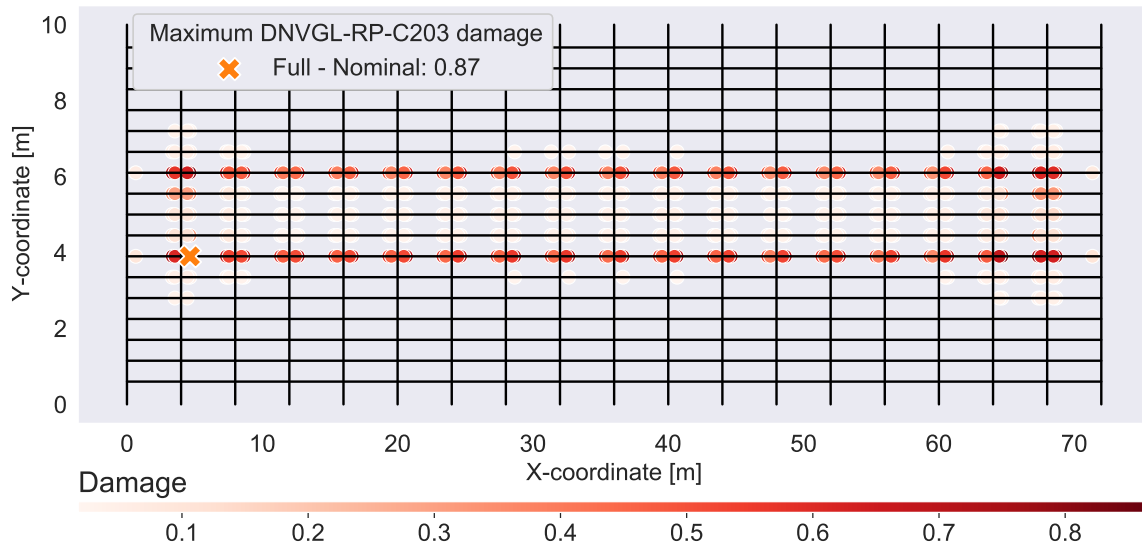
Figure 34: Stringer splice weld damage distribution in orthotropic deck.

Without stress raising geometries in the vicinity of the detail, similar load spectra for the nominal and hotspot analyses are expected. This is demonstrated in Figure 35, which shows the load spectra at the most damaged weld according to the full nominal model. Consequently, the damage calculated for the hotspot analysis is lower compared to the nominal analysis, shown in Figure 36. This is again as expected, because a less strict S-N curve is assigned for the hotspot analyses.
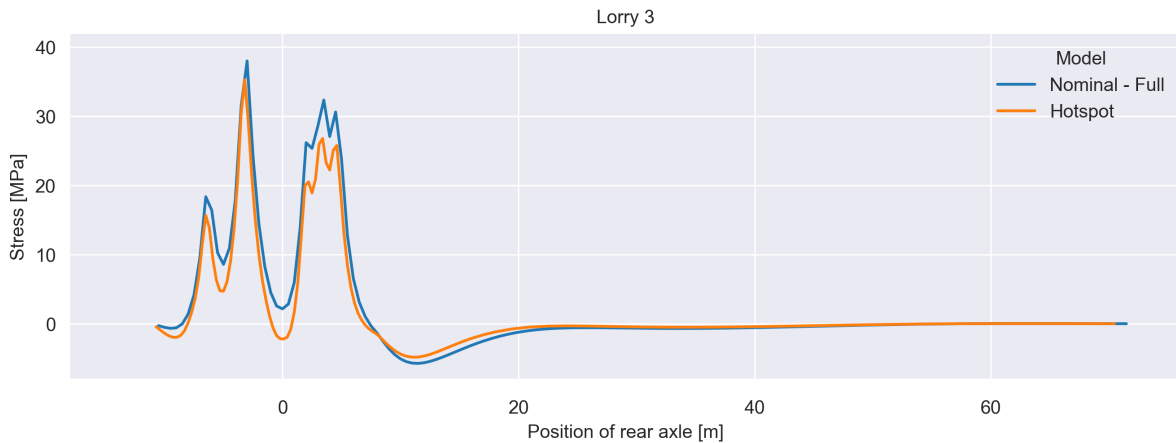
Figure 35: Stringer splice load spectra at most damage location according to full nominal analysis.

(a) Nominal - full.   (b) Hotspot.
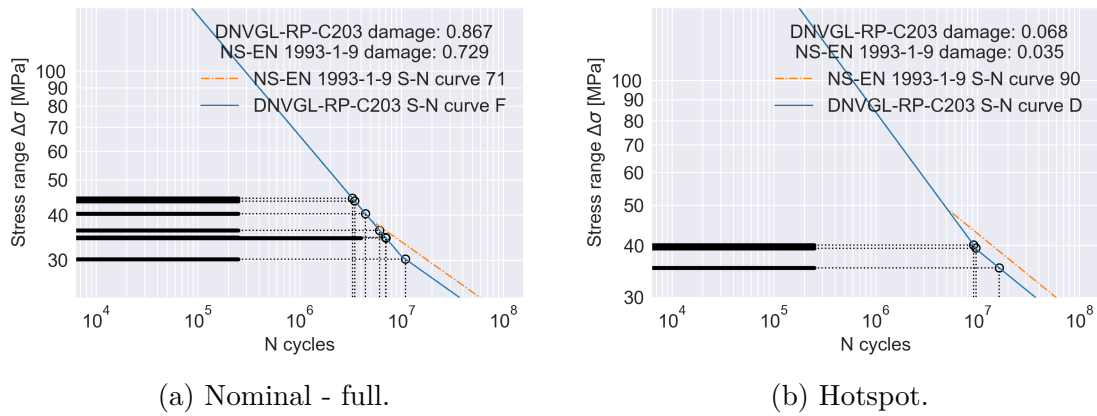
Figure 36: Stinger splice weld damage calculation at most damaged location according to full nominal analysis.

5.1.3 T-profile cutout welds

For the T-profile cutout welds, there are (as with the stringer-cover welds) differing results for the full and simplified nominal analyses, which can be seen in Figure 37. In this case, the simplified model also gives much larger damages than the full model. The two models both calculated the most damaged T-profile cutout weld close to the edge of the bridge, but at opposite sides, as shown in Figure 38.
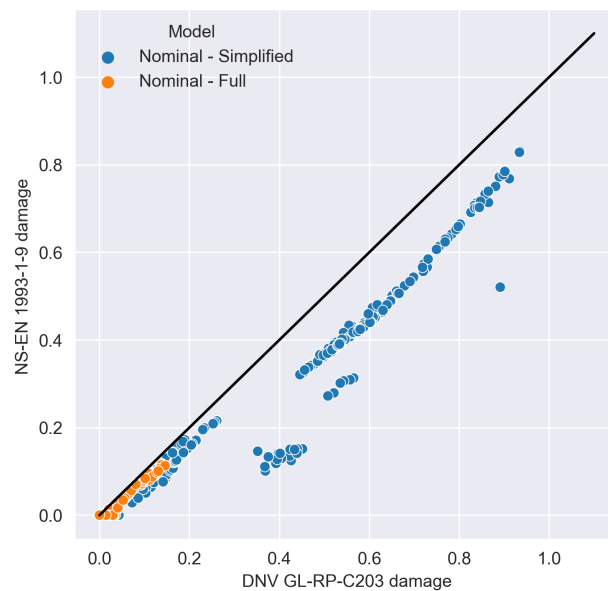
Figure 37: Nominal stress method damage for cutouts in orthotropic deck, full and simplified model on elastic supports.
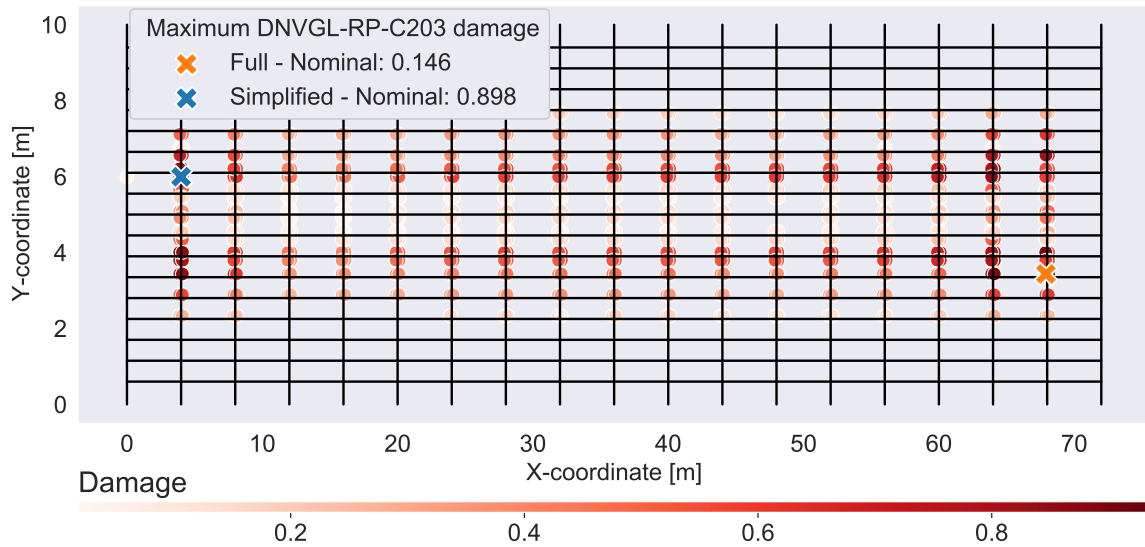
Figure 38: T-profile cutout weld damage distribution in orthotropic deck.

Figure 39 shows the load spectra at the most damaged location according to the full nominal model. Observe that the loads for both nominal models have the same general shape, and that they are of less magnitude than the hotspot model. Notably, as seen in Figure 40, the hotspot damage calculation exceeds the limit of $D \leq 1$, while the nominal full model damage is around $0.113 - 0.146$.
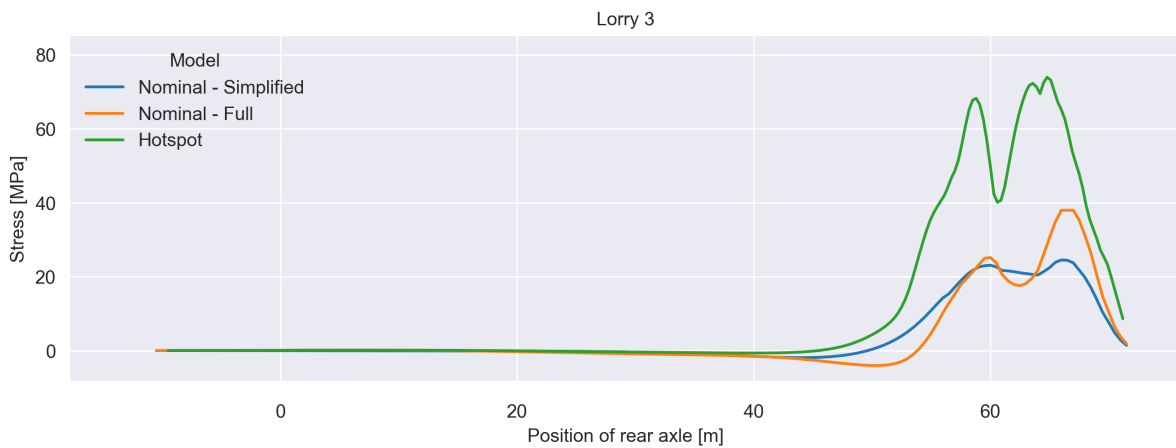
Figure 39: T-profile cutout weld load spectra at most damaged location according to full nominal analysis.

(a) Nominal - full.

(b) Hotspot.
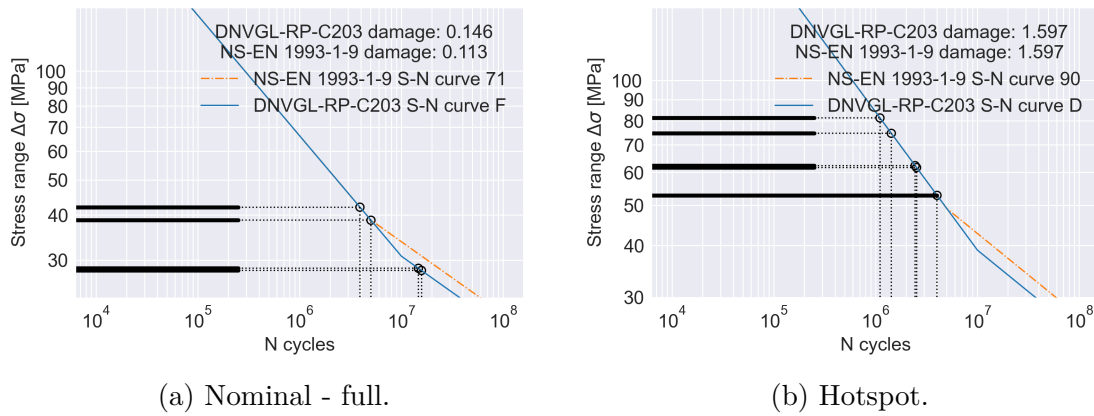
Figure 40: T-profile cutout weld damage calculation at most damaged location according to full nominal analysis.

For the most damaged T-profile cutout weld according to the simplified nominal analysis, damage calculation (visualized in Figure 42) is in agreement for the simplified and hotspot model. This is reflected in Figure 41, where the load on the hotspot model is a magnitude larger than the simplified model. For nominal analyses, this indicates that the detail category for this detail includes the stress raising effects in the hotspot analysis.
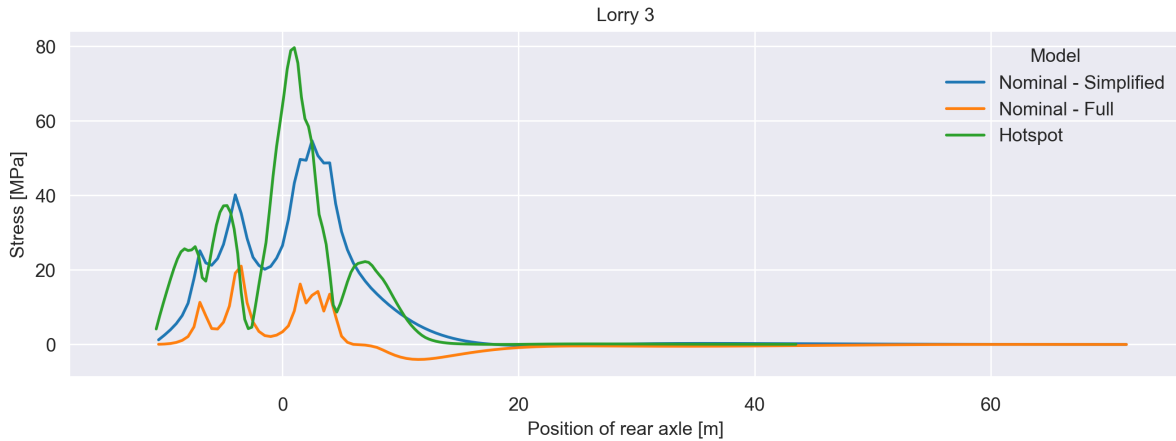
Figure 41: T-profile cutout weld load spectra at most damaged location according to simplified nominal analysis.

(a) Nominal - simplified.   (b) Hotspot.
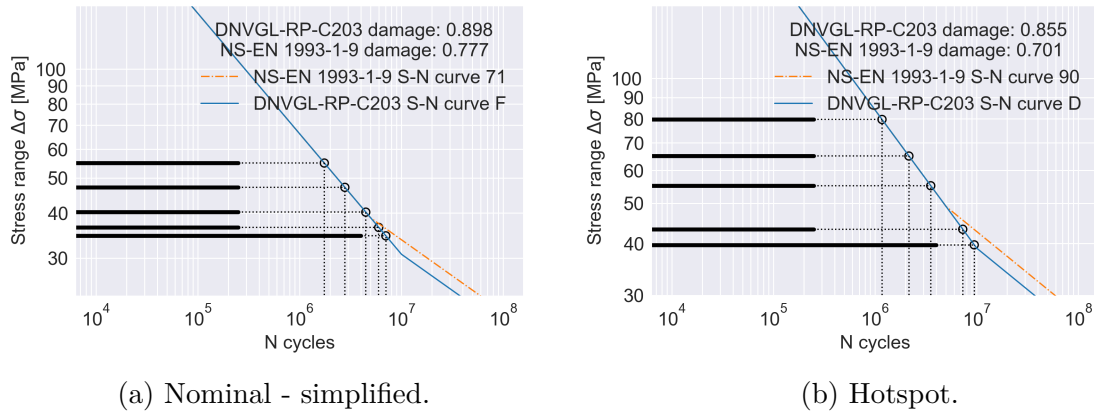
Figure 42: T-profile cutout weld damage calculation at most damaged location according to simplified nominal analysis.

5.2 Trusses

Analyses with both original dimensions suggested by Dr.techn. Olav Olsen AS (as presented in Section 4.1), and dimensions considered valid according to NS-EN 1993-1-9 have been performed. The results for the valid dimensions turned out to be highly unreasonable for both NS-EN 1993-1-9 and DNVGL-RP-C203. For the method presented in the former standard, the damage was estimated above 9000. Because of the extremely large damage values, the results for the valid dimensions will not be presented further. They can, however, be found in Appendix A.6.

The stresses calculated based on the approach described in DNVGL-RP-C203 were also applied when calculating damage using NS-EN 1993-1-9, as presented in Section 3.4.2. The stresses should be sampled approximately D/2 away from the intersection, where D is the chord diameter (Nussbaumer et al., 2011, p. 105). This would require interpolation of stresses in the beam elements. In order to simplify the analyses, the stresses have been conservatively sampled directly in the integration point of the B31 elements in the K-joint. The results are presented in the scatter plot shown in Figure 43. Many points had a damage equal to zero, and these have been removed to improve readability of the plot.
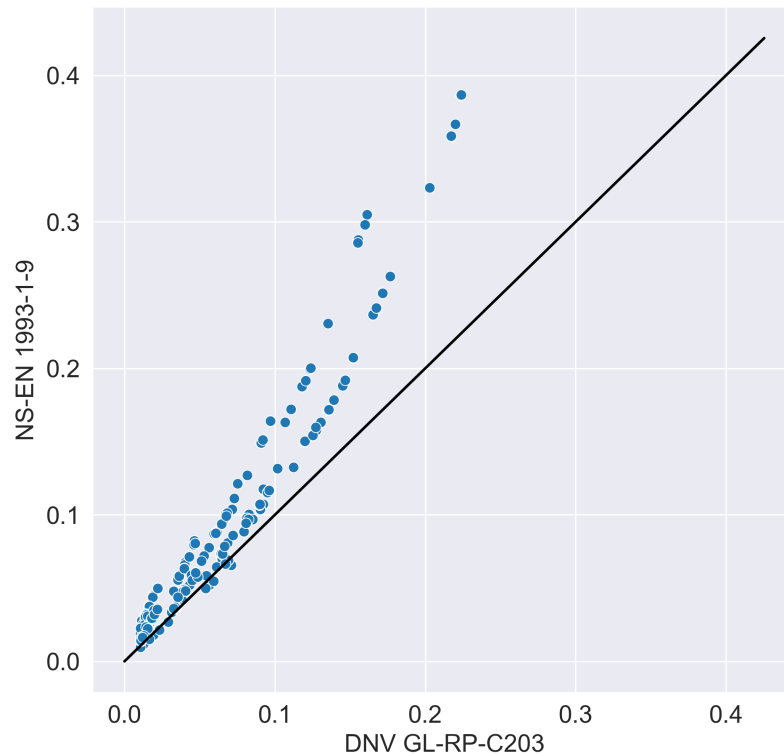
Figure 43: Damage calculated in both trusses.

Observe that most points in the truss have more NS-EN 1993-1-9 damage than DNVGL-RP-C203-damage, in contrast to the details the orthotropic deck. But some points behaved different, and had larger DNVGL-RP-C203 damage than NS-EN 1993-1-9 damage. This will be described further in Section 6.2.

5.2.1 Damage distribution in truss

Figure 44 illustrates how the damage is distributed in the *left* truss for NS-EN 1993-1-9. Each point in the figure represents the maximum damage of the eight points considered in the K-joints, as discussed in Section 3.4.2. Damage calculated using DNVGL-RP-C203 is similarly distributed, but of less magnitude. Figures 44a and 44b display the damage distribution at the 20 meter column support and at the bridge's mid span, respectively. They show that the maximum damages for chords and braces are not distributed in the same locations. The full damage distribution plot of the left truss can be found in Appendix A.7.
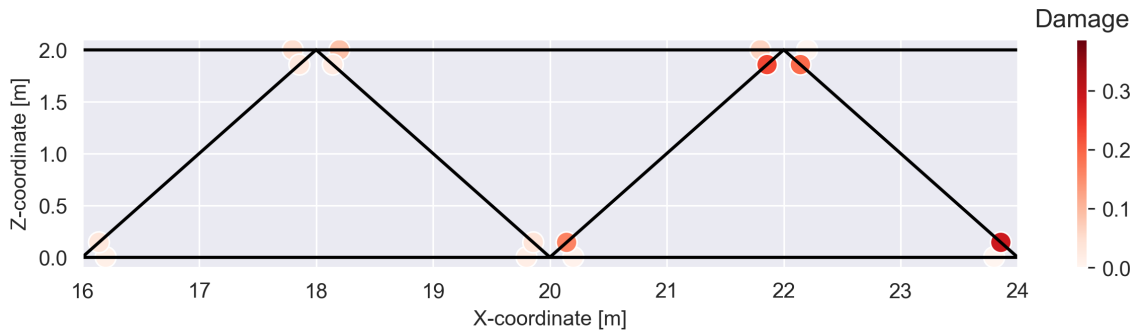
(a) Damage distribution at column support.
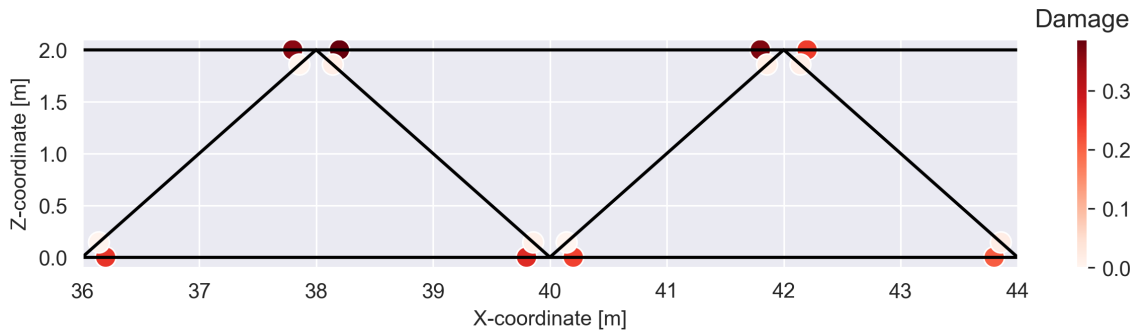
(b) Damage distribution at mid-span.

Figure 44: Damage distribution in left side truss. Calculations based on NS-EN 1993-1-9 S-N curves.

5.3 Design fatigue factors

Figure 45 displays the result of applying different DFFs to damages for all orthotropic deck details calculated with the nominal models. The results for the simplified model on the stringer cover welds are excluded, as these resulted in damages of 2 and above and were considered unreasonable to include in a study on the effect of different DFFs. In Figure 45d, a DFF obtained by a least squares curve fit is applied. This DFF was determined by optimizing the parameter to fit the damages calculated using DNVGL-RP-C203 to a curve with slope 1, at which NS-EN 1993-1-9 and DNVGL-RP-C203 damages are equal. The curve fit was performed with the function scipy.optmize.curve_fit from the Python module Scipy (Jones et al., 2001).

It should be noted that DNVGL-RP-C203 demands that damage should be below the usage factor η, as discussed in Section 3.3. To allow for comparison on a scatter plot, the damage has instead been normalized with respect to this usage factor. In this view, greater DFFs increase the damage calculated from DNVGL-RP-C203, and this is expressed as a translation of the data points on the scatter plots. For a DFF equal to 2 (as seen in Figure 45b), the damage data points are placed with a considerable portion on both sides of the unity line, but none on it except for smaller damage values. Compared to NS-EN

1993-1-9, a DFF of 1 gives a result significantly non-conservative, whereas a DFF of 3 gives a conservative result comparable to that of using a partial factor γ_{Mf} as seen in Figure 45e.

(a) $DFF = 1$

(b) $DFF = 2$

(c) $DFF = 3$

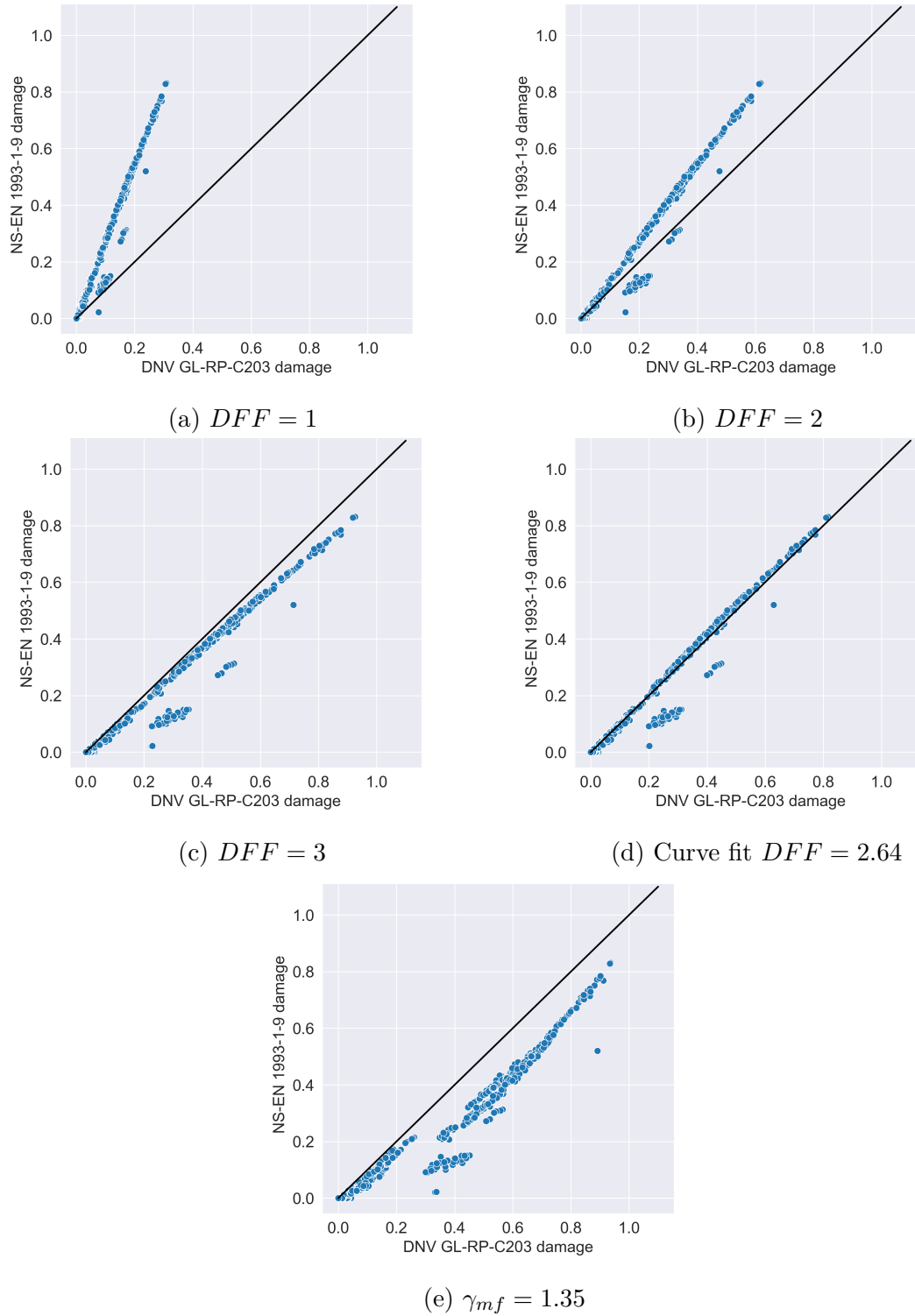(d) Curve fit $DFF = 2.64$

(e) $\gamma_{mf} = 1.35$

Figure 45: Damage comparison for all details.

6 Discussion

This section is structured in the same manner as the results section. Damage calculation for the orthotropic deck and trusses are discussed separately, due to the different nature of damage calculation. Safety implementation in the form of partial factors and design fatigue factors are discussed on the basis of results in the deck, as this resulted in a much larger amount of data points, and were deemed to be of better quality.

6.1 Orthotropic deck

As shown in Section 5.1, the results for damage in the orthotropic deck calculated with NS-EN 1993-1-9 turned out consistently less conservative than DNVGL-RP-C203 for all orthotropic deck details. This can be explained by the difference in S-N curves mentioned in Section 3.4. There are for smaller stress ranges $\Delta\sigma$ a difference in N cycles until failure of magnitude tens of millions. When applying the partial factor γ_{Mf} from NS-EN 1993-1-9 on S-N curves from DNVGL-RP-C203, damages are either equal for the two standards, or less for NS-EN 1993-1-9. For welds loaded with large stress ranges, S-N curves for both standards are similar and will give the same calculated damage. For welds with smaller stress ranges, DNVGL-RP-C203 will give more damage, resulting in clustering of data points below the equality line for the two standards.

6.1.1 Stringer-cover welds

With stringer-cover weld damages for the simplified nominal model larger than both the full nominal and hotspot models, the authors consider the simplified model unsuited for this type of detail. A probable reason for the large stringer-cover weld damages calculated for the simplified model, is that bending around the bridge's longitudinal axis is not properly accounted for when modeling transverse beams as elastic supports. This is indicated in Figure 46, which shows the deformation of the bridge with lorry 3 at the mid span for both the full and the simplified nominal model. The simplified model has springs placed only at the stringers in the model, not along the deck in between the stringers. For the models that include the transverse T-profile beams, a large part of the bending around the bridge's longitudinal axis is transferred to these beams. Without them and with only elastic supports at the stringers, this bending is likely to result in larger stresses in the deck plate, which is transferred to the webs of the longitudinal stringers.

(a) Full nominal model.
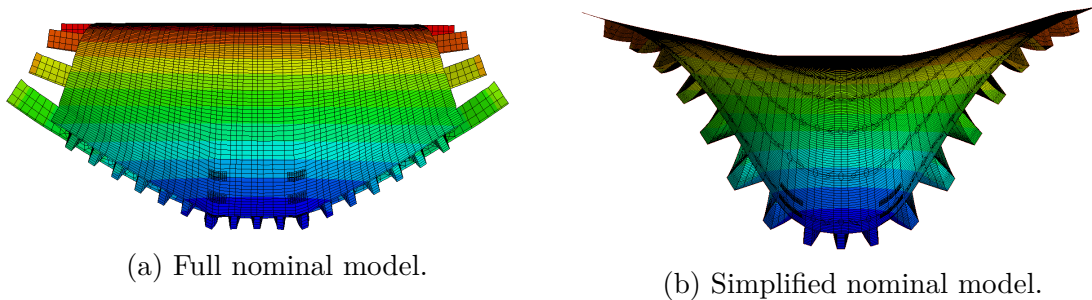
(b) Simplified nominal model.

Figure 46: Deformation plots of the orthotropic deck sectioned at the mid span of the bridge. Note that the trusses of the full nominal model has been removed for readability.

The full nominal model produced satisfactory results when compared to the hotspot analyses, as this model includes the transverse T-profile beams. The load spectra for the full nominal model (Figures 29 and 31) are similarly shaped as the hotspot models, with less magnitude. Although the simplified model on elastic supports is suggested by Nussbaumer for this detail, the stress raising geometry is not as severe as in the case of the T-profile cutout welds. Thus, the resulting similar damage calculated by the full nominal model and the hotspot model reflects the inherent stress concentration in the detail category for this detail when applying nominal analysis.

6.1.2 Stringer splice welds

For the stringer splice welds, the comparison between the nominal and hotspot analyses gave two important results. Firstly, the stringer splice weld is a detail without any stress raising geometry in its vicinity, meaning that any difference in the load spectra at the detail for nominal and hotspot analyses (Figure 35) would be due to element type and size. The small difference shown in Figure 35 is negligible and indicates that the global behavior of the S4R element full nominal model and the S8R element hotspot models are similar.

The second important result is that the damage calculated from these two models turned out so different even though they are exposed to the same loading. The authors would like to highlight that this is in accordance with the detail classification. For nominal analyses, the S-N curves are intended to include stress concentrations not taken into account in the finite element model. For the other details, this can be seen from their load spectra, where the nominal stress is similar in shape, but of a larger magnitude. For details without any stress concentrations for the hotspot analysis to pick up, one simply gets a less strict S-N curve. This should be used with caution, as the detail category selection for the stringer splice welds for nominal analysis could be considered to include some safety, which is omitted if one applies a hotspot approach for such a detail.

6.1.3 T-profile cutout welds

The T-profile cutout weld is the detail which first made it clear that an alternative modelling approach was required. This is because initial results from the nominal stress analyses on a finite element model with cutouts were poor compared to the results from the hotspot stress analyses. The simplified model with elastic supports as presented in Nussbaumer was therefore introduced due to problems with stress raising geometries for this detail. Given the results in Section 5.1.3, the simplified model is considered a good approach by the authors for this detail. As noted previously, damage calculation for the hotspot method and simplified model are in agreement at the most damaged location according to the simplified nominal analysis. However, this is not the case at the most damaged location according to the *full* nominal analysis. This is believed to be due to end effects in the finite element model.

The most damaged weld according to the simplified nominal analysis is located at the second T-profile beam from the leftmost bridge edge, whereas the most damaged weld according to the full nominal analysis is located at the second T-profile beam from the rightmost bridge edge. This subtle difference results in rather different shapes of the load spectra, albeit with similar maximum stress magnitude around 80 MPa. At the leftmost edge, the lighter frontal axles enter the bridge first, giving a jagged load spectra, before the heavier rear axles enter, which gives a maximum in the load spectra. At the rightmost edge this sequence is reversed, causing a less jagged spectra. As the lorries approach the weld in question, all axles are present on the bridge. When the lorries pass the weld, the frontal axles leave the bridge. These axles have a lighter load, and will therefore not affect the loading onto the weld as much, while the heavier rear axles are present. The less jagged load spectra at the weld at the rightmost edge of the bridge result in higher stress ranges when performing rainflow cycle counting, as the valleys and peaks are not disrupted. This explains the large damage calculated.

Inspection of stress extrapolation plots in the weld for the hotspot model reveals that for the full nominal model to give correct stresses for damage calculation, the stress sampling point is of major importance. Figure 47 shows the stress extrapolation for hotspot analysis for the cutout weld at the most damaged location, based on the results from the full nominal analysis. The extrapolation is shown for Lorry 3, with the rear axle positioned at 65.7 meters. In the hotspot analysis, stresses are sampled along the midpoints of the S8R elements, which have a size of $8mm \cdot 8mm$. The stresses are thus sampled at a distance from the hotspot of 4 mm, 12 mm, 20 mm etc. The stresses at the upper surface are the ones used for damage calculation, and the figure shows how the last 4 mm are extrapolated to the hotspot for this stress.
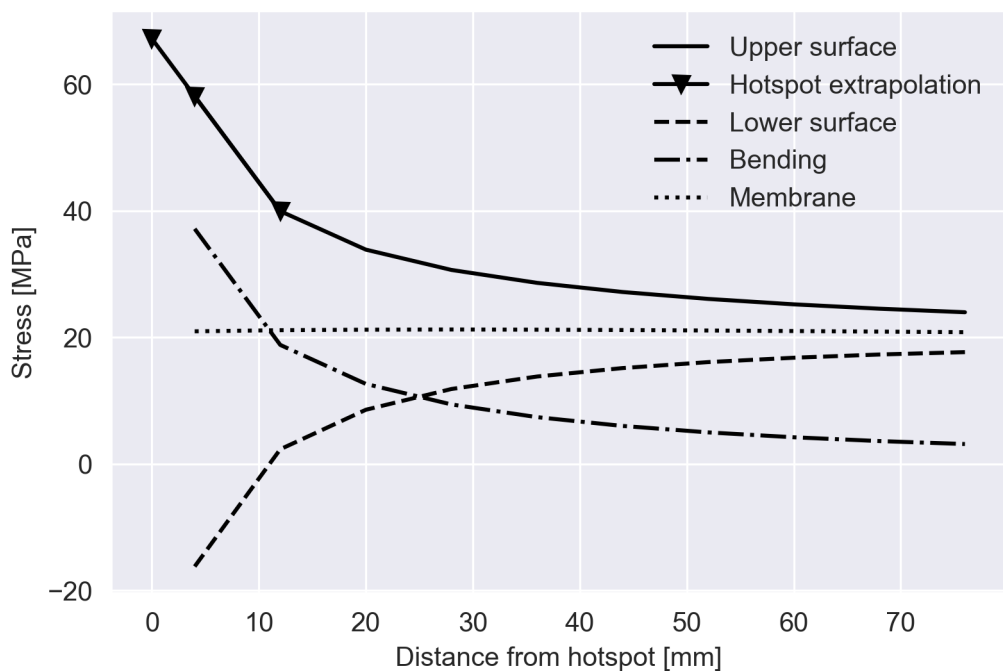
Figure 47: Hotspot stress extrapolation.

The abrupt change in the stress at the upper surface as one gets closer to the hotspot, reveals the difficulty of acquiring good results with a full nominal model. The outcome is very sensitive with respect to the position of the stress sampling point used in the nominal analysis for such an abrupt change. One could of course investigate the possibility of using a hotspot stress extrapolation to determine a suitable position for the stress sampling point for a full nominal analysis, though the authors consider this approach to be in conflict with the nominal stress method. The nominal method is based on stresses determined by classical analysis, and one runs the risk of positioning the sampling point in conflict with this. Neither is there a guarantee that the same distance from the hotspot is the optimal sampling point for all welds of this type in a full nominal analysis.

6.2   Trusses

The braces and chords considered in the K-joints display a different behavior than the orthotropic deck. As presented in Section 5.2, the calculated damage based on NS-EN 1993-1-9 is generally larger than damage calculated from DNVGL-RP-C203. According to the latter standard, the stresses tend to localize in the crown and saddle points (see Figure 13), meaning point 1, 3, 5 and 7 in Figure 14 (DNV AS, 2019b, p. 54). It is therefore of interest to identify where the largest damage value around the intersection of both brace and chord is.

The reason behind stress localizing in point 1, 3, 5 and 7 can be explained using basic mechanical knowledge as follows: Navier-Bernoulli's hypothesis states that plane sections remain plane. Based on the assumption that the material has a linear-elastic behaviour, the strain in the section will grow linearly in relation to the distance from the neutral axis. The stresses and strains will, according to Hooke's law, be proportional. As the distance from the neutral axis to points 1, 3, 5 and 7 are of maximum value, the stress in the fiber in one of these positions will be of maximum value as well. The in-between points (meaning point 2, 4, 6 and 8) are located closer to the neutral axis, and therefore, the stresses in these points will be smaller.

Calculated damage depends, as established through this report, on the fluctuation of stresses. The forces are as presented in Figure 48 below. From these plots, it can be observed that the axial force is the dominating force in the trusses, and bending moments (both in-plane and out-of-plane) are of small magnitude. The bending stresses can be connected to why the stresses localize in points 1, 3, 5 and 7. As bending stresses are linearly proportional to the distance from the neutral axis and the axial stress is constant through the entire section, they will either increase or decrease the total stress in the fiber located a maximum distance from the section centroid.
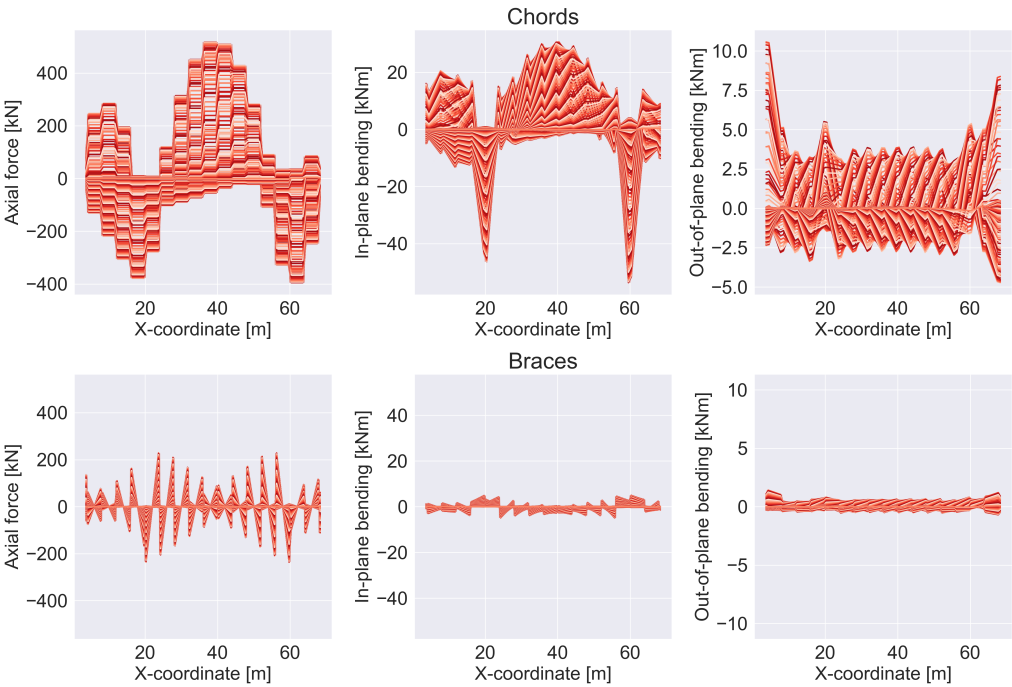

Figure 48: Force distribution in the lower K-joints of the left truss. Each line represents a time step of Lorry 3.

The distribution of damage calculated around the intersection of the braces and chords in the K-joint is shown in Figure 49 below. Figure 49a shows the damage calculated using DNVGL-RP-C203 as opposed to Figure 49b, where NS-EN 1993-1-9 have been used.

(a) DNVGL-RP-C203.
(b) NS-EN 1993-1-9.
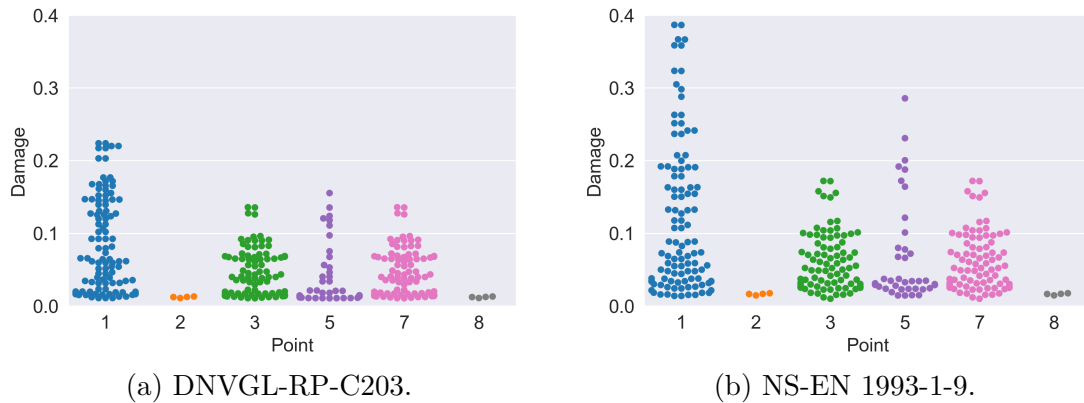
Figure 49: K-joint damage distribution at brace-chord intersection points in truss with original dimensions.

Figure 49 shows that damage calculated in the tubular K-joints with original dimensions for NS-EN 1993-1-9 and DNVGL-RP-C203 is similarly distributed. The only notable difference is the resulting damage from both standards. Using the Eurocode, maximum damage was approximately 0.39, and maximum damage resulting from DNVGL-RP-C203 turned out to be approximately 0.22. The maximum values are both found in point 1 in the intersection. As discussed (and expected), the largest stresses are found in this point, as well as in point 3, 5 and 7. Point 1 and 5 are located on the opposite side of each other in Figure 14, which will result in a larger stress in one point and a smaller stress in the opposite point due to the in-plane bending stress increasing or reducing the total stress in these points. Large in-plane bending also cause large fluctuations in the total stress, which are important for damage calculation. The same line of reasoning applies to point 3 and 7. However, it is observed that the damage values are more similar to each other in these points, both in shape and calculated damage values. This is due to out-of-plane bending being of such a small magnitude that it does not have a huge impact on the resulting damage. There is also some damage in point 2 and 8, which are the two closest points to point 1. Since the maximum stress is localized in the area around point 1, it makes sense that there will be some damage in these two points as well. No damage was calculated for point 4 and 6, which are the closest points around point 5.

A damage analysis for the valid dimensions of the truss section resulted in a similar distribution of damage around the intersection. The magnitude of damage, however, turned out to be *a lot* higher than 1 using both NS-EN 1993-1-9 and DNVGL-RP-C203. As mentioned in Section 5.2, the NS-EN 1993-1-9 damage was calculated to be approximately 9000, and for DNVGL-RP-C203, it was about 120. The stresses around the intersection are also of high magnitude (both in tension and compression) when analysing the model

with valid dimensions. The forces causing these stresses are illustrated in Figure 80 in the Appendix A.8. Because the cross-section is smaller, the total stresses will be higher in the intersection. From the figure, large fluctuations in the axial forces are observed. When calculating the axial stresses, there will also be large fluctuations in the stresses when applying the rainflow algorithm. As a consequence, the stress ranges will be much larger for the valid dimensions than the ranges calculated for the actual dimensions. Inserting these into the Palmgren-Miner summation rule for both NS-EN 1993-1-9 and DNVGL-RP-C203 yields damages of unreasonable values.

Another interesting observation is that the thickness effect, as discussed in Section 3.3, comes into play in the trusses. This only happens for the chords, as they have a thickness larger than the tubular joint reference thickness of 16 mm. The thickness term in the S-N equations effectively lowers the S-N curve, and might explain why some points in the truss have a larger DNVGL-RP-C203 damage than NS-EN 1993-1-9 damage. As mentioned in Section 3.4.2, NS-EN 1993-1-9 presents two single-sloped S-N curves, where the choice of either depends on a thickness ratio. A thickness ratio of 2 or more gives S-N curve 90 for NS-EN 1993-1-9, which is for smaller stress ranges still below the DNVGL-RP-C203 T-curve. As NS-EN 1993-1-9 fatigue calculation in joints are performed with S-N curves of a single slope $m = 5$ this difference grows significantly for higher stress ranges. NS-EN 1993-1-9 will for this reason give larger damages for all joints based on S-N curves alone. This also explains the huge difference in calculated damage for the two standards with truss dimensions valid according to NS-EN 1993-1-9.

6.2.1 Damage distribution in trusses

The damage is not distributed evenly in the truss, as discussed in Section 5.2.1. It is *not* uniformly distributed, with certain sections being more damaged than others, shown in Figure 44. The largest brace damages are observed at the intermediate supports of the bridge, while the largest chord damages are observed in the mid-span of the bridge. This can be explained with the help of the deformation pattern of the trusses as a lorry crosses the bridge, as shown in Figure 50.
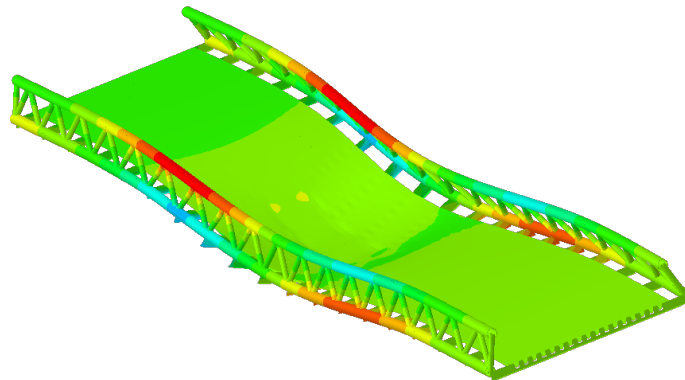

Figure 50: Deformation of the trusses and deck when lorry 3 is positioned in the middle of the bridge.

The figure shows that the trusses bend inwards towards the lorry as it crosses, giving the elements axial forces and bending moments resulting in tensile and compressive stresses. Because the axial forces are of such a large magnitude, the axial stresses will also be large. The bending stresses will be smaller, due to small bending moments (both in-plane and out-of-plane). This is pointed out in Figure 48. At the supports, the trusses are restrained against movement, and the forces tend to localize in the braces. Therefore, there will be large fluctuations in the brace-stresses as the lorries cross the bridge. As a consequence, the damage will be larger there.

The same line of reasoning applies to the top chords in the mid-span of the truss. As the lorry crosses, more and more tension forces will be transferred to the upper chords, which means more stress localization there. Because of stress ranges of significant value, the damage in the chord sections in the upper K-joints are large.

6.3 Design fatigue factors

The relationship between safety implementation in NS-EN 1993-1-9 and DNVGL-RP-C203 is to a degree linked for the bridge. NS-EN 1993-1-9 introduces partial factors, whose value is determined based on design philosophy and the consequence of failure. For bridges, the safe life method is prescribed by the Norwegian National Annex of NS-EN 1993-1-9, in which the partial factor is intended to ensure that the structure maintains integrity over its design life.

DNVGL-RP-C203 refers to DNVGL-OS-C101 for design fatigue factors. The DFFs are in this standard chosen based on the environment the detail is in, inspection regime, and ease of inspection. Though not stated explicitly, one can consider the design philosophy in DNVGL-RP-C203 to be similar to the damage tolerant method in NS-EN 1993-1-9. However - for details inaccessible for inspection, DNVGL-RP-C203 assigns a DFF equal to 3. The bridge in this thesis is most certainly accessible for inspection, but arguably the rest of the description for a detail with a DFF of 3 fits with the philosophy of safe life design. Figures 45e and 45c, which consider damage calculation with partial factor $\gamma_{Mf} = 1.35$ and design fatigue factor $DFF = 3$, lends support to this assessment as they give similar results.

The authors would like to stress that the Norwegian National Annex of NS-EN 1993-1-9 stipulates stricter partial factors than what the main part of this Eurocode does. Partial factors as specified outside the National Annex have not been investigated, and could give more divergent results between a detail given a DFF (based on being inaccessible for inspection), and a partial factor (based on a safe life designed structure with low consequences for failure). This indicates that the connection is only loosely based on the rules set in NS-EN 1993-1-9 and DNVGL-RP-C203.

6.4 Limitations

In order to narrow the modeling effort, few hotspot analyses has been performed. Hotspot analyses have only been performed for the most damaged welds based on the nominal analyses in order to assess the validity of the latter. Although this gives an indication of the relationship between hotspot and nominal analyses, it is not very extensive. This was not prioritized as this report focuses on comparing NS-EN 1993-1-9 and DNVGL-RP-C203, and any consequence of modeling errors here will be the same for damage calculation with both standards.

Loads are implemented in a simplified manner and could be more complex and closer to real life than in this report. The generic bridge has only one one-way driving lane, centered in the middle of the bridge, with pedestrian lanes on each side. The effect of lorries diverging from the driving lane center line as allowed for in NS-EN 1991-2, has also been excluded. Figures 28, 34 and 38 demonstrate that the damages in the orthotropic deck are located mostly where the wheels of the lorries pass. Including offsets from the lane center line is therefore likely to give favorable results, an effect of more interest in a built structure than a generic bridge intended for the comparison of two standards. These simplifications have been done to narrow the scope of the report, but comes at the cost of similar load distributions in the trusses at each side of the bridge.

Though not a limitation, the authors would like to note that damage has not been calculated using histograms, where stress ranges $\Delta\sigma$ are placed in stress range bins and their associated load cycles N are summed. This has been done to allow for better visualization on damage calculation plots, as this makes assessment of the differences between nominal and hotspot models easier. Although a histogram is suggested in both NS-EN 1993-1-9 (p. 30-32) and DNVGL-RP-C203 (p. 20), the approach in this report is equivalent to applying a histogram with a large number of bins.

7 Conclusions and suggestions for further work

The study has resulted in multiple valuable insights into the relationship between NS-EN 1993-1-9 and DNVGL-RP-C203, and has shown that a generic bridge is a useful tool for generating multiple realistic data points. Final conclusions on the deck and the truss, and suggestions for further work will be presented in the following.

7.1 Generic bridge

With NS-EN 1993-1-9 and DNVGL-RP-C203 approaching fatigue calculation slightly different at multiple points (such as S-N curves and procedures), there are many causes for divergent outcomes when comparing damage calculated by the two standards. In this regard, the use of a generic bridge as an analysis tool proved useful. By considering every possible location for the details, a large number of data points could be generated as presented in the scatter plots in this report. This avoids unfortunate sampling of data points skewed to any direction - an important feature as the scatter plots comparing NS-EN 1993-1-9 and DNVGL-RP-C203 show that damages can be clustered together at varying levels of divergence between the two standards.

7.2 Orthotropic deck

Both NS-EN 1993-1-9 and DNVGL-RP-C203 are well suited for fatigue analysis in the orthotropic deck. This gave a large set of data points to probe the relationship between safety implementation in the standards. NS-EN 1993-1-9 seems preferential for fatigue analysis in orthotropic decks as the less strict S-N curves in this standard results in less damage, and the details in an orthotropic deck are defined explicitly. For some details, nominal analysis requires modeling considerations to avoid stress raising geometries, but is otherwise very efficient.

7.3 Trusses

The fatigue analysis of the trusses were a challenge, with the most challenging part being NS-EN 1993-1-9 itself. One of many disadvantages with this standard is that NS-EN 1993-1-9 is not robust enough to cover dimensions larger than the ones specified. Also, it is unclear in describing what to do when this is the case.

In contrast, DNVGL-RP-C203 gives an elaborate way to analyze tubular joints of almost all dimensions. One thing Dr.techn. Olav Olsen AS was worried about when using this standard, was that the damage calculated using DNVGL-RP-C203 would be different compared to damage calculation using NS-EN 1993-1-9. This is the case, and is illustrated

clearly in Figure 49, where the maximum damage from NS-EN 1993-1-9 in point 1 is almost twice as large as the damage found from DNVGL-RP-C203 in the same point. Using this Recommended Practice will generate non-conservative results. Although this might be of concern if DNVGL-RP-C203 is to be used for design of structures governed by NS-EN 1993-1-9, there are several aspects to consider. First of all, DNVGL-RP-C203 is a document intended for structures placed in rough offshore environments, and is extensively used for this purpose. Thus, there is reason to believe that the non-conservative results when compared to NS-EN 1993-1-9 are due to the limitations associated with NS-EN 1993-1-9, and not any faults within DNVGL-RP-C203 itself. This is underlined implicitly by the results found for the orthotropic deck. For the relevant details here, both standards provide a thorough approach and they both generate comparable results, as opposed to the truss, where only DNVGL-RP-C203 presents a detailed approach.

7.4   Design fatigue factors and partial factors

This section only relates to results in the orthotropic deck, because NS-EN 1993-1-9 proved inferior to DNVGL-RP-C203 for fatigue calculation in the K-joints.

As mentioned in Section 3.3, use of partial factors from NS-EN 1993-1-9 can be applied in conjunction with DNVGL-RP-C203, though this has two major drawbacks. One is rather obvious in that one is not consistent in regards to which standard is used when designing a structure, and this might not be accepted by the contracting client and the proprietor of the standard. The other major drawback is that use of partial factors in damage calculation has been found to be rather conservative for DNVGL-RP-C203, as mentioned in Section 5.3. This is because the use of partial factors effectively lowers the S-N curve, placing a larger part of the stress ranges where the S-N curves in NS-EN 1993-1-9 and DNVGL-RP-C203 diverge. By comparing $\gamma_{Mf} = 1.35$ and $DFF = 3$ as in Figures 45c and 45e, one can see that less damage is calculated for DNVGL-RP-C203, while still being conservative relative to NS-EN 1993-1-9.

The authors would like to point out that if diverging from the rules stipulated in the standards is an option, a curve fitted DFF as performed in this report can be a good alternative approach. Curve fitted DFFs will circumvent the problem of borrowing rules from another standard and get overly conservative results related to a DFF of 3, although this comes with its own problems. One is that the safety introduced by the DFF is no longer linked explicitly to any inspection regime as detailed in DNVGL-OS-C101, but implicitly to whichever safety approach in NS-EN 1993-1-9 it is curve fitted to. The other problem that might be of concern is that a curve-fitted DFF will give DNVGL-RP-C203 damages both conservative and non-conservative relative to NS-EN 1993-1-9.

In conclusion, safety in fatigue analysis can be implemented in multiple ways. Less damage can be calculated with DNVGL-RP-C203 by combining rules from NS-EN 1993-1-9 and DNVGL-RP-C203 or adjusting DNVGL-RP-C203 to fit NS-EN 1993-1-9. The authors believe that the results in this report indicate that such approaches can be reasonable.

7.5   Suggestions for further work

The subject covered in this report is wide and complex. Especially on the subject of damage in the trusses, there is a potential for more work to be done. The authors have identified points which could be further elaborated in the future by building on the same techniques used in this report.

7.5.1   Trusses

In this report, the truss was analysed with the original dimensions suggested by Dr.techn. Olav Olsen AS and dimensions valid according to NS-EN 1993-1-9. The original dimensions gave reasonable stresses well below the yield strength of construction steels, and demonstrated how the single sloped S-N curves of NS-EN 1993-1-9 discussed in Section 3.4 cause NS-EN 1993-1-9 to calculate damage of higher magnitude than DNVGL-RP-C203. The study on the valid dimensions gave unreasonable results with damages well above 9000 for NS-EN 1993-1-9, due to the high stress ranges resulting from only reducing the dimensions of the truss members.

Further study on fatigue in the trusses of a generic bridge with valid truss dimensions can thus be a good candidate for further work on the topic of comparing NS-EN 1993-1-9 and DNVGL-RP-C203. This would require some consideration regarding the structure to avoid large stress ranges in the truss. Unfortunately, this cannot be done by changing the cross sections of the truss, as this is limited by NS-EN 1993-1-9. The authors would like to suggest two different approaches. The first and simplest approach would be to scale down the axial loads from the trucks, something which unfortunately would be in violation of the loads that the Eurocodes stipulate. A second (but more elaborate) approach would be to place the trucks to one of the sides of the bridge, which is likely to cause less damage in the truss at the opposite side. A drawback with this approach is that the truss closest to the trucks might experience stresses exceeding the yield strength of the steel.

7.5.2   Thickness effects

Finally, the authors would like to suggest investigating details where damage calculation diverges more than those investigated in this report. This can be done by increasing the thickness of the detail members above the reference thickness in DNVGL-RP-C203. This has only been briefly investigated in the original truss dimensions. For details in the deck, some details are given different S-N curves based on thicknesses. This was briefly brought up in Section 4.2.3, but as the thickness of the T-profile cross beam web was at the limits of the S-N curve designation, it was ignored.

References

Aardal, A. B. (2012). *Utmattingsstandarden DNV-RP-C203 mot Eurokode 3, del 1-9: Utmattingspåkjente konstruksjoner.* Master thesis, Norwegian University of Life Sciences. Available at: `http://hdl.handle.net/11250/188983` (Accessed: 2021-01-20).

Bell, K. (2014). *An engineering approach to Finite Element Analysis of linear structural mechanics problems.* 1st ed. Fagbokforlaget.

Callister W. D. & Rethwisch, D. G. (2015). *Materials Science and Engineering.* 9th ed. Wiley.

Campbell, F. C., ed. (2008). *Elements of Metallurgy and Engineering Alloys.* 1st ed. Materials Park: ASM International.

Cook, R. D., Malkus, D. S., Plesha, M. E., and Witt, R. J. (2002). *Concepts and applications of finite element analysis.* 4th ed. Wiley.

CRM Engineering Services (2021). *Simple Tubular Joint SCF.* Available at: `https://www.simple-tubular-scf.com/` (Accessed: 2021-03-06).

Dahle, E. A. and Smith-Solbakken, M. (2020). Alexander Kielland-ulykken. *Store Norske Leksikon.* Available at: `https://snl.no/Alexander_Kielland-ulykken` (Accessed: 2021-02-13).

Dewesoft (2021). *Fatigue Analysis, Damage calculation, Rainflow counting.* Available at: `https://training.dewesoft.com/storage/pro/courses/fatigue-analysis.pdf` (Accessed: 2021-05-11).

DNV AS (2019a). *DNVGL-OS-C101: Design of offshore steel structures, general - LFRD method.* Available at: `https://rules.dnv.com/docs/pdf/DNV/OS/2019-07/DNVGL-OS-C101.pdf` (Accessed: 2021-01-28).

— (2019b). *DNVGL-RP-C203: Fatigue design of offshore steel structures.* Available at: `https://oilgas.standards.dnvgl.com/download/dnvgl-rp-c203-fatigue-design-of-offshore-steel-structures` (Accessed: 2021-01-28).

Dowling, N. E. (2013). *Mechanical Behavior of Materials : Engineering Methods for Deformation, Fracture and Fatigue.* 4th ed. Pearson Education.

European Committee for Standardization (2021). *Structural: Eurocodes.* Available at: `https://www.cen.eu/work/areas/construction/eurocodes/pages/default.aspx` (Accessed: 2021-04-05).

Hellevik, L.R. (2020). *Numerical Methods for Engineers.* Available at: `https://folk.ntnu.no/leifh/teaching/tkt4140/` (Accessed: 2021-02-12).

Hiatt, J. (2019). *Rainflow Counting.* Available at: `https://community.sw.siemens.com/s/article/rainflow-counting` (Accessed: 2021-04-20).

Janiszewski, P. (2020). *rainflow*. Available at: `https://pypi.org/project/rainflow/` (Accessed: 2021-03-22).

Jones, E., Oliphant, T., Peterson, P., et al. (2001). *SciPy: Open source scientific tools for Python*. Available at: `http://www.scipy.org/` (Accessed: 2021-03-26).

Larsen, P. K. (2010). *Dimensjonering av stålkonstruksjoner*. 2nd ed. Fagbokforlaget.

Lotsberg, I. (2016). *Fatigue Design of Marine Structures*. Cambridge University Press.

Lovegrove, P. (2021). *DNV GL changes name to DNV as it gears up for decade of transformation*. Available at: `https://www.dnv.com/news/dnv-gl-changes-name-to-dnv-as-it-gears-up-for-decade-of-transformation-194340` (Accessed: 2021-03-05).

Nussbaumer, A., Borges, L., and Davaine, L. (2011). *Fatigue design of steel and composite structures : Eurocode 3: design steel structures: Part 1-9 - Fatigue : Eurocode 4: design of composite steel and concrete structures*. 1st ed. Wiley-Blackwell ECCS Ernst & Sohn.

Schijve, J. (2004). *Fatigue of Structures and Materials*. 1st ed. Springer.

Simulia (2020). *Abaqus 6.14 Analysis User's Guide*. Available at: `http://130.149.89.49:2080/v6.14/books/usb/default.htm` (Accessed: 2021-02-13).

Standard Norge (2009). *NS-EN 1993-2:2006+NA:2009 Eurocode 3: Design of steel structures - Part 2: Steel bridges*. Available at: `https://www.standard.no/no/Nettbutikk/produktkatalogen/Produktpresentasjon/?ProductID=405251` (Accessed: 2021-01-28).

— (2010a). *NS-EN 1991-2:2003+NA:2010 Eurocode 1: Actions on structures - Part 2: Traffic loads on bridges*. Available at: `https://www.standard.no/no/Nettbutikk/produktkatalogen/Produktpresentasjon/?ProductID=425440` (Accessed: 2021-01-28).

— (2010b). *NS-EN 1993-1-9:2005+NA:2010 Eurocode 3: Design of steel structures - Part 1-9: Fatigue*. Available at: `https://www.standard.no/no/Nettbutikk/produktkatalogen/Produktpresentasjon/?ProductID=416513` (Accessed: 2021-01-28).

— (2021). *About us*. Available at: `https://www.standard.no/en/toppvalg/about-us/#.YLjW8i0ePu0` (Accessed: 2021-04-05).

Statens Vegvesen (2015). *Håndbok N400 Bruprosjektering: Prosjektering av bruer, ferjekaier og andre bærende konstruksjoner*. Available at: `https://www.vegvesen.no/_attachment/865860/binary/1030718?fast_title=Håndbok+N400+Bruprosjektering.pdf` (Accessed: 2021-01-28).

Total Materia (2010). *Linear Elastic Fracture Mechanics: Part One*. Available at: `https://www.totalmateria.com/page.aspx?ID=CheckArticle&site=KTS&NM=299` (Accessed: 2021-04-10).

Vinogradov, Alexey (2019a). "Lecture 11: Fatigue Damage Characterization". [PowerPoint presentation]. *TMM 4195 Fatigue Design.* Available at: `https://ntnu.blackboard.com` (Accessed: 2021-04-07).

— (2019b). "Lecture 13-1: Fatigue Design". [PowerPoint presentation]. *TMM 4195 Fatigue Design.* Available at: `https://ntnu.blackboard.com` (Accessed: 2021-04-07).

— (2019c). "Lecture 2: Stress-based approach". [PowerPoint presentation]. *TMM 4195 Fatigue Design.* Available at: `https://ntnu.blackboard.com` (Accessed: 2021-04-07).

A   Appendix

Further results and theory relevant for the details in the orthotropic deck and trusses are presented in this appendix. The Python scripts used to automate the finite element analyses and extraction of them are presented at the end.

A.1 S-N Curves

DNVGL-RP-C203 defines the maximum for all S-N curves as curve B1. As S-N curve B1 (and B2) has a slope of $m = 4$ instead of $m = 3$ for less than $N = 10^7$ cycles, S-N curves C and C1 have multiple slopes. The S-N curve pairs B1/160, B2/140, C/125 and C1/112 are therefore not included in Figure 51.
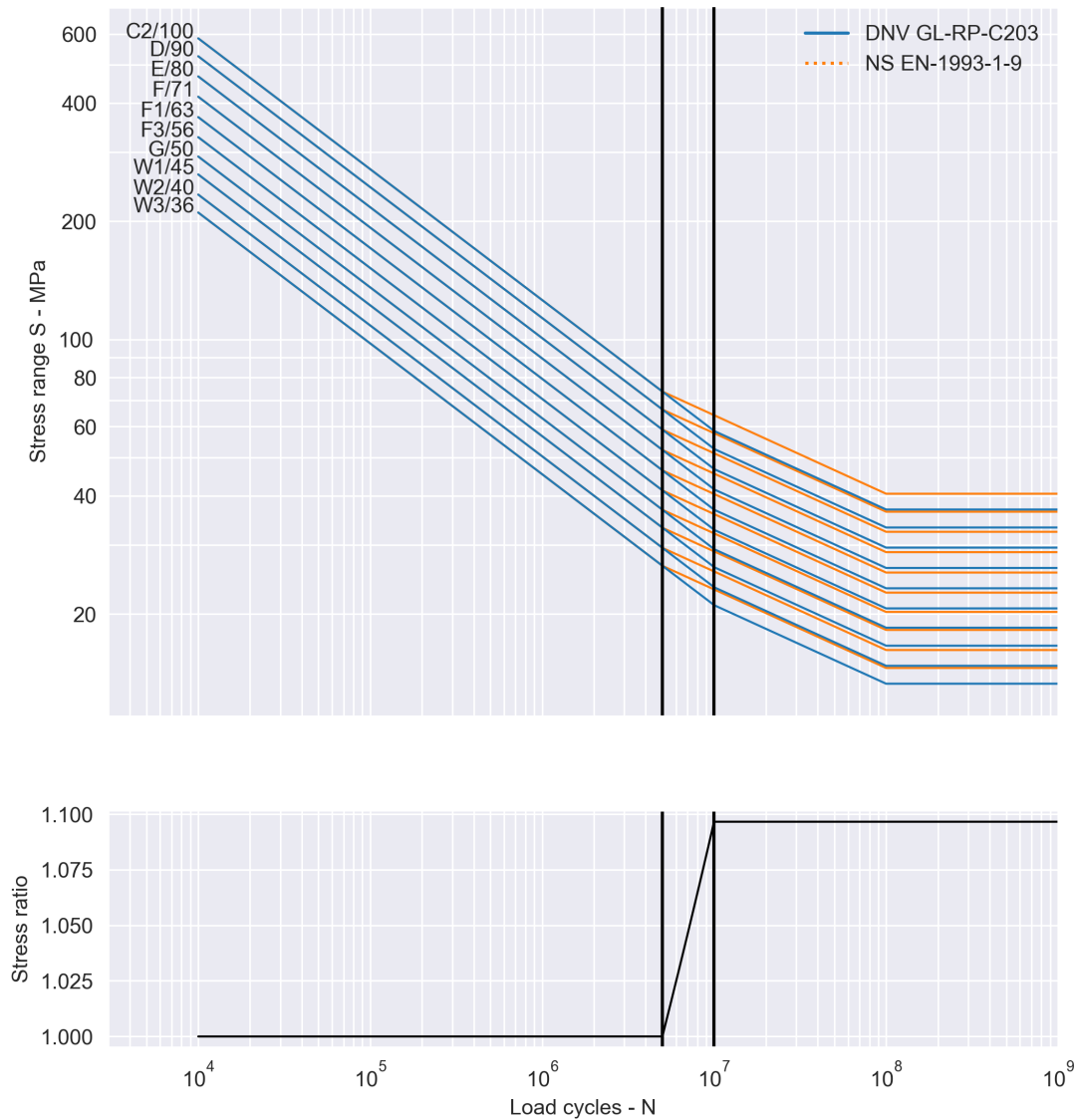

Figure 51: S-N curve comparison for NS-EN 1993-1-9 and DNVGL-RP-C203.

A.2 Construction drawings

The figures in this section show detailed dimensions of the generic bridge presented in Section 4.
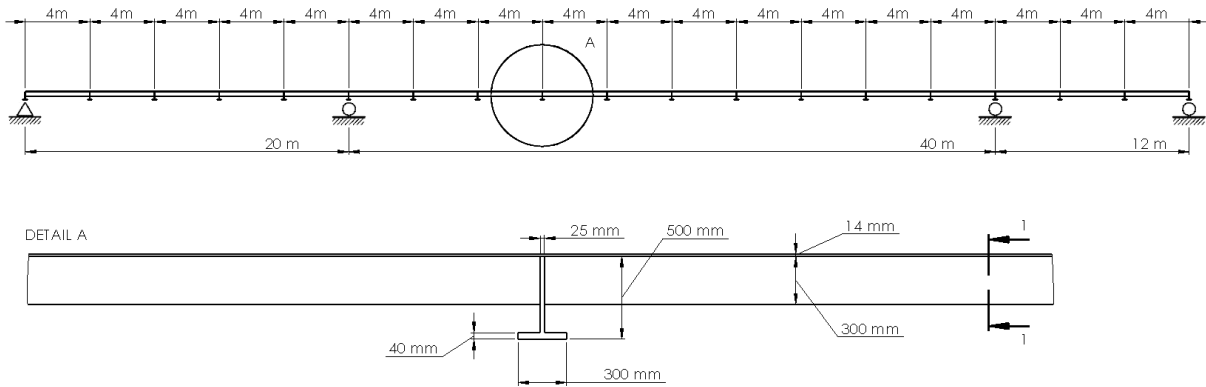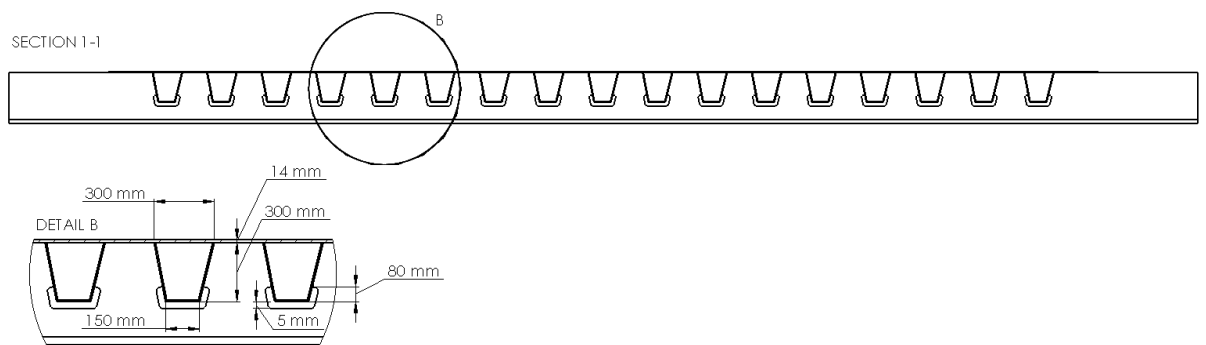

Figure 52: Bridge support layout.

Figure 53: Bridge transverse T-profile beam cutouts and longitudinal trapezoidal stringers geometry.
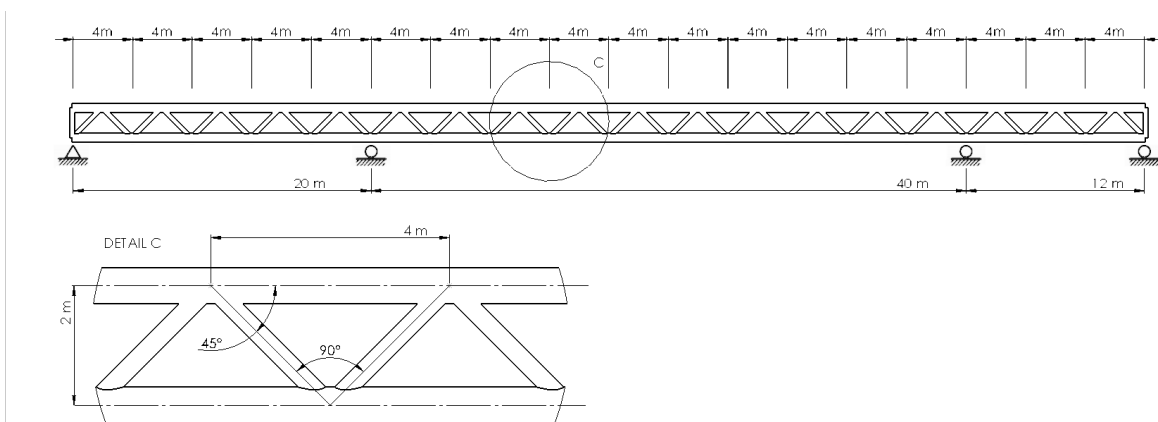

Figure 54: Truss geometry.

A.3   Mesh calibration

As discussed in section 2.4.4, element calibration was performed in accordance with NS-EN 1993-1-9. As all details considered for fatigue in the orthotropic deck are located on the longitudinal stringers, only one calibration is required for an element mesh of S8R elements with size $8mm \cdot 8mm$.

The geometry shown in Figure 6 was modelled in Abaqus FEA as seen in Figure 55 below, with inputs as listed in Table 9 to calibrate the element mesh by comparing SCFs. The plate with a tubular insert was modelled with 6965 S8R elements. A partition was added to ensure a regular $t \cdot t$ mesh in the hotspot where stress was to be sampled for calibration. Loading was applied with a magnitude of 100 MPa chosen for simplification of SCF calculation. The stress at the intersection of the plate and tubular insert was 193 MPa, yielding a SCF of 1.93. This gives a result comparable to that of plotted values from the DNVGL-RP-C203 as seen in Figure 56, and S8R elements with $8mm \cdot 8mm$ element size in the hotspot region can be considered calibrated.
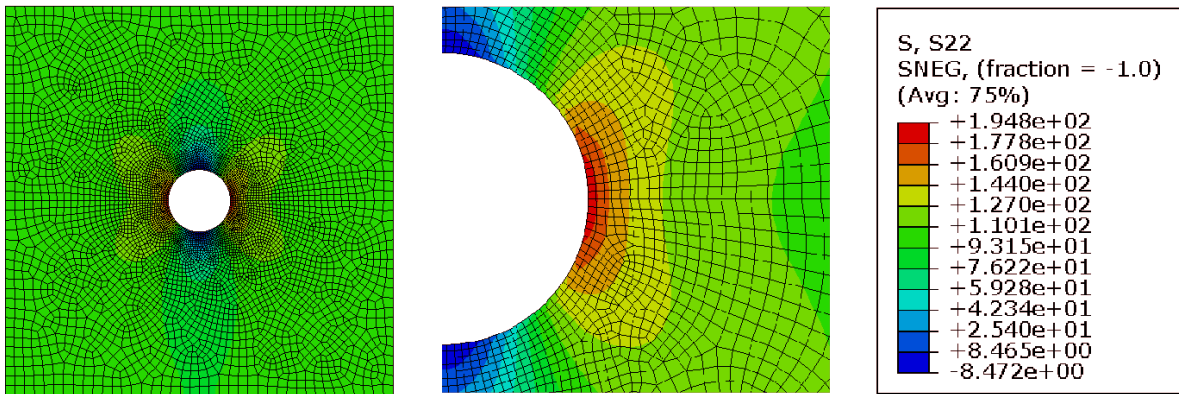
Figure 55: Calibration of mesh for hotspot method by comparison with experimental SCF values in DNVGL-RP-C203.

Table 9: Abaqus element calibration model inputs.

t_r	t_p	r	H	W^*
8 mm	8 mm	160 mm	40 mm	2000 mm

*Width of plate. Chosen large in the Abaqus
model to avoid end effects.
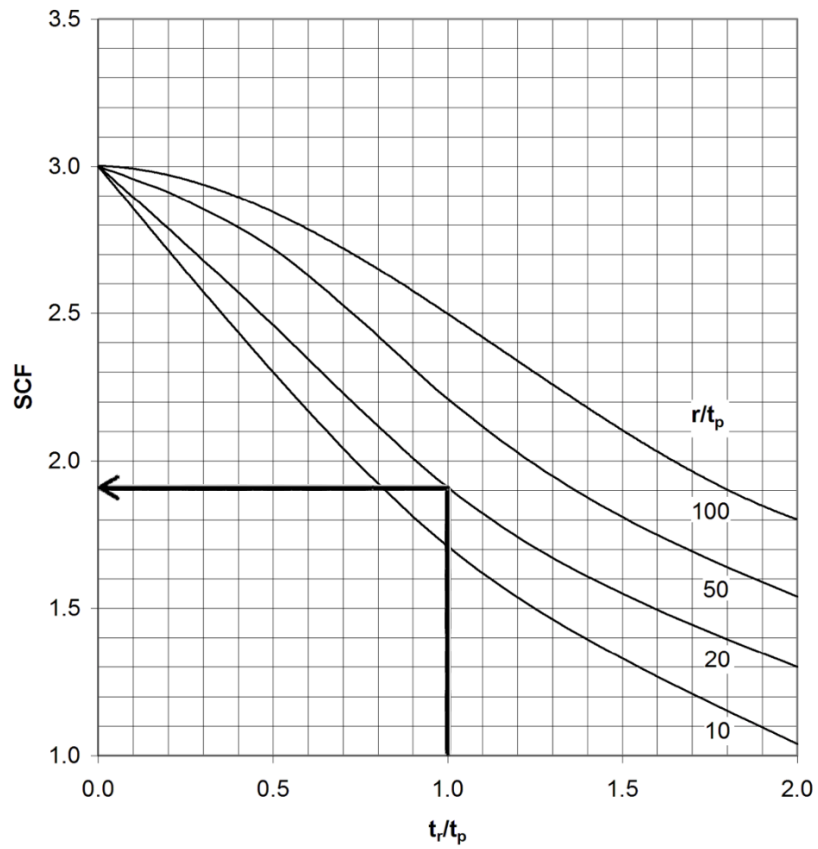
Figure 56: Stress concentration factor in plate with tubular insert with tube height H, thickness t_r and ratio $H/t_r = 5$ (DNV AS, 2019b, Figure C-4, p. 178).

A.4 Orthotropic deck details load spectra plots

The load spectra resulting from every lorry specified in FLM4 crossing the bridge are presented in this section. The following figures are results from nominal analyses performed in the most damaged locations in the details considered in the orthotropic deck. They are presented in the same order as in the main part of this report.

A.4.1 Stringer-cover welds
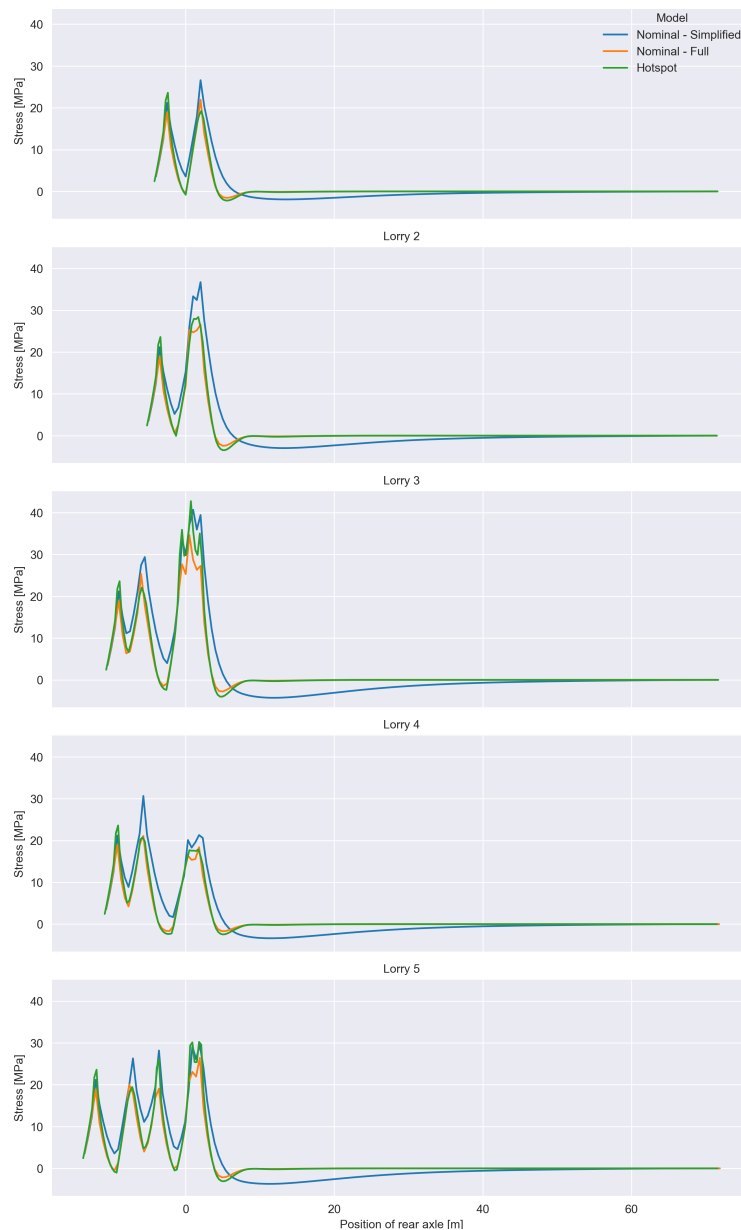
Figure 57: Stringer-cover weld load spectra at most damaged location according to full nominal analysis.
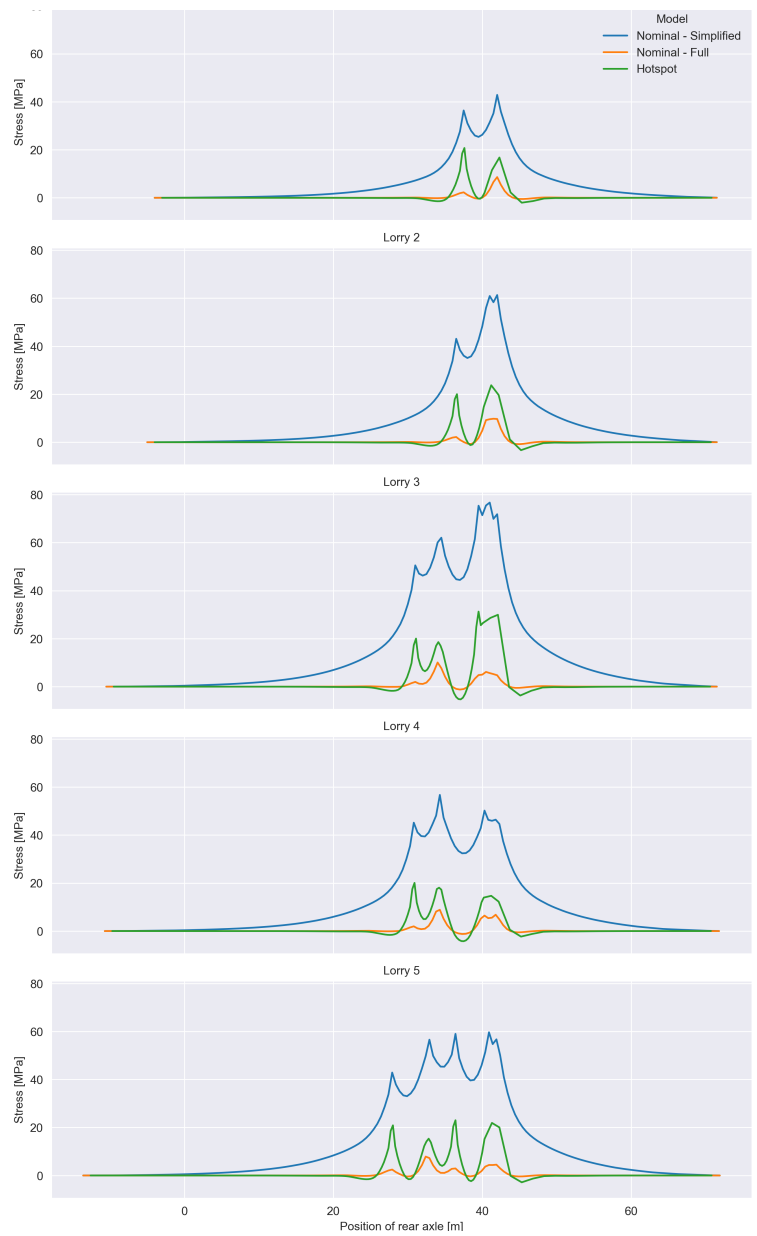
Figure 58: Stringer-cover weld load spectra at most damaged location according to simplified nominal analysis.

A.4.2 Stringer splices
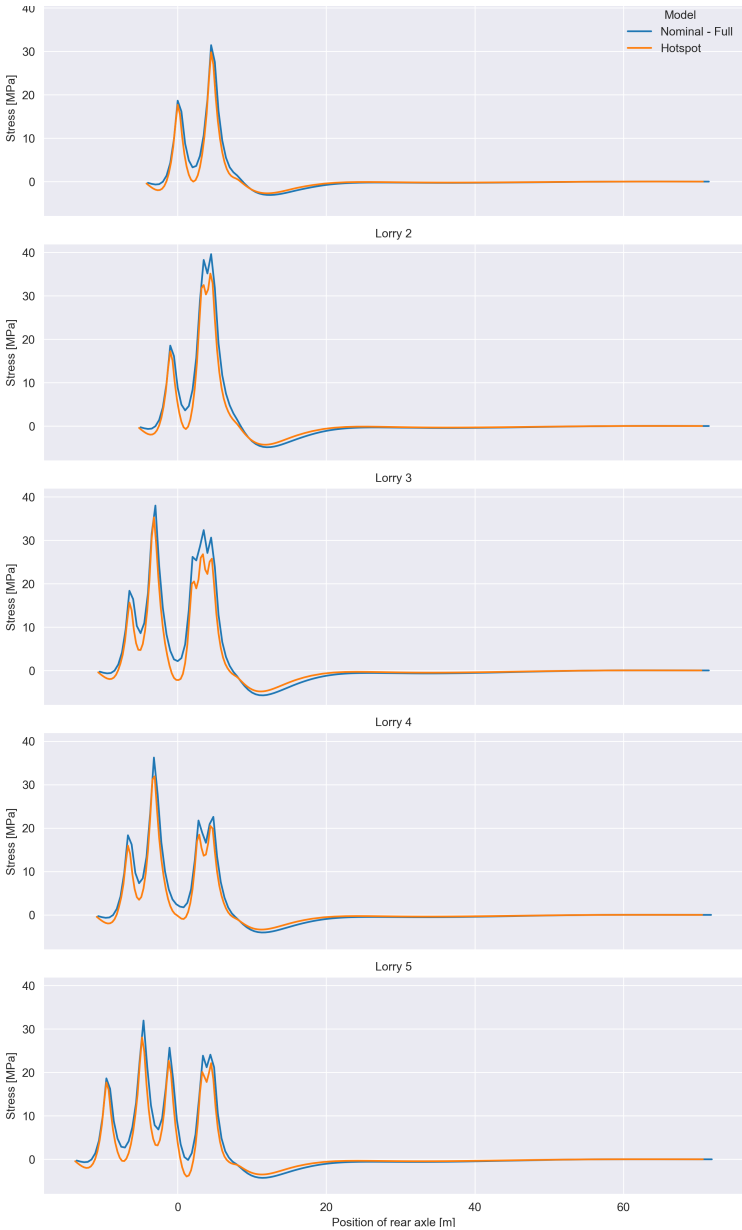
Figure 59: Stringer-cover weld load spectra at most damaged location according to full nominal analysis.

A.4.3   T-profile cutout welds
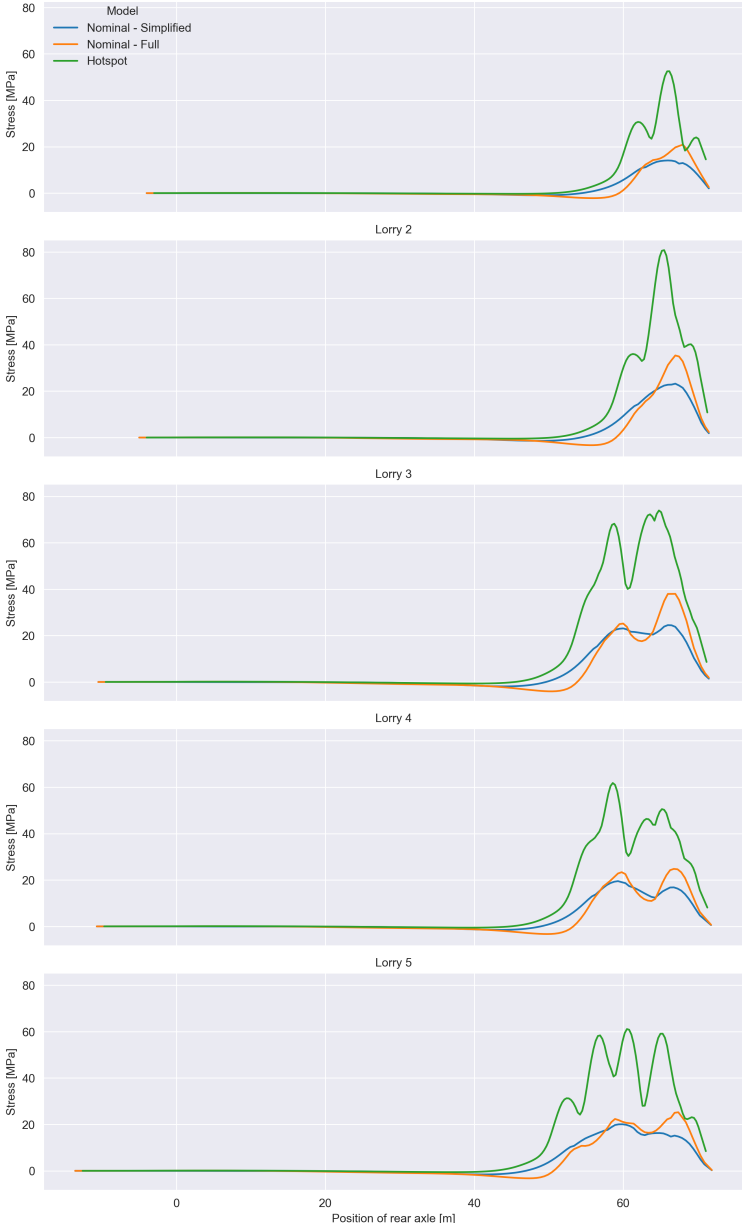
Figure 60: T-profile cutout weld load spectra at most damaged location according to full nominal analysis.
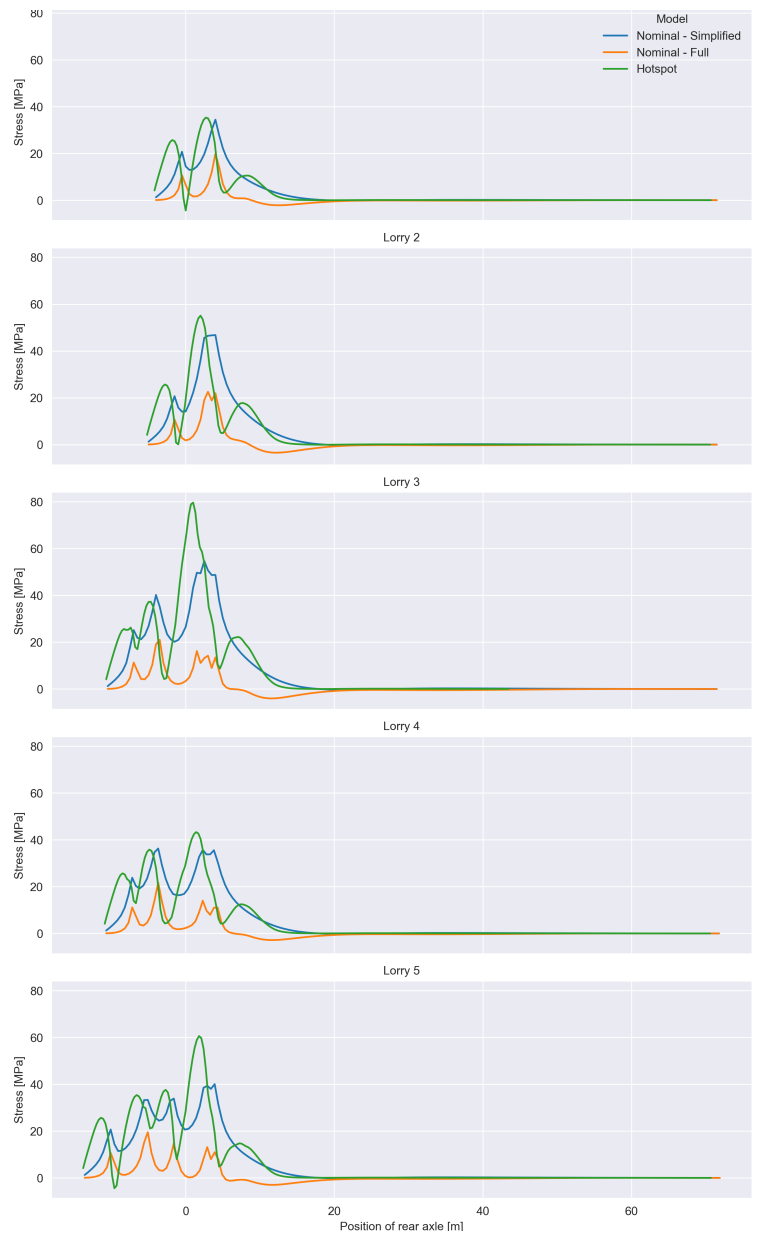
Figure 61: T-profile cutout weld load spectra at most damaged location according to simplified nominal analysis.

A.5 Orthotropic deck details damage scatter plots

Scatter plots are presented in this section for damages calculated with partial factor $\gamma_{Mf} = 1.35$ and design fatigue factors $DFF = 1$, 2, and 3, as well as a curve fitted $DFF = 2.64$. Partial factor plots found in Section 5.1 are repeated here for readability.

A.5.1 Stringer-cover welds

Figure 62: Nominal stress method damage for stringer-cover welds in orthotropic deck, full and simplified model on elastic supports. Partial factor $\gamma_{mf} = 1.35$.

Figure 63: Nominal stress method damage for stringer-cover welds in orthotropic deck, full and simplified model on elastic supports. Design fatigue factor $DFF = 1$.

Figure 64: Nominal stress method damage for stringer-cover welds in orthotropic deck, full and simplified model on elastic supports. Design fatigue factor $DFF = 2$.
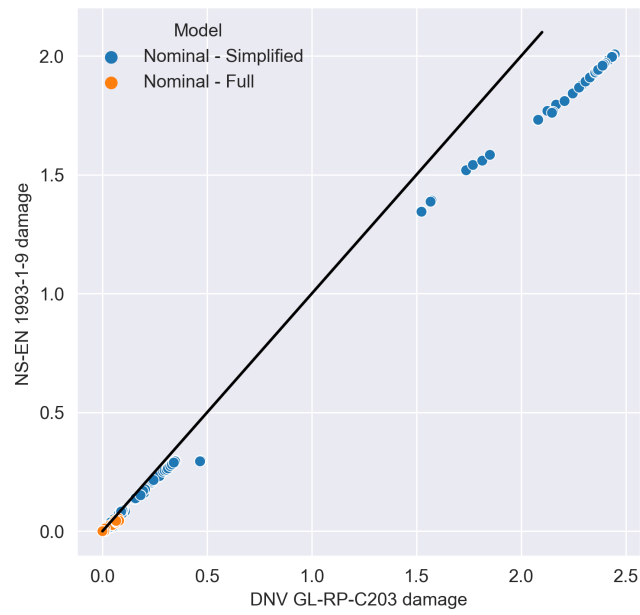
Figure 65: Nominal stress method damage for stringer-cover welds in orthotropic deck, full and simplified model on elastic supports. Design fatigue factor $DFF = 3$.
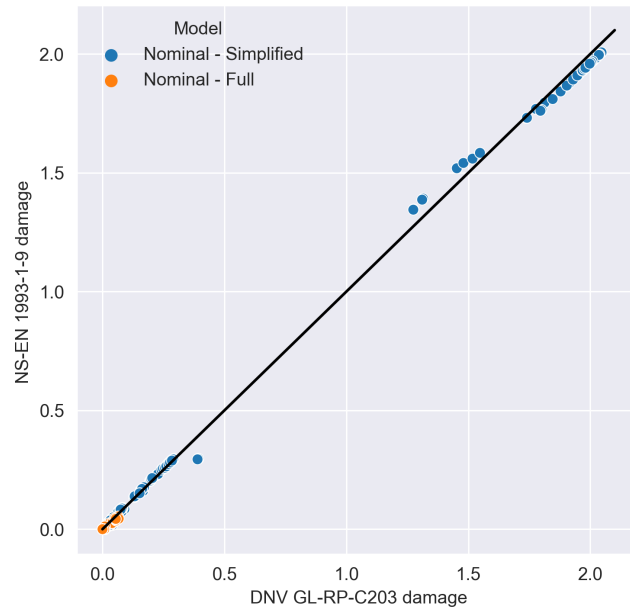
Figure 66: Nominal stress method damage for stringer-cover welds in orthotropic deck, full and simplified model on elastic supports. Curve fit Design fatigue factor $DFF = 2.64$.

A.5.2 Stringer splices

The simplified model with elastic supports was not used to determine nominal stresses for the stringer splice welds in the orthotropic deck.
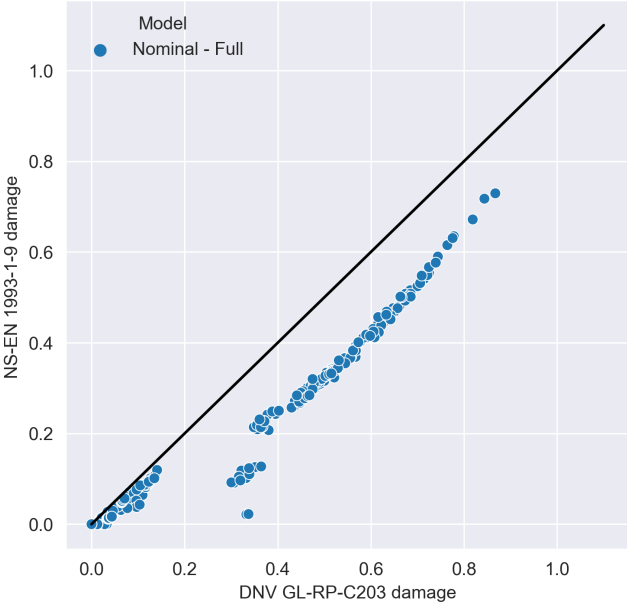
Figure 67: Nominal stress method damage for stringer splices in orthotropic deck, full model. Partial factor $\gamma_{mf} = 1.35$.
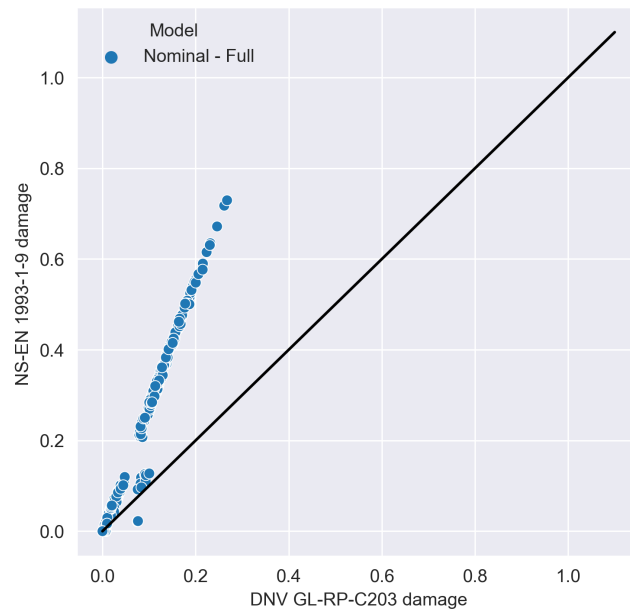
Figure 68: Nominal stress method damage for stringer splices in orthotropic deck, full model. Design fatigue factor $DFF = 1$.
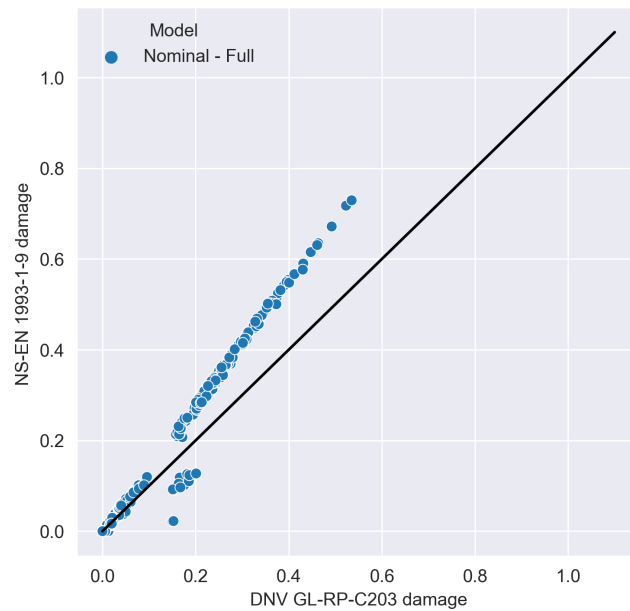
Figure 69: Nominal stress method damage for stringer splices in orthotropic deck, full model. Design fatigue factor $DFF = 2$.
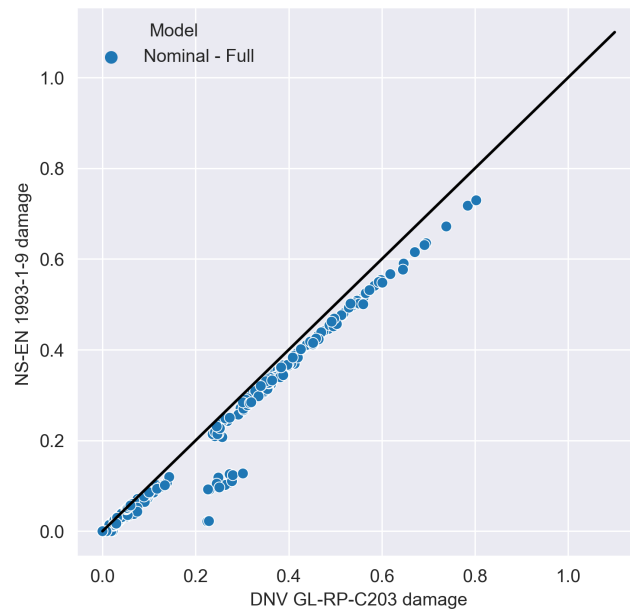
Figure 70: Nominal stress method damage for stringer splices in orthotropic deck, full model. Design fatigue factor $DFF = 3$.
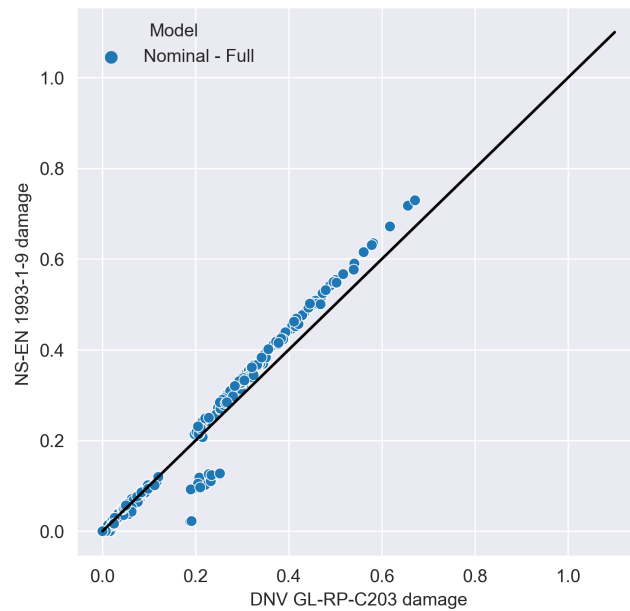
Figure 71: Nominal stress method damage for stringer splices in orthotropic deck, full model. Curve fit design fatigue factor $DFF = 2.64$.

A.5.3 T-profile cutout welds
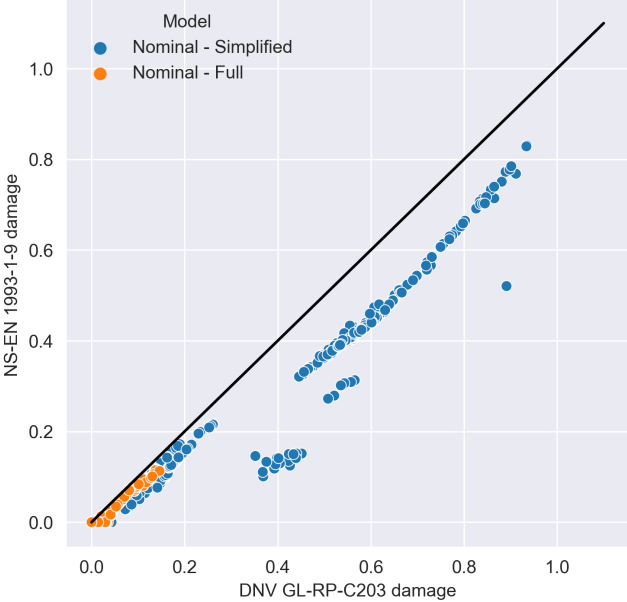
Figure 72: Nominal stress method damage for cutouts in orthotropic deck, full and simplified model on elastic supports. Partial factor $\gamma_{mf} = 1.35$.
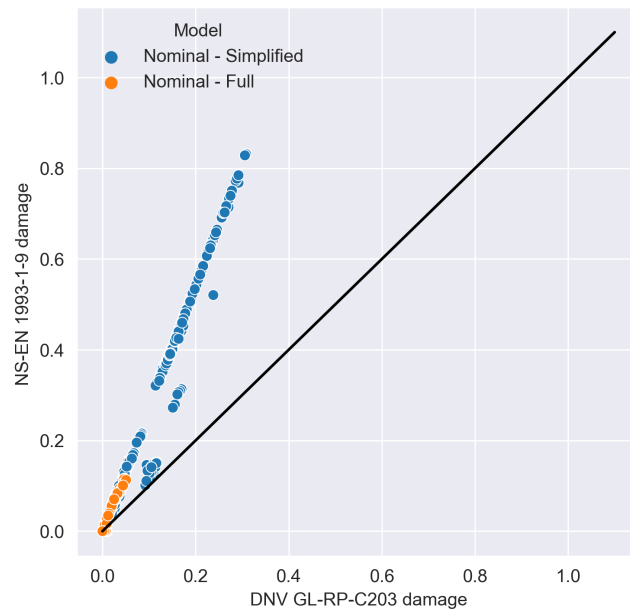
Figure 73: Nominal stress method damage for cutouts in orthotropic deck, full and simplified model on elastic supports. Design fatigue factor $DFF = 1$.
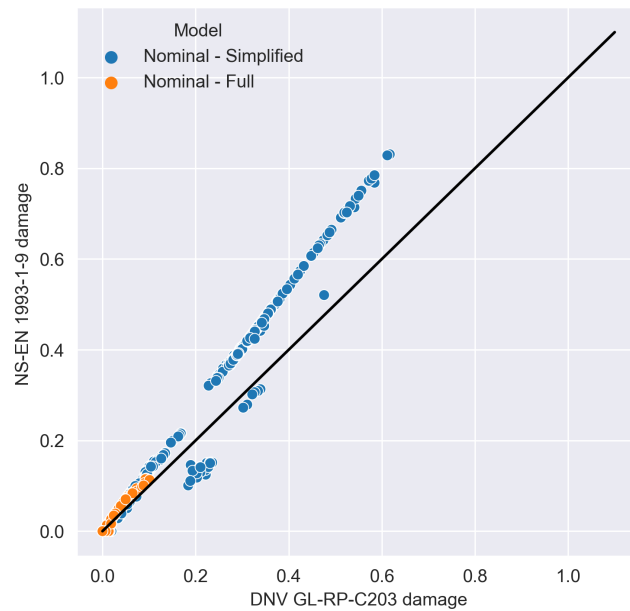
Figure 74: Nominal stress method damage for cutouts in orthotropic deck, full and simplified model on elastic supports. Design fatigue factor $DFF = 2$.
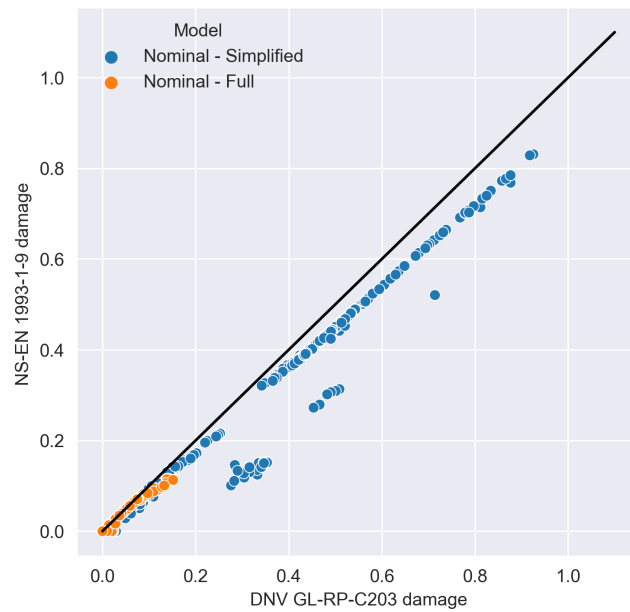
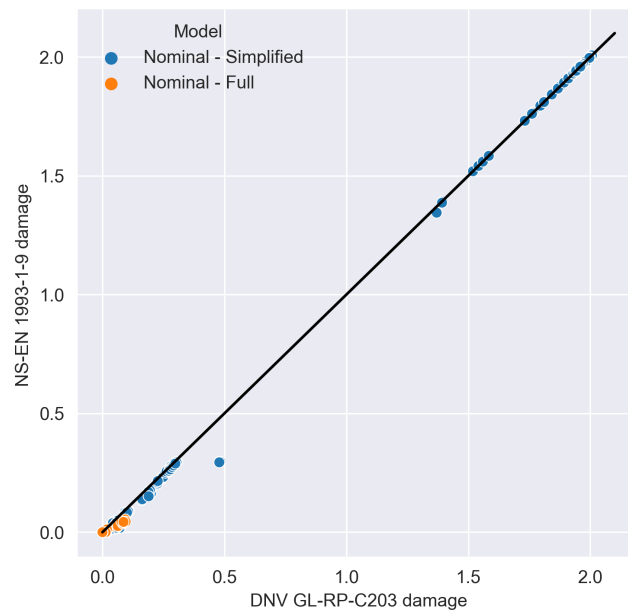Figure 75: Nominal stress method damage for cutouts in orthotropic deck, full and simplified model on elastic supports. Design fatigue factor $DFF = 3$.
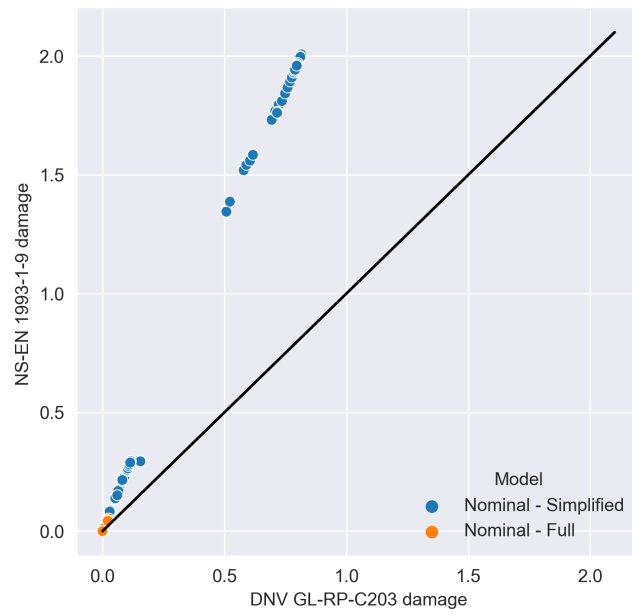

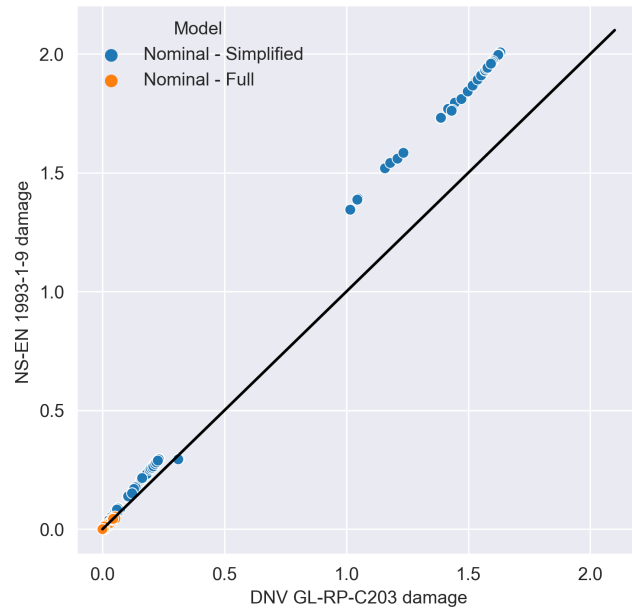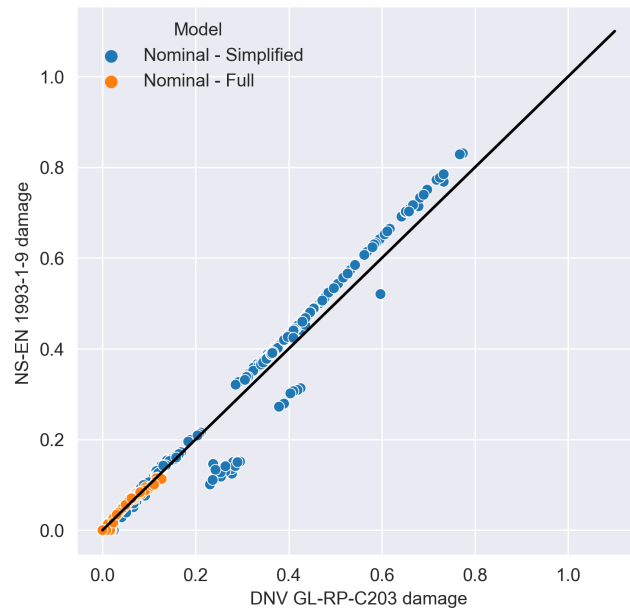Figure 76: Nominal stress method damage for cutouts in orthotropic deck, full and simplified model on elastic supports. Curve fit design fatigue factor $DFF = 2.64$.

A.6 Damage calculation for trusses with valid dimensions

The results from the analysis of the truss with valid dimensions according to NS-EN 1993-1-9 are presented here. Figure 77 shows the calculated damages in the integration points of the B31 elements in each K-joint. The maximum damage calculated for NS-EN 1993-1-9 turned out to be over 9000, whereas the calculated DNVGL-RP-C203 damage turned out to be about 120.
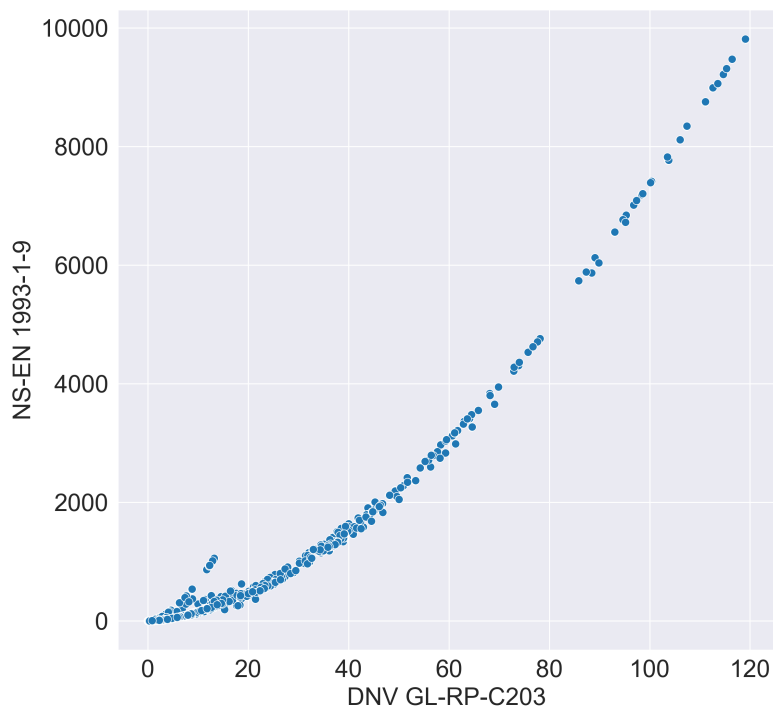
Figure 77: Damage calculated for the truss, using both NS-EN 1993-1-9 and DNVGL-RP-C203. Dimensions are within the validity range described in NS-EN 1993-1-9.

Figure 78a below shows the damage calculated in the eight points around the intersection between brace and chord. The values on the y-axes (or damage-axes) are also adjusted to each other to improve readability, as damage calculated using DNVGL-RP-C203 is so small compared to NS-EN 1993-1-9 damage.
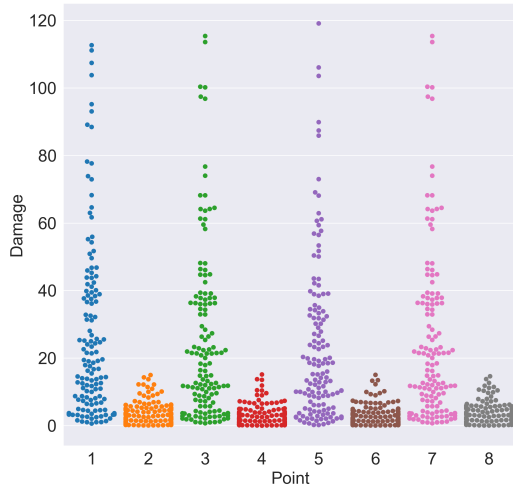
(a) DNVGL-RP-C203.
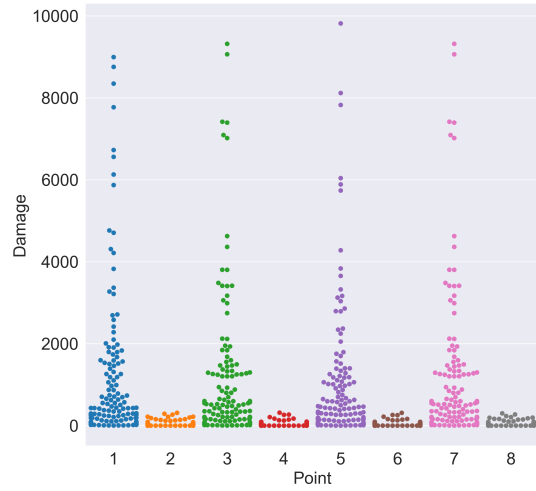
(b) NS-EN 1993-1-9.

Figure 78: K-joint damage distribution at brace-chord intersection points. Truss dimensions within the validity range of NS-EN 1993-1-9.

Observe that every point are significantly damaged with values well above 1. The distribution of damage is also very similar in points 1, 3, 5, and 7, where the maximum damage in each of them are equivalent to the maximum total damage resulting from both standards, as shown in Figure 77. The same is observed in the in-between points 2, 4, 6 and 8, although the maximum damage for these points are much smaller.

A.7 Full damage distribution plots for truss

The full damage distribution plot for the left truss analysed with original dimensions is presented in Figure 79 below. It has been split in half and rotated 90° to keep them both on the same page, as well as for readability reasons.
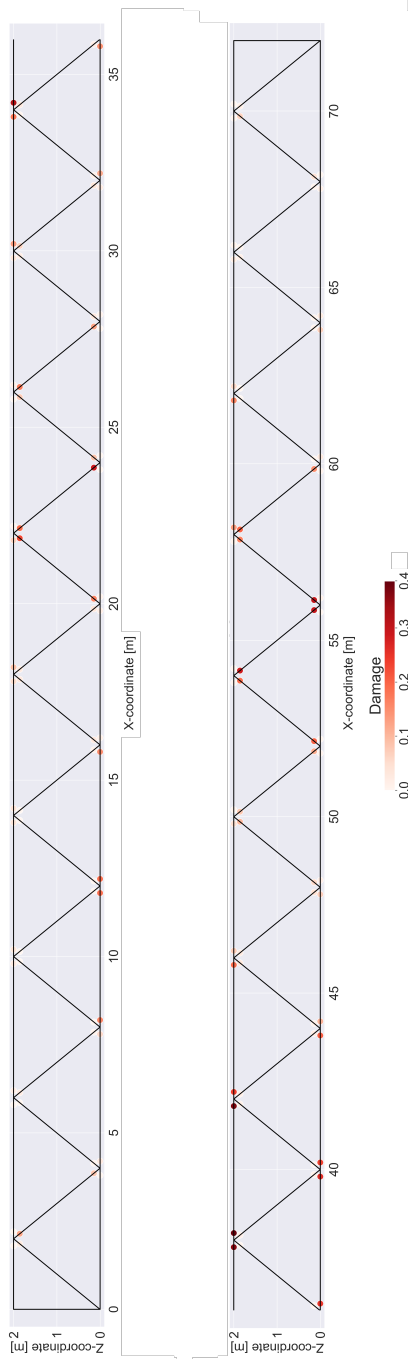
Figure 79: Damage distribution in left side truss. Damage calculation based on NS-EN 1993-1-9.

A.8 Force distribution in left truss with valid dimensions

Figure 80 shows the force distribution in the lower part of the left truss, plotted for both braces and chords. The plot is used to show that the damage is mainly a result from localization of axial stresses in the elements of the truss.
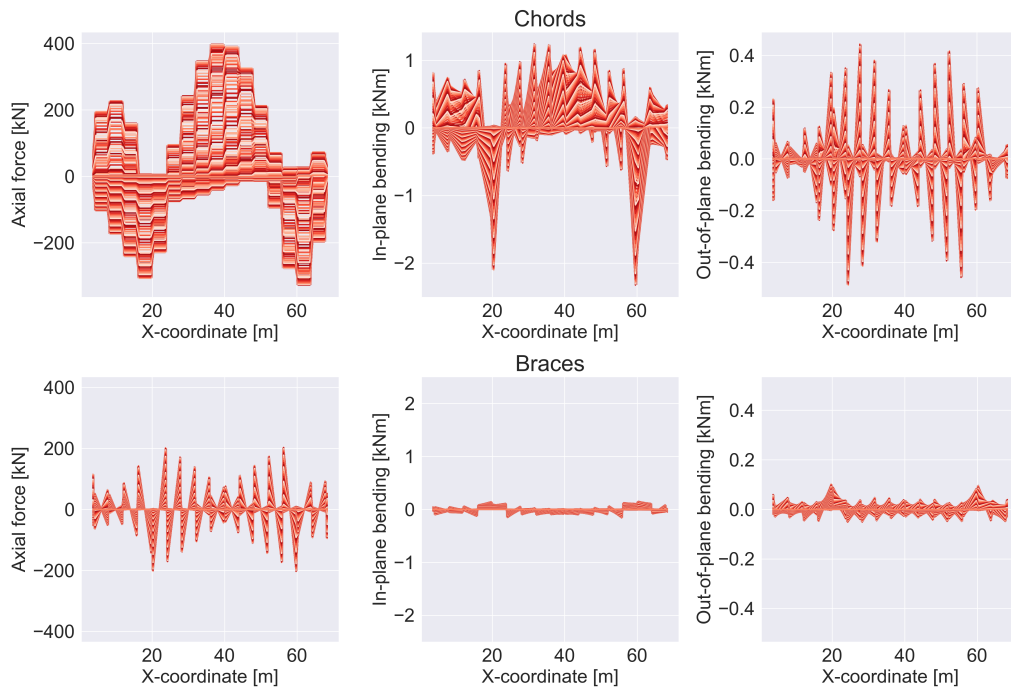
Figure 80: Force distribution in the lower K-joints of the left truss, valid dimensions.

A.9 Python Scripts

The main scripts in this thesis are presented in this section. Note that the Python scripts used for Abaqus FEA input file generation and sampling of output stresses are presented in a generalized manner.

A.9.1 Abaqus FEA input file generation

```python
# -*- coding: utf-8 -*-
import os
import shutil


"""
Script for generation of Abaqus input files for FLM4 with Eurocode
    ↪ 1991-2.

Nils Arne Rakstad
"""



scaleFactor = 1000

#import from TrafficModels.py
from TrafficModels import *



#create Fatigue load model 4 (FLM4)
FLM = FLM(4,'FLM4')
FLM.createLorries()
l1 = FLM.getLorry(1)
l2 = FLM.getLorry(2)
l3 = FLM.getLorry(3)
l4 = FLM.getLorry(4)
l5 = FLM.getLorry(5)
lorries = {'L1':l1,'L2':l2,'L3':l3,'L4':l4,'L5':l5}

V2_startValues= {'A':0.25, 'B':0.25,'C':0.25}

wheelPressure = {'A':274.122, 'B':148.809, 'C':242.247}

#lane
laneNumber = 1
```

```
#Input for different lanes. Y-offset across the deck
ys={1 : 5}
offset = 0


folderName = # Link to folder where FLM ODB-files are stored
runFolder = r'..\..\..' #relative link to Abaqus files



inputText = """**
#### use include statements to include parts such as the bridge and
    ↪ wheel sets in the Fatigue Load Models
*include, input={folderName}\\ # inputFile.inp
**
** ASSEMBLY
### Insert assembly instances here. Node and element sets.###
**
{wheelAssemblyText}
**
** Constraint: Truck
*Tie, name=Truck, adjust=no, position tolerance=0.01, no thickness
{tieText}
**
*End Assembly
** MATERIALS
### Define material properties
**
**
** BOUNDARY CONDITIONS
### Insert boundary conditions
** ----------------------------------------------------------------
**
** STEP: Truck
**
*Step, name=Truck, nlgeom=NO
*Static
1., 1., 1e-05, 1.
**
** LOADS
**
** Name: A Type: Pressure
*Dsload
{loadText}
**
** OUTPUT REQUESTS
**
```

```
*Restart, write, frequency=0
**
** FIELD OUTPUT: F-Output-1
**
*Output, field
*Node Output
CF, RF, U
*Element Output, directions=YES
LE, NFORC, P, PE, PEEQ, PEMAG, S, SF
*Contact Output
CDISP, CSTRESS
**
** HISTORY OUTPUT: H-Output-1
**
*Output, history, variable=PRESELECT
*End Step
"""

inputTextAssemblyWheel = """**
*Instance, name=DECK{wheelName}, part=FLM_4_{wheelType}
        {x}, {y}, 0.0005
*End Instance
**
"""



inputTextTie = """DECK{wheelName}.Tie, "Orthotropic cover-1".Plate"""

loadText = "DECK{wheelName}.DECK,␣P,␣{pressure}"

#iterate over all lorries:
for lorryName,lorry in lorries.items():
    fileNames=[]

    #gt lorry axle.
    axles = lorry.getAxles()

    xLastAxle = lorry.getX(1)
    axleNumbers = list(lorry.getAxleNumers())
    xFirstAxle = lorry.getX(axleNumbers[-1])

    lorryLength = xFirstAxle - xLastAxle
    lastAxleAt = xLastAxle - lorryLength
```

```python
lastAxleCoordiantes = []
fileDir = os.path.join(folderName,FLM.name)

if not os.path.isdir(fileDir):
    os.makedirs(fileDir)

fileDir = os.path.join(fileDir,lorryName)

if not os.path.isdir(fileDir):
    os.makedirs(fileDir)

fileDir = os.path.join(fileDir,str(round(offset,1)))
if not os.path.isdir(fileDir):
    os.makedirs(fileDir)


#set x = -1*lorry length. This places the first axle at the bridge.
x=lorryLength*-1
i=0


#Bridge length, adjust for other bridges.
modelLength = 72
while x < modelLength:

    assemblyString = ""
    tieString = ""
    loadString = ""

    i += 1

    fileName = '{}_{}_Dist_{}.inp'.format(lorryName,round(x,1),round(
        ↪ offset,1))

    file = os.path.join(fileDir, fileName)
    f=open(file,'w')
    wheels_included = {}

    for axle in axles:
        position,area,kN,wheel_type = axles[axle]
        xAxle = x + position
        scaleLoad = kN/100.0*scaleFactor
        if not wheel_type in wheels_included:
            wheels_included[wheel_type]=0
            wheelName = wheel_type
```

```python
            else:
                wheels_included[wheel_type] += 1
                wheelName = "{}_{}".format(wheel_type,wheels_included[
                    ↪ wheel_type])


            if xAxle > 0 and xAxle < modelLength:


                pressure = wheelPressure[wheel_type] * scaleLoad
                loadString += loadText.format(wheelName=wheelName,pressure=
                    ↪ pressure) + '\n'
                y = ys[laneNumber] + offset
                assemblyString += inputTextAssemblyWheel.format(wheelName=
                    ↪ wheelName,wheelType=wheel_type,x=xAxle,y=y)
                tieString += inputTextTie.format(wheelName=wheelName)+'\n'




    posFirstAxle = xFirstAxle + x
    posLastAxle = xLastAxle + x
    x = x+0.5

    f.write(inputText.format(folderName=runFolder,wheelAssemblyText=
        ↪ assemblyString[:-1],tieText=tieString[:-1], loadText=
        ↪ loadString[:-1]))
    f.close()
    fileNames.append(fileName)

#Create script that runs all inp-files on laptop
fileNameBat = os.path.join(fileDir,'runAll.bat')
fBat = open(fileNameBat,'w')
for fileName in fileNames:
    fBat.write('call abaqus j={} cpus=2 ask_delete=OFF interactive\n'.
        ↪ format(fileName[:-4]))
fBat.close()


#create script that runs all inp-files on data-cluster
fileNameJobaba = os.path.join(fileDir,'jobaba')
fJobaba = open(fileNameJobaba,'w')


fJobaba.write("#!/bin/bash\n\n#SBATCH -J abaqus\n#SBATCH -o abaqus.%j.
    ↪ out\n#SBATCH -n 4\n#SBATCH --ntasks-per-core=1\n\nsingularity 
    ↪ run -B /opt:/opt /opt/ohpc/pub/apps/centos7.img <<EOF\nsource /
    ↪ opt/ohpc/pub/apps/intel/compilers_and_libraries/linux/bin/
```

```
          ↪ compilervars.sh␣intel64\n\nunset␣SLURM_GTIDS\n")

    for fileName in fileNames:
        fJobaba.write("/opt/ohpc/pub/apps/abaqus/Commands/abq2019␣job={}␣
            ↪ cpus=$SLURM_NTASKS␣double␣interactive\n".format(fileName
            ↪ [:-4]))
    fJobaba.write('EOF\n')
    fJobaba.close()
```

```
# -*- coding: utf-8 -*-

"""
Script for generation of lorries for FLM in Eurocode 1991-2.

Nils Arne Rakstad
"""


class Lorry():
    def __init__(self,name,printOn):
        self.name = name
        self.axles = {}
        if printOn:
            print("Create␣Loory␣{}".format(self.name))

    def getX(self,axleNumber):
        """ Return x coordiante for a specified axle number """
        if axleNumber in self.axles:
            x,area,load,wheelType = self.axles[axleNumber]
            return x
        else:
            print("Axle␣number␣{}␣not␣found␣for␣{}".format(axleNumber,self
                ↪ .name))
            print("Returning␣x=␣0")
            x = 0
        return x

    def getWheelArea(self,wheelType):
        """Return length and width for predfined wheels. According to
            ↪ table 4.8 in EN-1991-2.
        Input:
            wheelType: - string - ['A','B','C']"""
        if wheelType == 'A':
            length = 0.32
```

```python
            width = 0.22
            area = length * width
        if wheelType == 'B':
            length = 0.32
            width = 0.54
            area = length * width
        if wheelType == 'C':
            length = 0.32
            width = 0.27
            area = length * width
        return length,width,area


    def addAxleWidth(self,width):
        """Add width between wheels at a axle.
        Input:
            width - float - distance between wheels at a axle. """
        self.width = width


    def getAxleWidth(self):
        return self.width


    def getAxleNumers(self):
        "Return axle numbers "

        return self.axles.keys()


    def addAxle(self, axleNumber, xAdd=None, area=0, load=0, x=0, printOn=
    ↪ False):
        """add axle and load
        Input:
            axleNumber - integer - axle number
            xAdd - float - space from previos axis [m] (Set 0 for first
                ↪ axis)
            x - float - location of axis. If not xAdd is used
            area - float or 'A,B'C' - area of tyre pressue [m2]
            load - float - load [kN]
            """
        if xAdd:
            if axleNumber > 1:
                previousAxle = axleNumber - 1
                xPrev = self.getX(previousAxle)
                x = xAdd + xPrev
            else:
                x = xAdd
```

```python
        if area == 'A':

            wheelType = 'A'
            area = self.getWheelArea(wheelType)
        elif area == 'B':

            wheelType = 'B'
            area = self.getWheelArea(wheelType)
        elif area == 'C':

            wheelType = 'C'
            area = self.getWheelArea(wheelType)
        else:
            wheelType = 'User Defined'

        self.axles[axleNumber]=x,area,load,wheelType
        if printOn:
            print("Axle {} added. X = {}, Load = {} kN, wheel type: {}".
                ↪ format(axleNumber, round(x,1), load, wheelType))


    def getAxle(self, axle):
        """ return axle properties for a specified axle
        Return:
            x - float - location of axle [m] (x=0 for last axle)
            area - float - area of tyre pressue [m2]
            load - float - load [kN]
            wheelType - string - 'A','B','C', 'User Defined'
        """
        if axle in self.axles:
            return self.axles[axle]
        else:
            print("Axle {} not defined. Available axle: {}".format(axle,
                ↪ self.axle.keys()))
            pass

    def getAxles(self):
        """ return axles properties """
        return self.axles

    def getNumberOfAxles(self):
        """ get number of defined axles """
        return len(self.axles)
```

```python
class FLM():
    def __init__(self, modelNumber,name):
        self.modelNumber = modelNumber
        self.name = name
        self.lorries={} #Store lorry objects

        self.numberOfPassings = 0 #total number of lorries
        self.looriesPassings = {} #passes per lorry

    def getModel(self):
        return self.model

    def getName(self):
        return self.name

    def addLorry(self,lorryNumber,lorryObject):
        """ Add a lorry object to FLM model
        Input:
            lorryNumber - int - lorry number in FLM
            lorryObject - Lorry - Lorry object
            """

        self.lorries[lorryNumber] = lorryObject

    def createLorries(self,printOn=False):
        if self.modelNumber == 3:
            l1 = Lorry('FLM3_1',printOn)
            l1.addAxle(1,0,'C',120,printOn)
            l1.addAxle(2,1.2,'C',120,printOn)
            l1.addAxle(3,6.0,'C',120,printOn)
            l1.addAxle(4,1.2,'C',120,printOn)
            self.lorries[1] = l1

        if self.modelNumber == 4:
            l1 = Lorry('FLM4_1',printOn)
            l1.addAxle(1,0,'B',130,printOn)
            l1.addAxle(2,4.5,'A',70,printOn)
            self.lorries[1] = l1

            l2 = Lorry('FLM4_2',printOn)
            l2.addAxle(1,0,'B',120,printOn)
            l2.addAxle(2,1.3,'B',120,printOn)
            l2.addAxle(3,4.2,'A',70,printOn)
            self.lorries[2] = l2
```

```python
        l3 = Lorry('FLM4_3',printOn)
        l3.addAxle(1,0,'C',90,printOn)
        l3.addAxle(2,1.3,'C',90,printOn)
        l3.addAxle(3,1.3,'C',90,printOn)
        l3.addAxle(4,5.2,'B',150,printOn)
        l3.addAxle(5,3.2,'A',70,printOn)
        self.lorries[3] = l3

        l4 = Lorry('FLM4_4',printOn)
        l4.addAxle(1,0,'B',90,printOn)
        l4.addAxle(2,1.8,'B',90,printOn)
        l4.addAxle(3,6,'B',140,printOn)
        l4.addAxle(4,3.4,'A',70,printOn)
        self.lorries[4] = l4

        l5 = Lorry('FLM4_5',printOn)
        l5.addAxle(1,0,'C',80)
        l5.addAxle(2,1.3,'C',80)
        l5.addAxle(3,4.4,'C',90)
        l5.addAxle(4,3.6,'B',130)
        l5.addAxle(5,4.8,'A',70)
        self.lorries[5] = l5



    def getLorries(self):
        """ Return dictonary with lorries defined in FLM model"""
        return self.lorries

    def getLorry(self,lorryNumber):
        """Return a defiend lorry for FLM model
        Input:
            lorryNumber - int - lorry number in self.lorries dictonary
        Return:
            lorryObject (self.lorries[lorryNumber])
            """
        if lorryNumber in self.lorries:
            return self.lorries[lorryNumber]
        else:
            print('Lorry {} not defined'.format(lorryNumber))
            print('Lorries defined {}'.format(self.lorries.keys()))
            pass

    def addLorryPassings(self,lorryNumber,passings,fixedNumber=False):
        if passings <= 1:
```

```python
            "assume ratio of total passings"
            lorryPassings = self.numberOfPassings * passings

        elif passings <= 100:
            "assume ratio in persent of total passings "
            lorryPassings = self.numberOfPassings * passings/100.0

        else:
            lorryPassings = passings

        if fixedNumber == True:
            lorryPassings = passings

        self.looriesPassings[lorryNumber]=lorryPassings

def addTotalPassings(self, numberOfPassings):
    self.numberOfPassings = numberOfPassings

def getTotalPassings(self):
    return self.numberOfPassings

def getLorryPassings(self,lorryNumber=None):
    if not lorryNumber:
        return self.looriesPassings

    else:
        if lorryNumber in self.looriesPassings:
            return self.looriesPassings[lorryNumber]
        else:
            print('Number of passings not defined for {}'.format(
                lorryNumber))
```

A.9.2 Abaqus FEA output scripting

```python
# -*- coding: utf-8 -*-
from odbAccess import openOdb
import os
from glob import glob

ODB_main_folder = #link to FLM ODB-file folder
TXTpath =#link to where outputfile should be stored
txt_name = [name of analysis]+"␣output"

os.chdir(TXTpath)

#Create .txt-file
f= open(txt_name+".txt","w+")
f.write("analysis;lorry;dist;element;integrationpoint;s22_neg;
    ↪ maxPrincipal_neg;mises_neg;s22_pos;maxPrincipal_pos;mises_pos\n")

os.chdir(ODB_main_folder)
dirs = os.listdir(".")

for directory in dirs:
        os.chdir(directory)
        ODBpath = ODB_main_folder+"\\"+directory+"\\"+os.listdir(".")[0]
        os.chdir(os.listdir(".")[0])

        filenames= glob('*.odb')

        for name in filenames:
                splitnames = name.split(".")
                jobname = splitnames[0]
                dist = float(name.split("_")[1])
                lorry = name.split("_")[0]

                #Opening the odb file
                try:
                        odb = openOdb(name)
                except:
                        continue

                try:
                        step = odb.steps["Truck"]
                        history = step.historyRegions
                        fatigueSet = odb.rootAssembly.elementSets["
                            ↪ FATIGUE_SET"]
```

```python
            field = step.frames[-1].fieldOutputs["S"]
            subField = field.getSubset(region=fatigueSet)
    except:
            odb.close()
            continue


    element_label = []
    integration_point = []
    s22_neg=[]
    maxPrincipal_neg = []
    mises_neg =[]
    s22_pos =[]
    maxPrincipal_pos=[]
    mises_pos =[]

    for element in subField.values:

            if element.integrationPoint in [3,4]:
                    continue

            integration_point.append(element.integrationPoint)
            element_label.append(element.elementLabel)

            if element.sectionPoint.description == "SNEG, (
                ↪ fraction = -1.0)":
                    s22_neg.append(element.data[0])
                    if abs(element.maxInPlanePrincipal) > abs(
                        ↪ element.minInPlanePrincipal):
                            maxPrincipal_neg.append(element.
                                ↪ maxInPlanePrincipal)
                    else:
                            maxPrincipal_neg.append(element.
                                ↪ minInPlanePrincipal)
                    mises_neg.append(element.mises)

            elif element.sectionPoint.description == "SPOS, (
                ↪ fraction = 1.0)":
                    s22_pos.append(element.data[0])
                    if abs(element.maxInPlanePrincipal) > abs(
                        ↪ element.minInPlanePrincipal):
                            maxPrincipal_pos.append(element.
                                ↪ maxInPlanePrincipal)
                    else:
```

```
                            maxPrincipal_pos.append(element.
                                ↪ minInPlanePrincipal)
                      mises_pos.append(element.mises)

           odb.close()

           os.chdir(TXTpath) #Changing folder for organizational
               ↪ purposes

           f.write("␣".join(analysisFolder.split("␣")[1:])+";"+lorry+"
               ↪ ;"+str(dist)+";"+str(element_label)+";"+str(
               ↪ integration_point)+";"+str(s22_neg)+";"+str(
               ↪ maxPrincipal_neg)+";"+str(mises_neg)+";"+str(s22_pos
               ↪ )+";"+str(maxPrincipal_pos)+";"+str(mises_pos)+"\n")

           os.chdir(ODBpath)

       os.chdir("..")
       os.chdir("..")

f.close()
```

A.9.3 Stress concentration factors

```python
# -*- coding: utf-8 -*-
#This script implemments the stress concentration factors given in DNVGL
   ↪ -RP-C203 appendix B for details relevant for the joints used in
   ↪ the report

import numpy as np

def B1_F1(beta, gamma, alpha):
    '''
    Calculates short chord correction factor F1 of tab B.1
    '''
    F1 = 1 - (0.83 * beta - 0.56 * (beta**2) - 0.02)*(gamma**0.23) * np.
       ↪ exp(-0.21 * (gamma ** -1.16) * (alpha ** 2.5))

    return F1

def B1_F2(beta, gamma, alpha):
    '''
    Calculates short chord correction factor F2 of tab B.1
    '''
    F2 = 1 - ( 1.43 * beta - 0.97 * (beta ** 2) - 0.03) * (gamma ** 0.04)
       ↪ * np.exp(-0.71 * (gamma ** -1.38) * (alpha ** 2.5))

    return F2

def B1_F3(beta, gamma, alpha):
    '''
    Calculates short chord correction factor F3 of tab B.1
    '''
    F3 = 1- 0.55 * (beta**1.8) * (gamma**0.16)*np.exp(-0.49*(gamma**-0.89)
       ↪ *(alpha**1.8))

    return F3

def B3_F4(beta, gamma, alpha):

    '''
    Calculates short chord correction factor F4 of tab B.4
    '''

    F4 = 1 - 1.07 * (beta**1.88) * np.exp(-0.16 * (gamma**-1.06) * (alpha
       ↪ **12.4))
```

```python
    return F4

def eq_1(t, T, d, D, theta, L):

    '''
    Calculates SCF for chord saddle eq.1 tab B-1

    Parameters
    ----------
    t : float
        Brace thickness.
    T : float
        Chord thickness.
    d : float
        Brace diameter.
    D : float
        Chord diameter.
    theta : float
        Angle in radians between brace and chord.
    L : float
        Length of joint.

    Returns
    -------
    scf_chord_saddle : float
        SCF for chord saddle.
    '''

    tau = t/T
    beta =d/D
    gamma = D/(2*T)
    alpha = (2*L)/D

    scf_chord_saddle = gamma * (tau**1.1)*(1.11 - 3*((beta-0.52)**2))*(np.
        ↪ sin(theta)**1.6)

    if alpha < 12:
        F1 = B1_F1(beta, gamma, alpha)
        scf_chord_saddle = scf_chord_saddle * F1
        print("alpha_<_12")

    return scf_chord_saddle

def eq_2(t, T, d, D, theta, L):
```

```python
    '''
    Calculates SCF for chord crown eq.2 tab B-1

    Parameters
    ----------
    t : float
        Brace thickness.
    T : float
        Chord thickness.
    d : float
        Brace diameter.
    D : float
        Chord diameter.
    theta : float
        Angle in radians between brace and chord.
    L : float
        Length of joint.

    Returns
    -------
    scf_chord_crown : float
        SCF for chord crown.
    '''

    tau = t/T
    beta =d/D
    gamma = D/(2*T)
    alpha = (2*L)/D

    scf_chord_crown = (gamma**0.2)*tau*(2.65 + 5*((beta-0.65)**2))+tau*
        ↪ beta*(0.25*alpha-3)*np.sin(theta)

    return scf_chord_crown

def eq_3(t, T, d, D, theta, L):

    '''
    Calculates SCF for brace saddle eq.3 tab B-1

    Parameters
    ----------
    t : float
        Brace thickness.
    T : float
        Chord thickness.
```

```
    d : float
        Brace diameter.
    D : float
        Chord diameter.
    theta : float
        Angle in radians between brace and chord.
    L : float
        Length of joint.


    Returns
    -------
    scf_brace_saddle : float
        SCF for brace saddle.
    '''

    tau = t/T
    beta =d/D
    gamma = D/(2*T)
    alpha = (2*L)/D

    scf_brace_saddle = 1.3 + gamma * (tau**0.52) * (alpha ** 0.1) * (0.187
        ↪ - 1.25 * (beta ** 1.1) * (beta - 0.96)) * (np.sin(theta) **
        ↪ (2.7 - 0.01 * alpha))

    if alpha < 12:
        F1 = B1_F1(beta, gamma, alpha)
        scf_brace_saddle = scf_brace_saddle * F1
        print("alpha␣<␣12")

    return scf_brace_saddle

def eq_4(t, T, d, D, theta, L):
    '''
    Calculates SCF for brace crown eq.4 tab B-1

    Parameters
    ----------
    t : float
        Brace thickness.
    T : float
        Chord thickness.
    d : float
        Brace diameter.
    D : float
        Chord diameter.
```

```
        theta : float
            Angle in radians between brace and chord.
        L : float
            Length of joint.

        Returns
        -------
        scf_brace_crown : float
            SCF for brace crown.
        '''


        tau = t/T
        beta =d/D
        gamma = D/(2*T)
        alpha = (2*L)/D

        scf_brace_crown = 3 + (gamma ** 1.2)*(0.12*np.exp(-4 * beta) + 0.011 *
        ↪   (beta ** 2) - 0.045) + beta * tau * (0.1 * alpha - 1.2)

        return scf_brace_crown

def eq_5(t, T, d, D, theta, L, C = 0.7):
        '''
        Calculates SCF for chord saddle eq.5 tab B-1

        Parameters
        ----------
        t : float
            Brace thickness.
        T : float
            Chord thickness.
        d : float
            Brace diameter.
        D : float
            Chord diameter.
        theta : float
            Angle in radians between brace and chord.
        L : float
            Length of joint.
        C : float
            Chord-end fixity parameter, typically C = 0.7 as specified at the
            ↪   end of tab B.1.

        Returns
        -------
```

```python
    scf_chord_saddle : float
        SCF for chord saddle.
    '''
    tau = t/T
    beta =d/D
    gamma = D/(2*T)
    alpha = (2*L)/D
    C1 = 2 * (C - 0.5)

    SCF_eq_1 = eq_1(t, T, d, D, theta, L)

    scf_chord_saddle = SCF_eq_1 + C1 * (0.8 * alpha - 6) * tau * (beta **
        ↪ 2) * ((1 - (beta ** 2))**0.5) * (np.sin(2*theta)**2)

    if alpha < 12:
        F2 = B1_F2(beta, gamma, alpha)
        scf_chord_saddle = scf_chord_saddle * F2
        print("alpha < 12")

    return scf_chord_saddle

def eq_6a(t, T, d, D, theta, L, C = 0.7):
    '''
    Calculates SCF for chord crown eq.6a tab B-1

    Parameters
    ----------
    t : float
        Brace thickness.
    T : float
        Chord thickness.
    d : float
        Brace diameter.
    D : float
        Chord diameter.
    theta : float
        Angle in radians between brace and chord.
    L : float
        Length of joint.
    C : float
        Chord-end fixity parameter, typically C = 0.7 as specified at the
            ↪  end of tab B.1.

    Returns
    -------
```

```python
    scf_chord_crown : float
        SCF for chord crown.
    '''
    tau = t/T
    beta =d/D
    gamma = D/(2*T)
    alpha = (2*L)/D
    C2 = C/2

    scf_chord_crown = (gamma ** 0.2) * tau * (2.65 + 5 * ((beta - 0.65) **
        ↪ 2)) + tau * beta * (C2 * alpha -3) * np.sin(theta)

    return scf_chord_crown

def eq_6c(t, T, d, D, theta, L):
    '''
    Calculates SCF for brace sadle eq.6c tab B-1. Note that this is not
        ↪ any equation listed in tab B.1. Brace saddle is calculated by
        ↪ eq_3, but with another short chord correction factor. Thus a
        ↪ fictious equation numer 6c is added for programming purposes

    Parameters
    ----------
    t : float
        Brace thickness.
    T : float
        Chord thickness.
    d : float
        Brace diameter.
    D : float
        Chord diameter.
    theta : float
        Angle in radians between brace and chord.
    L : float
        Length of joint.

    Returns
    -------
    scf_brace_saddle : float
        SCF for brace saddle.
    '''

    beta =d/D
    gamma = D/(2*T)
    alpha = (2*L)/D
```

```python
    scf_brace_saddle = eq_3(t, T, d, D, theta, L)

    if alpha < 12:
        F2 = B1_F2(beta, gamma, alpha)
        scf_brace_saddle = scf_brace_saddle * F2
        print("alpha < 12")

    return scf_brace_saddle

def eq_7a(t, T, d, D, theta, L, C = 0.7):
    '''
    Calculates SCF for brace crown eq.7a tab B-1.

    Parameters
    ----------
    t : float
        Brace thickness.
    T : float
        Chord thickness.
    d : float
        Brace diameter.
    D : float
        Chord diameter.
    theta : float
        Angle in radians between brace and chord.
    L : float
        Length of joint.
    C : float
        Chord-end fixity parameter, typically C = 0.7 as specified at the
        ↪   end of tab B.1.

    Returns
    -------
    scf_brace_crown : float
        SCF for brace crown.
    '''

    tau = t/T
    beta =d/D
    gamma = D/(2*T)
    alpha = (2*L)/D
    C3 = C/5
```

```python
    scf_brace_crown = 3 + (gamma ** 1.2) * (0.12 * np.exp(-4 * beta) +
        ↪ 0.011 * (beta ** 2) - 0.045) + beta * tau * (C3 * alpha - 1.2)

    return scf_brace_crown

def eq_8(t, T, d, D, theta, L):
    '''
    Calculates SCF for chord crown eq.8 tab B-1.

    Parameters
    ----------
    t : float
        Brace thickness.
    T : float
        Chord thickness.
    d : float
        Brace diameter.
    D : float
        Chord diameter.
    theta : float
        Angle in radians between brace and chord.
    L : float
        Length of joint.

    Returns
    -------
    scf_chord_crown : float
        SCF for chord crown.
    '''

    beta =d/D
    gamma = D/(2*T)
    tau = t/T

    scf_chord_crown = 1.45 * beta *(tau ** 0.85) * (gamma ** (1 - 0.68 *
        ↪ beta)) * (np.sin(theta) ** 0.7)

    return scf_chord_crown

def eq_9(t, T, d, D, theta, L):
    '''
    Calculates SCF for brace crown eq.9 tab B-1.

    Parameters
    ----------
```

```python
    t : float
        Brace thickness.
    T : float
        Chord thickness.
    d : float
        Brace diameter.
    D : float
        Chord diameter.
    theta : float
        Angle in radians between brace and chord.
    L : float
        Length of joint.


    Returns
    -------
    scf_brace_crown : float
        SCF for brace crown.
    '''
    tau = t/T
    beta =d/D
    gamma = D/(2*T)

    scf_brace_crown = 1 + 0.65 * beta * (tau ** 0.4) * (gamma ** (1.09 -
        ↪ 0.77 * beta)) * (np.sin(theta) ** (0.06 * gamma - 1.16))

    return scf_brace_crown

def eq_10(t,T,d,D, theta, L):
    '''
    Calculates SCF for chord saddle eq.10 tab B-1.

    Parameters
    ----------
    t : float
        Brace thickness.
    T : float
        Chord thickness.
    d : float
        Brace diameter.
    D : float
        Chord diameter.
    theta : float
        Angle in radians between brace and chord.
    L : float
        Length of joint.
```

```python
    Returns
    -------
    scf_chord_saddle : float
        SCF for chord saddle.
    '''
    gamma = D/(2*T)
    tau = t/T
    beta = d/D
    scf_chord_saddle = gamma * tau * beta * (1.7 - 1.05*(beta**3))*(np.sin
        ↪ (theta)**1.6)
    alpha = 2*L/D

    if alpha < 12:
        F3 = B1_F3(beta, gamma, alpha)
        scf_chord_saddle = scf_chord_saddle * F3
        print("alpha␣<␣12")

    return scf_chord_saddle

def eq_11(t,T,d,D, theta, L):
    '''
    Calculates SCF for Brace saddle eq.11 tab B-1.

    Parameters
    ----------
    t : float
        Brace thickness.
    T : float
        Chord thickness.
    d : float
        Brace diameter.
    D : float
        Chord diameter.
    theta : float
        Angle in radians between brace and chord.
    L : float
        Length of joint.

    Returns
    -------
    scf_brace_saddle : float
        SCF for brace saddle.
    '''
    gamma = D/(2*T)
```

```python
    tau = t/T
    beta = d/D

    scf_eq_10 = eq_10(t, T, d, D, theta, L)

    scf_brace_saddle = (tau ** -0.54) * (gamma ** -0.05) * (0.99 - 0.47 *
        ↪ beta + 0.08 * (beta ** 4)) * scf_eq_10

    alpha = 2*L/D

    if alpha < 12:
        F3 = B1_F3(beta, gamma, alpha)
        scf_brace_saddle = scf_brace_saddle * F3
        print("alpha < 12")

    return scf_brace_saddle

def eq_20(t_a, t_b, T, d_a, d_b, D, theta_a, theta_b, L, g=None):
    '''
    Calculates SCF for Chord eq.20 tab B-3.

    Parameters
    ----------
    t_a : float
        Brace A thickness.
    t_b : float
        Brace B thickness
    T : float
        Chord thickness.
    d_a : float
        Brace A diameter.
    d_b : float
        Brace B diameter.
    D : float
        Chord diameter.
    theta_a : float
        Angle in radians between brace A and chord.
    theta_b : float
        Angle in radians between brace B and chord.
    L : float
        Length of joint.
    g : float
        Gap between braces at chord surface

    Returns
```

```
    -------
    scf_chord_a : float
        SCF for Chord at Brace A.
    scf_chord_b : float
        SCF for Chord at Brace B.
    '''

    if g == None:
        g_a = np.tan(np.pi/2-theta_a)*D/2 - abs(d_a/2 / np.cos(np.pi- (np.
            ↪ pi/2 - theta_b)))
        g_b = np.tan(np.pi/2-theta_b)*D/2 - abs(d_b/2 / np.cos(np.pi- (np.
            ↪ pi/2 - theta_b)))
        g=g_a+g_b

    tau_a = t_a/T
    tau_b = t_b/T
    beta_a = d_a/D
    beta_b = d_b/D
    gamma = D/(2*T)
    zeta = g/D
    beta_max = max(beta_a, beta_b)
    beta_min = min (beta_a, beta_b)
    theta_max = max(theta_a, theta_b)
    theta_min = min(theta_a, theta_b)

    scf_chord_a = (tau_a**0.9)*(gamma**0.5)*(0.67-(beta_a**2)+1.16*beta_a)
        ↪ *np.sin(theta_a)*((np.sin(theta_max)/np.sin(theta_min))**0.3)
        ↪ *((beta_max/beta_min)**0.3)*(1.64 + 0.29*(beta_a**-0.38)*np.
        ↪ arctan(8*zeta))
    scf_chord_b = (tau_b**0.9)*(gamma**0.5)*(0.67-(beta_b**2)+1.16*beta_b)
        ↪ *np.sin(theta_b)*((np.sin(theta_max)/np.sin(theta_min))**0.3)
        ↪ *((beta_max/beta_min)**0.3)*(1.64 + 0.29*(beta_b**-0.38)*np.
        ↪ arctan(8*zeta))
    return scf_chord_a, scf_chord_b

def eq_21(t_a, t_b, T, d_a, d_b, D, theta_a, theta_b, L, overlap_brace =
    ↪ "a", g=None):
    '''
    Calculates SCF for Brace eq.21 tab B-3.

    Parameters
    ----------
    t_a : float
        Brace A thickness.
    t_b : float
```

```
        Brace B thickness
T : float
    Chord thickness.
d_a : float
    Brace A diameter.
d_b : float
    Brace B diameter.
D : float
    Chord diameter.
theta_a : float
    Angle in radians between brace A and chord.
theta_b : float
    Angle in radians between brace B and chord.
L : float
    Length of joint.
overlap_brace : str
    Choice of overlap brace.
g : float
    Gap between braces at chord surface

Returns
-------
scf_brace_a : float
    SCF for Brace A.
scf_brace_b : float
    SCF for Brace B.
'''

if g == None:
    g_a = np.tan(np.pi/2-theta_a)*D/2 - abs(d_a/2 / np.cos(np.pi- (np.
        ↪ pi/2 - theta_b)))
    g_b = np.tan(np.pi/2-theta_b)*D/2 - abs(d_b/2 / np.cos(np.pi- (np.
        ↪ pi/2 - theta_b)))
    g=g_a+g_b

tau_a = t_a/T
tau_b = t_b/T
beta_a = d_a/D
beta_b = d_b/D
gamma = D/(2*T)
zeta = g/D
theta_max = max(theta_a, theta_b)
theta_min = min(theta_a, theta_b)

if g >= 0:
```

```python
            c_a = 0
            c_b = 0
        else:
            if overlap_brace == "a":
                c_a = 1.0
                c_b = 0.5
            elif overlap_brace == "b":
                c_b = 1.0
                c_a = 0.5


    scf_chord_a, scf_chord_b = eq_20(t_a, t_b, T, d_a, d_b, D, theta_a,
        ↪ theta_b, L, g)
    scf_brace_a = 1 + (1.97 - 1.57 * (beta_a**0.25))*(tau_a**-0.14)*(np.
        ↪ sin(theta_a)**0.7)*scf_chord_a + (np.sin(theta_max+theta_min)
        ↪ **1.8)*(0.131 - 0.084*np.arctan(14*zeta+4.2*beta_a))*c_a*(
        ↪ beta_a**1.5)*(gamma**0.5)*(tau_a**-1.22)
    scf_brace_b = 1 + (1.97 - 1.57 * (beta_b**0.25))*(tau_b**-0.14)*(np.
        ↪ sin(theta_b)**0.7)*scf_chord_b + (np.sin(theta_max+theta_min)
        ↪ **1.8)*(0.131 - 0.084*np.arctan(14*zeta+4.2*beta_b))*c_b*(
        ↪ beta_b**1.5)*(gamma**0.5)*(tau_b**-1.22)

    return scf_brace_a, scf_brace_b

def eq_22_chord(t_a, t_b, T, d_a, d_b, D, theta_a, theta_b, L, g=None):
    '''
    Calculates SCF for Chord eq.22 tab B-3.

    Parameters
    ----------
    t_a : float
        Brace A thickness.
    t_b : float
        Brace B thickness
    T : float
        Chord thickness.
    d_a : float
        Brace A diameter.
    d_b : float
        Brace B diameter.
    D : float
        Chord diameter.
    theta_a : float
        Angle in radians between brace A and chord.
    theta_b : float
```

```
        Angle in radians between brace B and chord.
    L : float
        Length of joint.
    g : float
        Gap between braces at chord surface


    Returns
    -------
    scf_chord_a : float
        SCF for Chord at Brace A.
    scf_chord_b : float
        SCF for Chord at Brace B.
    '''

    if g == None:
        g_a = np.tan(np.pi/2-theta_a)*D/2 - abs(d_a/2 / np.cos(np.pi- (np.
            ↪ pi/2 - theta_b)))
        g_b = np.tan(np.pi/2-theta_b)*D/2 - abs(d_b/2 / np.cos(np.pi- (np.
            ↪ pi/2 - theta_b)))
        g=g_a+g_b

    scf_chord_a = eq_8(t_a, T, d_a, D, theta_a, L)
    scf_chord_b = eq_8(t_b, T, d_b, D, theta_b, L)

    if abs(g) / (d_a + d_b - abs(g)) > 0.3 and g < 0:
        scf_chord_a = scf_chord_a*1.2
        scf_chord_b = scf_chord_b*1.2

    return scf_chord_a, scf_chord_b

def eq_22_brace(t_a, t_b, T, d_a, d_b, D, theta_a, theta_b, L,
    ↪ overlap_brace="a", g=None):
    '''
    Calculates SCF for Brace eq.22 tab B-3.

    Parameters
    ----------
    t_a : float
        Brace A thickness.
    t_b : float
        Brace B thickness
    T : float
        Chord thickness.
    d_a : float
        Brace A diameter.
```

```python
    d_b : float
        Brace B diameter.
    D : float
        Chord diameter.
    theta_a : float
        Angle in radians between brace A and chord.
    theta_b : float
        Angle in radians between brace B and chord.
    L : float
        Length of joint.
    overlap_brace : str
        Choice of overlap brace.
    g : float
        Gap between braces at chord surface

    Returns
    -------
    scf_brace_a : float
        SCF for Brace A.
    scf_brace_b : float
        SCF for Brace B.
    '''

    if g == None:
        g_a = np.tan(np.pi/2-theta_a)*D/2 - abs(d_a/2 / np.cos(np.pi- (np.
            ↪ pi/2 - theta_b)))
        g_b = np.tan(np.pi/2-theta_b)*D/2 - abs(d_b/2 / np.cos(np.pi- (np.
            ↪ pi/2 - theta_b)))
        g=g_a+g_b

    beta_a = d_a/D
    beta_b = d_b/D

    scf_brace_a = eq_9(t_a, T, d_a, D, theta_a, L)
    scf_brace_b = eq_9(t_b, T, d_b, D, theta_b, L)

    if g < 0:
        if overlap_brace=="a":
            scf_brace_a = scf_brace_a * (0.9 + 0.4 *beta_a)
        elif overlap_brace=="b":
            scf_brace_b = scf_brace_b * (0.9 + 0.4 *beta_b)

    return scf_brace_a, scf_brace_b

def eq_23(t_a, t_b, T, d_a, d_b, D, theta_a, theta_b, L, g=None):
```

```python
'''
Calculates SCF for Chord eq.23 tab B-3.

Parameters
----------
t_a : float
    Brace A thickness.
t_b : float
    Brace B thickness
T : float
    Chord thickness.
d_a : float
    Brace A diameter.
d_b : float
    Brace B diameter.
D : float
    Chord diameter.
theta_a : float
    Angle in radians between brace A and chord.
theta_b : float
    Angle in radians between brace B and chord.
L : float
    Length of joint.
g : float
    Gap between braces at chord surface

Returns
-------
scf_chord_a : float
    SCF for Chord at Brace A.
scf_chord_b : float
    SCF for Chord at Brace B.
'''

if g == None:
    g_a = np.tan(np.pi/2-theta_a)*D/2 - abs(d_a/2 / np.cos(np.pi- (np.
        ↪ pi/2 - theta_b)))
    g_b = np.tan(np.pi/2-theta_b)*D/2 - abs(d_b/2 / np.cos(np.pi- (np.
        ↪ pi/2 - theta_b)))
    g=g_a+g_b

scf_eq_10_a = eq_10(t_a, T, d_a, D, theta_a, L)
scf_eq_10_b = eq_10(t_b, T, d_b, D, theta_b, L)
beta_a = d_a/D
beta_b = d_b/D
```

```python
    gamma = D/(2*T)
    zeta = g/D
    beta_max = max(beta_a, beta_b)

    x_a = 1 + (zeta * np.sin(theta_a))/beta_a
    x_b = 1 + (zeta * np.sin(theta_b))/beta_b
    alpha = 2*L/D

    F4_a = B3_F4(beta_a, gamma, alpha)
    scf_chord_a = scf_eq_10_a * (1-0.08*((beta_b*gamma)**0.5)*np.exp(-0.8*
        ↪ x_a)) + scf_eq_10_b*(1-0.08 * ((beta_a*gamma)**0.5)*np.exp
        ↪ (-0.8*x_a))*(2.05*(beta_max**0.5)*np.exp(-1.3*x_a))
    scf_chord_a = scf_chord_a * F4_a

    F4_b = B3_F4(beta_b, gamma, alpha)
    scf_chord_b = scf_eq_10_b * (1-0.08*((beta_a*gamma)**0.5)*np.exp(-0.8*
        ↪ x_b)) + scf_eq_10_a*(1-0.08 * ((beta_b*gamma)**0.5)*np.exp
        ↪ (-0.8*x_b))*(2.05*(beta_max**0.5)*np.exp(-1.3*x_b))
    scf_chord_b = scf_chord_b * F4_b

    return scf_chord_a, scf_chord_b

def eq_24(t_a, t_b, T, d_a, d_b, D, theta_a, theta_b, L, g=None):
    '''
    Calculates SCF for Brace eq.24 tab B-3.

    Parameters
    ----------
    t_a : float
        Brace A thickness.
    t_b : float
        Brace B thickness
    T : float
        Chord thickness.
    d_a : float
        Brace A diameter.
    d_b : float
        Brace B diameter.
    D : float
        Chord diameter.
    theta_a : float
        Angle in radians between brace A and chord.
    theta_b : float
        Angle in radians between brace B and chord.
    L : float
```

```
    Length of joint.
overlap_brace : str
    Choice of overlap brace.
g : float
    Gap between braces at chord surface

Returns
-------
scf_brace_a : float
    SCF for Brace A.
scf_brace_b : float
    SCF for Brace B.
'''


if g == None:
    g_a = np.tan(np.pi/2-theta_a)*D/2 - abs(d_a/2 / np.cos(np.pi- (np.
        ↪ pi/2 - theta_b)))
    g_b = np.tan(np.pi/2-theta_b)*D/2 - abs(d_b/2 / np.cos(np.pi- (np.
        ↪ pi/2 - theta_b)))
    g=g_a+g_b

scf_eq_23_a, scf_eq_23_b = eq_23(t_a, t_b, T, d_a, d_b, D, theta_a,
    ↪ theta_b, L, g)
tau_a = t_a/T
tau_b = t_b/T
beta_a = d_a/D
beta_b = d_b/D
gamma = D/(2*T)
alpha = 2*L/D

F4_a = B3_F4(beta_a, gamma, alpha)
scf_brace_a = (tau_a**-0.54) * (gamma**-0.05) * (0.99 - 0.47 *beta_a +
    ↪ 0.08 * (beta_a**4))*scf_eq_23_a
scf_brace_a = scf_brace_a * F4_a

F4_b = B3_F4(beta_b, gamma, alpha)
scf_brace_b = (tau_b**-0.54) * (gamma**-0.05) * (0.99 - 0.47 *beta_b +
    ↪ 0.08 * (beta_b**4))*scf_eq_23_b
scf_brace_b = scf_brace_b * F4_b

return scf_brace_a, scf_brace_b
```